2010

TARGETED POLYMERIC BIOMATERIALS FOR THE PREVENTION OF POST SURGICAL ADHESIONS

John M. Medley
University of Kentucky, jmmedl0@engr.uky.edu

ABSTRACT OF DISSERTATION

John M. Medley

The Graduate School

University of Kentucky

2010

TARGETED POLYMERIC BIOMATERIALS FOR THE PREVENTION OF POST SURGICAL ADHESIONS

ABSTRACT OF DISSERTATION

A dissertation submitted in partial fulfillment of the
requirements for the degree of Doctor of Philosophy in the
College of Engineering
at the University of Kentucky

By
John M. Medley

Lexington, Kentucky

Director: Dr. Thomas D. Dziubla, Assistant Professor of Chemical Engineering

Lexington, Kentucky

2010

ABSTRACT OF DISSERTATION

TARGETED POLYMERIC BIOMATERIALS FOR THE PREVENTION OF POST SURGICAL ADHESIONS

Despite recent advances in surgical technique and the development of numerous therapeutic agents, the formation post surgical adhesions (PSA) continues to cause complications for many patients. In this research, we have employed a rational system to develop a novel treatment to address this clinical need. Based on an understanding of the biochemical events that lead to PSA formation, a series of targeted polymeric biomaterials was designed to interrupt the fibrin gel matrix propagation and suppress PSA formation.

Using group transfer polymerization, a series of well controlled block copolymers of polyacrylic acid and poly(ethylene glycol-methacrylate) based materials was synthesized. Subsequent functionalization with the pentapeptide Cys-Arg-Glu-Lys-Ala (CREKA) was employed to target the materials to fibrin as a marker of pro-adhesive sites. While preliminary testing of the untargeted materials verified their ability to suppress non-specific protein adsorption to model surfaces, numerous *in vitro* tests were conducted to study the ability to inhibit fibrin gel propagation. The ability to inhibit both the rate and quantity of fibrinogen deposition to a fibrin coated surface has been demonstrated. In addition, the rate of fibrin gel propagation and the degree of cellular attachment can modulated.

Taking advantage of the systematic variation in structure facilitated by the robust synthetic methodology employed, statistical analysis was used to elucidate the structure-property relationships governing the performance of these materials. The most important factors that lead to enhanced performance in *in vitro* tests are the length of PEG chain and number of peptide units conjugated to the polymer: increasing PEG chain length and increasing the number of peptides conjugated to the polymer both improve performance in all tests. The synthetic methods that have been developed, in conjunction with the experimental results, will be used to direct future studies, including cytotoxicity and animal studies.

KEYWORDS: Biomaterials, Post Surgical Adhesions,
Targeting, Fibrin Gel Matrix, Fibrinogen

John M. Medley

February 22, 2010

TARGETED POLYMERIC BIOMATERIALS FOR THE PREVENTION OF POST SURGICAL ADHESIONS

By

John M. Medley

Dr. Thomas D. Dziubla
Director of Dissertation

Prof. Stephen Rankin
Director of Graduate Studies

February 22, 2010
Date

RULES FOR THE USE OF DISSERTATIONS

Unpublished dissertations submitted for the Doctor's degree and deposited in the University of Kentucky Library are as a rule open for inspection, but are to be used only with due regard to the rights of the authors. Bibliographical references may be noted, but quotations or summaries of parts may be published only with the permission of the author, and with the usual scholarly acknowledgements.

Extensive copying or publication of the dissertation in whole or in part also requires the consent of the Dean of the Graduate School of the University of Kentucky.

A library that borrows this dissertation for use by its patrons is expected to secure the signature of each user.

Name Date

DISSERTATION

John M. Medley

The Graduate School

University of Kentucky

2010

TARGETED POLYMERIC BIOMATERIALS FOR THE PREVENTION OF POST SURGICAL ADHESIONS

DISSERTATION

A dissertation submitted in partial fulfillment of the
requirements for the degree of Doctor of Philosophy in the
College of Engineering
at the University of Kentucky

By
John M. Medley

Lexington, Kentucky

Director: Dr. Thomas D. Dziubla, Assistant Professor of Chemical Engineering

Lexington, Kentucky

2010

Dedication

To My Family – Rachel, Will, and Christopher

Thank you for your tireless support and enduring patience. Without them, I would never have had the courage to embark on this exciting new endeavor.

ACKNOWLEDGEMENTS

First, I would like to express my gratitude to my advisor, Dr. Tom Dziubla. Thank you for allowing me the freedom to pursue my interests while helping me keep my focus on the big picture.

Much of this work would have been impossible without the assistance of several dedicated colleagues. Specifically, I would like to thank Eric Beane for his efforts in developing the HPLC methodology and for his assistance with QCM studies. John Heisterberg's work on the QCM was invaluable. I would like to express my gratitude to Sharath Sundararaj for his assistance in investigating cellular attachment and to Paritosh Wassamwar and Dr. Trevor Creamer for their assistance in performing the circular dichroism measurements. Thanks to the members of my committee for their thoughtful suggestions and for their assistance in planning this project.

Finally, I would like to acknowledge the University of Kentucky Graduate School and the Department of Chemical and Materials Engineering for their generous funding.

TABLE OF CONTENTS

LIST OF TABLES

LIST OF FIGURES

CHAPTER 1. INTRODUCTION

Post-surgical adhesions (PSA), abnormal fibrous linkages between adjacent tissue surfaces, represent one of the most common and significant complications facing surgical recovery today. It is believed that the vast majority of surgical patients experience this complication [1-2]. While, in most cases, these adhesions are not problematic, many patients require subsequent treatment(s) to correct the complications that arise. Approximately 440,000 adhesiolysis procedures are performed each year in the United States at an estimated total cost of over $1 billion [3-4]. Numerous strategies have been investigated to reduce adhesion formation, including changes in surgical technique and the development of adhesion barrier strategies. Unfortunately, no method has yet been devised that provides general applicability and affords adequate protection.

In this research, we have developed a new targeted polymeric material designed to address this problem by assembling at pro-adhesive sites and providing protection against PSA formation. The preliminary data contained herein suggest that this material may provide a novel approach to the prevention of post surgical adhesions. *In vitro* studies have demonstrated the ability of these synthetic polymeric materials to assemble onto model surfaces and prevent the early steps (e.g., protein absorption, fibrin growth, cellular attachment) in the event cascade that leads to PSA formation.

A rational design approach was used to identify the molecular properties that can be used to engineer a potential treatment to meet a specific medical condition. Based on the physiology and pathology of post surgical adhesion formation, polymeric materials were designed to interact with the fibrin gel matrix and suppress its development. These polymers incorporated peptide targeting units to control the interactions with fibrin and

polyethylene glycol units to form a surface layer that resists subsequent fibrin deposition. Preliminary testing demonstrated the viability of the concept, while more thorough experiments confirmed the ability to modulate the series of biochemical events that lead to adhesion formation. As anticipated, the structure of the polymer employed exerts dramatic influence on the ability of these materials to function as designed. Based on the encouraging results obtained from these experiments, *in vivo* studies are planned to assess the function of these materials in a rabbit model.

CHAPTER 2. BACKGROUND

Based on review published in:

> Biological Interactions on Materials Surfaces Understanding and Controlling Protein, Cell, and Tissue Responses Puleo, David A.; Bizios, Rena (Eds.) 2009 [5]. Used with permission.

2.1. Problem Statement

Each year in the United States, millions of people submit themselves to abdominal surgery for a variety of reasons, including gynecological reconstruction, tumor removal, and Cesarean sections [1-2]. While the success rate and recovery times for the initial surgeries are continually improving, complications frequently occur. One major complication of abdominal surgery, occurring in the vast majority of patients, is the formation of tissue adhesion. While it is impossible to determine the incidence rate with certainty, several studies indicate that post surgical adhesion formation occurs in 65 – 97% of abdominal surgery patients [1-4]. This acellular, collagen rich tissue often forms when an organ is damaged due to inadvertent desiccation or trauma during surgery. During healing, this damaged tissue often becomes permanently attached to adjacent tissues by the formation of a fibrous scar, as shown in **Figure 2-1**. While the nearly ubiquitous formation of adhesions is not generally problematic, numerous problems can arise that require subsequent physician care. Many patients experience abdominal or pelvic pain, intestinal obstructions, infertility, and increased difficulty in subsequent surgical procedures. In addition to the immeasurable costs in patient pain and suffering, an estimated 440,000 adhesiolysis procedures are performed in the United States each year [3-4].

2.2. Post-surgical Adhesion (PSA) Formation

The mechanism of these formations has been shown to follow the same basic pathway as intraperitoneal wound healing. The cells, proteins, and tissues involved in this mechanism, which have been described in numerous review articles, are shown graphically in **Figure 2-2** and can be summarized as a sequence of eight steps, as described in **Table 2-1** [6-8]. When this process initiates on an open surface, typical wound healing is observed, including the associated scar tissue formation. If an opposing surface is bridged by the Fibrin Gel Matrix (FGM) (see **Table 2-1, step 6**), the resulting scar tissue can permanently connect these surfaces, resulting in the formation of post surgical adhesions.

Depending where these adhesions form, a variety of complications are possible. If the adhesions involve the intestines, bowel obstructions can result [9-11]. In female patients, adhesions can obstruct the fallopian tubes and result in reduced fertility [9, 12-13]. Following surgery, many patients experience abdominal pain, which is believed to be a result of reduced mobility of the organs within the abdominal cavity [9, 12, 14-15]. Finally, subsequent surgeries can be complicated as tissue adhesions may interfere with the surgeon's access to organs [16-17]. Adhesions also form in areas of the body outside of the abdominal cavity. Numerous medical specialties, including cardiosurgery, neurosurgery, and orthopedic surgery, are plagued by the formation of complications arising due to postsurgical adhesion [18-23].

The costs associated with PSA in the United States are substantial. Approximately 300,000 hospital readmissions annually are either directly or indirectly related to the formation of PSA; the annual financial expenditure for pertinent treatment costs exceeds

$1.3 billion [3, 8]. Based on the significant financial costs and the immeasurable cost in terms of patient discomfort, the need either to eliminate or reduce the incidence and severity of PSA is apparent.

2.3. Methods of PSA Prevention and Control

Based on the well-characterized PSA formation mechanism, researchers and physicians have developed numerous approaches to prevent their formation. These approaches can be classified into four general categories: modification of surgical technique, pharmaceutical approaches, liquid instillates, and adhesion barriers. While none of these techniques can eliminate the incidence of PSA completely, each approach has demonstrated encouraging results, with research continuing along all four directions.

2.3.1. Modification of Surgical Technique

Since PSAs are known to form as the result of tissue trauma, it is logical that the number and severity of PSA can be reduced by reducing the trauma to tissues during surgery. Simple changes, such as implementing the use of non-powdered surgical gloves, can reduce desiccation of the peritoneum and have a positive impact. During open abdominal surgery, the peritoneum is often sutured closed to aid healing. This practice increases the length of surgery and, since the peritoneum is known to heal rapidly via island implantation, it has recently been questioned [24-26]. Several studies have recently been conducted to assess the necessity of suturing the peritoneum and its affect on the formation of PSA; the results have been mixed [1-2, 13, 24-26]. As described in **Section 2.5**, the presence of suture materials can induce an exacerbated wound healing response, due to the foreign body reaction, and promote PSA formation [27].

Another common surgical procedure, installation of prophylactic drainage tubes following abdominal surgeries, has also been a subject of investigation [28]. Often performed as an effort either to remove excess serum and blood (to reduce infection) or to provide an early warning of surgical complications, the necessity of this technique is uncertain [29-32]. In fact, the presence of drainage tubes can increase the likelihood of infection following abdominal surgery and has been shown to increase the incidence of PSA [31].

Recent investigations suggest that increasing the oxygenation of tissues in the abdominal cavity may affect the biochemistry of the wound healing process. Reduced oxygen levels in tissue (e.g., due decreased blood flow) can reduce the ratio of tissue plasminogen activator (tPA) to plasminogen activator inhibitor-1 (PAI-1) present in that tissue [33]. Since plasmin is necessary to break down the fibrin gel matrix (see **Table 2-1, step 6**), this reduced oxygen level may contribute to increased PSA formation. Oxygenating tissues during surgery has demonstrated some success at reducing the impact of PSA [33].

Since PSA is a result of trauma to the internal organ surfaces, reductions in the incision size, shortening the time of surgery and the overall invasiveness of the procedure should result in a reduction of PSA. Indeed, laparoscopic surgical methods have resulted in a major reduction in the incidence and severity of PSA [34-36]. Unfortunately, not all surgeries, such as gynecological reconstruction or emergency procedures, are amendable to laparoscopic methods. In addition, even though the incidence of PSA is reduced, laparoscopy can result in some tissue trauma with PSA formation still a likely outcome. Implementation of improved surgical procedures, while effective at reducing the

incidence and severity of adhesions, does not eliminate the risk of PSA formation. A significant clinical need still exists for alternative interventions to inhibit PSA formation.

2.3.2. Pharmaceutical Interventions

Since PSA formation is a product of uncontrolled wound healing, by pharmacologically intervening in this process, it may be possible to reduce the effect of pathways leading to tissue adhesions. However, implementation of these techniques has been frustrated by the complex biochemical nature of the wound healing process. For example, while it may be desirable to modify the healing process at the site of basement membrane exposure, biological approaches can potentially disrupt the beneficial healing throughout the body, resulting in more severe post-surgical complications.

Initial attempts to employ pharmaceutical agents focused on the reduction of tissue trauma. Local application of anti-inflammatory medications (i.e., ibuprofen, steroids, antihistamines, etc.) has been used to reduce inflammation at the surgical site. Interestingly, these therapies have demonstrated some efficacy during preclinical trials at reducing the formation of PSA [37-38]. This result is likely due to the understood link between excessive inflammation and fibrosis [39].

Similarly, attempts at mitigating oxidative stress at the wound site have also been employed to suppress the formation of PSA. While generation of oxygen radicals (typically from the leukocyte respiratory burst) [40-41] is a necessary part of the wound healing cascade, an excessive amount is known to activate collagen producing cells resulting in exaggerated levels of fibrosis [42-43]. It is logical to expect, then, that administration of antioxidant molecules would suppress formation of collagen rich tissues

[44]. Melatonin, vitamin E, and catalase have all shown some promise in reducing the severity of post surgical adhesion formation [44-47].

Heparin, a naturally occurring anticoagulant, interrupts various steps of the coagulation cascade and inactivates thrombin. Used to treat numerous pathologies and to create biologically-passivated surfaces, heparin has been investigated as an agent to reduce PSA formation. The results of these investigations, however, have been disappointing [48].

The most beneficial pharmaceutical interventions have employed fibrinolytic agents to reduce PSA formation. These enzymes, occurring naturally in the body, play a key role in the degradation of blood clots. As a result of trauma caused by surgery, production of these enzymes is suppressed [49-50]. It was proposed that the formation of PSA can be prevented by accelerating the degradation of fibrin deposits with locally delivered fibrinolytic agents to break down the fibrin gel matrix (FGM). This adhesive fibrin gel matrix is responsible for the formation of the initial deleterious union of adjacent tissue surfaces. Early investigations involved treatment with bacterially-derived streptokinase, a protein that catalyzes formation of plasmin which, in turn, breaks down the fibrin mesh of blood clots [51]. Increased plasmin activation proved beneficial in both animals and in humans and resulted in the commercialization of “Varidase” in the 1970s [52-54]. Additional investigations used the plasminogen activator enzyme, urokinase, and plasmin directly via intraperitoneal injection; mixed results and potentially immunogenic responses were observed [55-56]. Despite these inconsistencies, direct management of fibrin, the primary adhesive protein, represents an attractive PSA prevention strategy. Recent studies, focusing on the use of recombinant tissue plasminogen activator (rt-PA)

demonstrated significant potential to successfully address PSA formation [50]. While the use of tissue plasminogen activators has shown efficacy in reducing the incidence of PSA formation, they have been shown to increase the risk of hemorrhage in many applications [2, 57-58].

Oral delivery of drugs to reduce PSA formation has recently been investigated [59]. Chymases, naturally occurring proteases, stimulate accumulation of neutrophils and other inflammatory cells at the trauma site; these enzymes cleave procollagen into collagen fibrils, a primary step in the formation of the collagen rich tissue bridge. It was hypothesized that, by inhibiting/slowing the formation of collagen fibrils, the FGM could break down before PSA formation can occur. A recent study employed oral delivery of NK3201, a novel chymase inhibitor, showed significant reduction in chymase activity and, thereby, suppressed PSA formation in a hamster model [59].

2.3.3. Liquid Instillates

During surgery, saline solution is typically instilled into the body cavity to accomplish a number of goals. In addition to maintaining a clean surgical site (by removing blood and other biological debris), this solution also maintains hydration of exposed tissues. In an effort to reduce PSA formation, several alternate liquid instillates have been investigated.

Hyaluronic acid (HA), whose chemical structure is shown in **Table 2-2**, is a naturally-occurring biological polymer consisting of a long chain of disaccharide units with a molecular weight that can exceed 20 million Daltons. HA is a principal component of the extracellular matrix of tissues throughout the human body. HA can readily be broken down into its principle sugar molecules and metabolized within the body; these

degradation units, both monomeric and oligomeric, are potent signals for macrophage and cell recruitment, angiogenesis, and the presumed non-scarring, fetal-like, wound healing response [60-63]. Because of these properties, the use of HA has been investigated as a means to reduce PSA formation. If instilled prior to surgery, HA can effectively coat the organs in the abdominal cavity and provide protection against surgical trauma and tissue desiccation [64-65]. HA reduces the tissue adhesion score to 0.9 ± 1.1 versus 2.0 ± 0.8 obtained from the controls in a mouse model and has been approved for use by the FDA [64].

Several chemical modifications of HA have been formulated in order to improve its *in vivo* performance. By slowing HA degradation kinetics, it is believed that additional protection against PSA formation can be obtained. HA crosslinked with ferric ion (FeHA) reduced adhesion scores by 59% in clinical trials and led to the commercial product “Intergel” [66-67]. This product was withdrawn from the market after reports of additional complications, including pain and a foreign-body response attributed to the high iron content [48, 68]. By esterifying the hydroxyl groups on one HA chain with the carboxyl groups on another HA chain, it is possible to form an autocrosslinked HA derivative (HAx). This material forms a hydrogel and provides surface tissue protection for a longer duration. Tests in a rabbit model demonstrated the reduction in the adhesion score from 3.0 for controls to 0.5 in the treatment groups [69]. Clinical trials have also demonstrated reductions in adhesion scores of approximately 60% versus controls [70-71]. In addition, it is not clear whether these esterfied HA monomers possess the same degree of chemotacticity as native HA and, thereby, alter the rate of cellular infiltration and wound healing at the surgery site [72].

The most effective HA-derived liquid instillate employs crosslinked HA with another biologically-derived polymer, carboxymethylcellulose (CMC). CMC, whose structure is shown in **Table 2-2**, is a non-toxic material, used as a thickening agent in many food and drug products. CMC is not degraded in the body as rapidly as HA [69, 73-74]. After partial oxidation, HA can be chemically crosslinked with CMC; this chemical combination of HA with CMC, which is commercially available as "Sepracoat," results in an instillate with a residence time in the abdominal cavity of approximately seven days [66, 75-77]. This material has demonstrated significant protection against PSA formation in animal models but failed to convince the Federal Food and Drug Agency Panel of its clinical effectiveness against preventing adhesions in human patients [78].

Liquid instillates based on the chemistry of phospholipids have also been employed. These materials, whose general chemical structure is shown in **Table 2-2**, are amphiphilic: they have a polar, hydrophilic head group and a hydrophobic tail. This amphiphilicity accounts for the surfactant properties exhibited by these materials; they adhere to hydrophilic surfaces and form a protective boundary lubricating layer with their hydrophobic tails extending from the surface [79]. Several amphiphilic lipids (phospholipids, sphingolipids, galactolipids), have been tested to reduce PSA formation and demonstrated significant potential to reduce PSA formation [80-82]. In a rabbit model, these materials reduced the area of adhesion formation from 691 mm^2 to 191 mm^2 [80].

Another class of materials has been designed to provide protection in the abdominal cavity without pretreatment via hydroflotation. The saline solutions typically used for irrigation during surgical procedures fall into this category. "Adept," a

commercial product based on icodextrin, a polymeric starch, whose chemical structure is shown in **Table 2-2**, has been used for irrigation and rinsing during surgery [83]. After surgery, the polymeric starch is absorbed into the lymphatic system very slowly due to its high molecular weight [84]. Because of its high concentration, this material increases the osmotic pressure in the abdominal cavity and maintains an increased level of fluid [85]. The presence of this excess fluid results in tissue separation and has been shown to decrease PSA formation [84, 86-89]. In the rabbit dual uterine horn model, "Adept" increased the number of adhesion-free sites to 50% versus the 5% obtained for the untreated controls [84].

Polyethylene glycol (PEG), discussed in **Section 2.5**, has also been employed in efforts to reduce PSA formation. This material, often referred to as polyethylene oxide (PEO), was proven biocompatible in a number of applications and is under investigation for a number of additional uses [90]. PEG, whose chemical structure is shown in **Table 2-2**, consists of a series of repeating ether units with either hydroxyl or methoxy terminations at both ends. This structure renders PEG amphiphilic and resistant to protein adsorption. Soluble in many organic solvents, PEG is highly hydrophilic and can form a hydrated layer with a large excluded volume and high steric stabilization [90-91]. PEG surfaces present few binding sites for protein interactions; for this reason, adsorption of proteins, and subsequent adhesion of cells, is strongly inhibited. Injection of PEG into the peritoneal cavity has been moderately successful in preventing PSA formation [4]. Yet, because of their anti-adhesive nature, free PEG chains adhere poorly to surfaces. Attempts to increase the protective ability of PEG by crosslinking with CMC

into a viscous gel have achieved a 42% reduction in the American Fertility Society adhesion score versus the relevant controls [92].

A recent attempt to prevent PSA formation employed sequential use of solutions containing charged polypeptides [93]. A solution containing poly(L-lysine) (PLL) was instilled into the peritoneal cavity followed by a solution of poly(L-glutamate) (PLG) five minutes later. Positively-charged PLL, whose chemical structure is shown in **Table 2-2**, adheres to damaged tissues. Negatively-charged PLG, whose chemical structure is also shown in **Table 2-2**, associated with the positively-charged PLL on the surface and forms an insoluble film at the site of injury. In animal studies employing a mouse model, this system reduced the incidence of PSAs from 49.5% in the animals to 8.81% in treated animals [93-94]. Further implementation of these materials may be hampered because of toxicity concerns associated with the highly charged polyamines employed [93].

2.3.4. Adhesion Barriers

Currently, the most consistently effective methods that reduce the incidence and severity of PSA formation provide physical separation of wounded from surrounding tissues. By isolating damaged or potentially damaged surfaces from each other during the wound healing process, normal healing without the formation of PSAs was achieved [2, 8]. Because of the simplicity and efficacy of this approach, numerous barrier systems have been investigated.

The first adhesion barrier system investigated consisted of grafts of peritoneal tissue aimed at providing protection to areas of damaged peritoneum. The presence of necrotic graft material, however, promoted, rather than inhibited, PSA formation in animal trials [48]. Other attempts to protect tissues by stretching the nearby peritoneal

membrane also proved ineffective [48]. Decreased blood flow in this distorted tissue results in decreased plasmin activation and enhanced the formation of the fibrin gel matrix [48].

Another material that has been investigated for use as an adhesion barrier is poly(tetrafluoroethylene) (PTFE) [95]. Because PTFE is known to resist adhesion to most substances, it is a natural candidate for use as a PSA barrier. This material, whose structure is shown in **Table 2-2**, consists of a straight chain of carbon atoms onto which fluorine atoms are fully substituted. The fluorine atoms present an inert, electron-rich surface that prevents strong interactions with other materials. PTFE is readily available as an expanded mesh, commonly referred to as ePTFE, under the trade name "Gore-Tex Surgical Membrane" [96-97]. The presence of PFTE between damaged tissue surfaces prevents the FGM from bridging these tissues and, thus, prevents PSA formation [3, 98-101]. In animal tests employing a porcine model, PTFE reduced the adhesion score to 0.14 ± 0.12 versus the observed 1.33 ± 0.41 for controls [101].

The major drawbacks of PTFE result from its high degree of inertness. Since PTFE is so effective at preventing interactions with biological tissues, it typically must be sutured into place in the body [102]. In addition, PTFE is not biodegradable. Ideal for permanent prosthetic applications, the use of PTFE as an adhesion barrier can be problematic [99]. After the body has healed from the trauma induced by surgery, typically within about two weeks, the presence of the PTFE membrane at the site of trauma is undesirable. A second surgery, then, is typically necessary to remove this barrier material and ensure that unwanted complications are prevented [100].

Several barrier membranes have been investigated that overcome this limitation of PTFE. Designed to be readily biodegradable, such membranes often do not need suturing into position and, thus, subsequent removal. After the desired protection has been rendered, these membranes break down and are metabolized by the body. Numerous biodegradable materials have been investigated for use as adhesion barriers, including cellulose derivatives, hyaluronic acid derivatives, and PEG-based materials [102-107].

Oxidized regenerated cellulose (ORC) was employed to form a barrier that was successfully commercialized under the trade name “Interceed.” Cellulose, a naturally occurring polysaccharide, whose structure is shown in **Table 2-2**, is partially oxidized to improve aqueous solubility. This biodegradable material has a gauze-like consistency and can be applied directly to damaged tissues in order to prevent PSA. When properly applied, this material has shown a high degree of efficacy in reducing PSA formation in surgical procedures. There are, however, several limitations to the clinical use of “Interceed” [94, 99]. Because it is thrombogenic, contact with blood greatly increases the likelihood of subsequent surrounding tissue adhesion; because of this property, complete hemostasis must be achieved prior to *in situ* application of “Interceed.” In addition, application must be limited to a single layer of material in all areas; multiple layers may promote adhesions [48]. These difficult handling requirements render “Interceed” unsuitable for laparoscopic procedures and limit its general applicability to more invasive laparotomic procedures.

Barriers based on HA crosslinked with CMC are available under the trade name “Seprafilm.” This material is applied as rigid sheets that, once hydrated, form a protective gel on the abdominal tissue surface and prevent PSA formation. With a chemical

composition nearly identical to “Sepragel,” this material is readily biodegraded *in vivo* within about one week. Provided that a surgeon has knowledge and access to all areas of tissue damage, “Seprafilm” can be very effective at preventing PSA formation [102-104]. In animal studies employing a rat model, the total adhesion score was reduced to 4.15 ± 0.58 from 7.21 ± 0.52 obtained for the respective controls [77]. A meta-analysis of clinical data also demonstrated “Seprafilm” to be effective at lowering the incidence of PSAs in abdominal surgeries [108]. While this study mistakenly included a non-“Sepracoat” HA/CMC material in its analysis, it reported that patients receiving the “Sepracoat” were 8.71-times more likely ($p < 0.01$) to have no adhesions than the control group ($p < 0.01$) [108]. While the rigid structure of “Seprafilm” has traditionally prevented its use in laparoscopic surgery, newer techniques involving the use of rolled films has provided some limited laparoscopic use [109].

Since the number of procedures performed by laparoscopic surgery is continually increasing, the ability to apply antiadhesive therapies via this method is increasingly important. A material recently developed to address this clinical need is the two-component system commercially available as “SprayGel.” This system consists of a double-barrel syringe used to apply the contents to damaged tissue via laparoscopy. Each barrel contains a reactive PEG precursor solution. Upon mixing, an amine group from one component reacts with N-hydroxysuccinimide (NHS) ester in the other component to form a crosslinked hydrogel, as shown in **Table 2-2**. This crosslinked material degrades *in vivo* into PEG units that are rapidly removed from the body by renal clearance [105-106]. Since “SprayGel” is readily applicable in laparoscopic procedures, the major limitation for its use in PSA suppression is the surgeon’s awareness of, and access to,

damaged tissues. In clinical trials, this material showed significant efficacy because it reduced the mean adhesion tenacity score by 64.7% versus the values obtained for the untreated controls [110].

The aforementioned adhesion barriers have proven efficacious in reducing PSA formation in patients; for this reason, these commercially available products are enjoying success in the marketplace. Even with these methods, however, PSA formation is still occurring. For instance, in the 2007 meta-analysis of "Seprafilm" described earlier, of the 371 patients in the adhesion barrier treatment group (combined over several studies), 196 still had developed a post surgical adhesion [108]. With a prevention rate of only ~ 48%, multiple hypotheses have emerged to explain the persistent occurrence of PSA. If the surgeon is unaware of damaged tissue or if the damaged site is inaccessible, current barrier methods may not be effective and tissue adhesion formation remains a likely outcome. To overcome these deficiencies, many new strategies for the prevention of PSA are currently being investigated. Some of these investigations focus on combinations of techniques that have demonstrated success in the past. For example, various hydrogels have been loaded with either anti-inflammatory, antibiotic, or fibrinolytic agents, including budesonide, paclitaxel, or streptokinase [38, 46, 111-113]. In addition, changes to pertinent surgical technique are under investigation [31, 33, 59]. A brief summary of the most widely investigated PSA prevention methods is given in **Table 2-3**.

2.4. PSA Evaluation Methods

Perhaps one of the biggest impediments to the rapid development of PSA prevention strategies, especially to the testing of barrier materials, is the lack of a standard and widely used method to evaluate and compare pertinent performance. The

situation is complicated because various animal models are used and each clinical trial is conducted independently. Due to the complex interplay of the many facets of the wound healing process, inflammatory cascades, and anatomical aspects, *in vivo* studies are an integral part of PSA evaluation. Animal testing, however, is, by its nature, very complex, time consuming and limited in its ability to provide useful data comparisons among studies. In addition, large-scale screening of materials is not typically possible because of the associated high cost, time requirements, and ethical issues. Furthermore, in most animal models, failure of PSA treatment strategy does not always provide useful information regarding the underlying mechanism of failure. Methods of assessment have been primarily based on semi-quantitative animal models, including mouse, rat uterine horn, rabbit, and porcine; these models are summarized in **Table 2-4**. The results of such studies are typically scored based on visual observations (e.g., no adhesion, filmy avascular adhesion, vascularized adhesion, collagen rich adhesion) in an attempt to provide meaningful comparisons. Because of the large variability in the test methods and in data analysis, it is generally not possible to conduct meaningful comparisons between independent investigations. Results of material performance are often either confounded or obscured by the differences in the models and scoring systems employed.

Furthermore, there has been a significant lack of translational relevance from *in vivo* PSA treatment models to clinical application and success. A strong need exists to revisit the fundamental aspects of adhesion formation and obtain more information regarding the underlying mechanisms for both the success and failure of each treatment. Recent attempts to address these issues have focused on standardizing the methods of testing and quantifying tissue adhesion formation. A grading system, described in **Table**

2-5, was developed to evaluate three characteristics (specifically, extent, severity, and degree) of adhesion formation; application of these three measures assigns a total adhesion score [114]. While still semi-quantitative, this grading system provides some quantitative information and allows comparisons to be made between the results of various studies.

Most recently, complete quantitative investigations and *in vitro* models are being developed to allow for a rational optimization of potential treatments prior to large-scale animal tests. Investigators have reported preliminary results indicating that tissue adhesions can be reproducibly formed in a porcine model and analyzed using a tensile test system [115]. This tensile strength analysis method provides bulk modulus data of the formed scar tissue, allowing direct quantitative assessment of the quality and maturity of the adhesion and does not rely upon physical appearance alone [115].

In order to overcome many of these limitations, a comprehensive understanding of the nature of the mechanism controlling the PSA reduction is highly desirable. This result can be achieved by developing reproducible *in vitro* tests and systematically studying the effects of various materials on the results. If this work can then be correlated with the results of *in vivo* studies, the relative importance of various *in vitro* tests can be assessed and development of additional PSA prevention strategies can be carried out in a much more systematic and efficient manner.

2.5. Biomaterials

2.5.1. Background

Over the past three decades, the medical field has benefitted greatly from numerous advances in material properties. Since the early 1980s, several definitions have been proposed to describe the field of biomaterials [116-118]. The main concepts that are generally regarded as important in designing a biomaterial are that something interact with the body in a desired manner and that it provide the desired function. One widely used definition of a biomaterial was promulgated in 1987: “A biomaterial is a nonviable material used in a medical device, intended to interact with biological systems” [119]. This broad field of study encompasses a wide array of materials and devices, ranging from simple disposable catheters and syringes to complex, permanently implanted devices such as artificial joints and pacemakers. Recent advances have enabled the development of increasingly complex biomaterial devices, such as those used for tissue engineering and artificial organs [118, 120-121]. As these devices have become more complex and permanent, understanding and controlling the interactions of the component materials with the body has become increasingly important.

2.5.2. Biomaterial Interactions

Consisting principally of cells, proteins, and extracellular matrix, natural tissue is a complex, active material. Each component contributes unique functionality to the tissue, and the synergistic effect of these components creates a sophisticated composite system. Conversely, typical synthetic biomedical implants consist of much more homogeneous materials that have been optimized for a particular function. As a result,

implant materials are often inferior to natural tissues in many ways, including strength, elasticity, and capacity for self-repair.

Another difficulty with biomaterials is that implants are rarely constructed from materials native to the patient. When a biomaterial is implanted into the body, a complex series of biochemical events is triggered. Initially, the body's response is focused on hemostasis. During the ensuing inflammatory phase, the body attempts to isolate or remove any injurious agents using its natural defenses. Depending on the nature of the biomaterial, this inflammation typically relies on the action of macrophages and is of relatively short (less than one week) duration. If inflammation persists for more than approximately 1 week, chronic inflammation, characterized by the presence of monocytes in the affected area, may result. Over time, these monocytes may differentiate into macrophages and lead to the formation of foreign body giant cells. [7-9, 122-126].

In the absence of chronic inflammation, the repair and remodeling phase of healing continues and the implant site is stabilized. The implant is incorporated into a collagenous fibrous capsule. The nature of this capsule is dictated by both the composition and structure of the implant material and by the location of the implant [125, 127-129]. For non-toxic, non-degradable materials, minimal fibrosis may be observed [130-131]. If implants are composed of more reactive materials, the resulting encapsulation becomes more extensive and consists primarily of collagen with some fibroblasts and macrophages [125, 131]. Materials that elicit a strong foreign body response result in the formation of a thick, fibrous capsule formation and may impede integration of the implant with native tissue. Finally, if a more pronounced incompatibility is seen, a more significant immunological response may be induced. In

this instance, rejection of the implant by the immune system or remote effects may occur [125]. With these difficulties, it is apparent that conventional implant technology leaves much to be desired.

Recent advances in biomedical research have focused on controlling the body's response to implant materials by careful selection and engineering. If the effect of these biomaterials on the body can be controlled, implants with much better function and applicability can be imagined. Numerous attempts to modulate the body's response have been investigated. For example, the use of materials such as Dacron® and Gore® for use in vascular grafts and the use of modern alloys in articular replacements have greatly improved the function of these implants and reduced the incidence and severity of adverse reactions in the body. The poor biointegration often seen with these materials and their inherent inability to repair damage still represent significant deficits in their long-term function [132]. The development of more complex biomaterials remains a major area of research and shows great promise to address a number of critical needs in the medical field.

The body's response to biomaterials is very similar to the previously described post surgical adhesion formation process (see **Section 2.2**). These parallels provide insight into the desired properties of materials employed for the prevention of PSA. Strategies that have previously been shown to attenuate the foreign body response observed with implanted biomaterials are expected to provide excellent opportunities for reducing the incidence of PSA. It is thought that, by minimizing the body's response, development of an extended FGM matrix can be controlled in much the same way that many successful biomaterials avoid a strong foreign body response.

2.5.3. Polyethylene Glycol

One particular material that is the subject of much current research is polyethylene glycol (PEG). This material, often referred to as polyethylene oxide (PEO) in higher molecular weight forms, has been shown to be biocompatible in a number of applications and is under investigation for a variety of additional uses. PEG consists of a series of repeating $–(CH_2CH_2O)–$ units with hydroxyl terminations at both ends. This structure results in PEG's having an amphiphilic nature that renders it resistant to protein adsorption.

While soluble in many organic solvents, PEG is highly hydrophilic and has been shown to form PEGylated surfaces with a hydrated layer with a large excluded volume and high steric stabilization [90-91]. Such a surface presents few binding sites for protein interactions, and the adsorption of protein and subsequent adhesion of cells is strongly inhibited. Recent studies incorporating low concentrations of PEG into polylactic acid have been shown to reduce the level of cellular adhesion dramatically [133]. In addition to its resistance to fouling, PEG can also form hydrogels. In this form, PEG's consistency can be tailored to match the native or surrounding tissue for implant applications.

This unique structure, coupled with its lack of toxicity, has led to PEG's investigation for use in numerous biomaterials applications. Many controlled drug delivery systems exploit PEG to create "stealth" technologies. Nanoscale materials can be injected into the bloodstream; since they are unable to be seen by immune cells, they can achieve very long circulation times and extend drug delivery therapy. Other drug delivery systems employ PEG in stationary reservoir systems to avoid fibrous capsule

formation [134]. More recently, PEG has been investigated for use in biosensor and numerous other biomedical applications [135]. This wide-ranging applicability at rendering surfaces resistant to cell and protein adhesion and well-characterized biocompatibility suggest that PEG should be an ideal material for use in PSA adhesion technologies.

2.6. Targeting and Controlled Delivery

Successful medical treatment of many conditions is hampered by numerous factors. In order to treat a disease in the body, it is often necessary to deliver a drug to a specific area and to maintain therapeutic concentrations for an extended period of time [134]. The desire to maintain these concentrations, frequent dosing at high levels can lead to systematic complications. For example, many chemotherapies for the treatment of cancers require daily dosing and can lead to side effects including nausea, loss of hair, and anemia [136-140].

In order to maximize the efficacy of treatments and to reduce these side effects, it would be advantageous to deliver the desired drugs to the affected areas of the body and release them at a rate that would maintain the therapeutic concentration in the local area. Vigorous research is underway to investigate technologies that will facilitate such treatments. Many advanced drug delivery systems have been designed to extend the therapeutic treatment window. These systems vary from relatively simple extended release tablets to complicated pulsatile delivery systems with feedback loops that respond to changes in the physiological environment [134, 141-145].

Another technique that can be used to minimize side effects while achieving the maximum benefit from a treatment relies on delivering the therapy only to the affected

area(s) of the body. Simple embodiments of this concept include external application of ice to swollen joints, injection of anti-inflammatory drugs, or the application of topical antibiotics. The treatment of many disease conditions, however, requires that potentially toxic drugs be delivered to specific areas within the body. In order to address this goal, drug delivery systems have been developed to deliver agents specifically to affected areas of the body.

For therapeutic agents delivered via the vasculature, this targeted drug delivery can occur through two unique mechanisms. Passive targeting often relies on the enhanced permeability and retention (EPR) effect to facilitate delivery of drugs to tumor sites [146-149]. Because of their rapid growth, tumor sites often develop vasculature with large pores. This "leaky" vasculature allows nanosized drug carriers to reach these sites, where they are able to release therapeutic agents at the pathological sites. Alternatively, active targeting relies on specific ligand-target interactions to direct drugs to the desired site in the body. Recent developments in chemical and biochemical techniques have led to advances in the area of active targeting. By designing drugs or drug carriers to seek out these specific sites in the body, the efficacy of therapeutic treatments can be enhanced while the potential for adverse side effects can be greatly reduced [146, 150-152]. Major advances in this field have demonstrated excellent results in the treatment of numerous cancers, diabetes, and vascular disease [153-160].

This active targeting can be carried out using a variety of targeting units. Antibodies for specific molecules, including fibrin, can be conjugated to nanoparticles or liposomes in order to direct targeting [161]. These antibodies, however, are not ideal for targeting of small molecules. Because of their very large size (~ 150 kDa), the antibody

could mask the effect of polymers delivered to surfaces. In addition, since they are biologically derived, they are likely to elicit an undesired response in the body. Aptamers, small strands of nucleic acid, can also be employed to provide specific binding to molecules [162-163]. These targeting units can be isolated by iterative selection and amplification *in vitro* from a random pool of nucleic acid strands. A similar approach using bacteriophages for amplification can be employed to select peptide units for targeting [164]. These targeting approaches result in the identification of small, easily synthesized molecules that can then be incorporated onto the therapeutic molecule or carrier [163, 165-167].

These small targeting units provide advantages over antibody targeting. First, since the targeting unit is relatively small, multiple groups can be incorporated into the structure to amplify the effect of targeting without the likelihood of masking the protective properties of the polymers. In addition, since they are not biologically derived, they have a low probability of eliciting an immunological response from the body.

2.6.1. CREKA Targeting Peptide

A particular targeting technology has recently been developed as a means to target drug carriers to tumor cells based on the presence of clotted plasma proteins that accumulate due to the leaky vascular associated with rapidly growing tumors [168-170]. This new targeting agent, based on the pentapeptide unit Cysteine-Arginine-Glutamic Acid-Lysine-Alanine (CREKA), has been shown to enhance delivery of nanoparticles and nanoworms to tumor sites. In initial investigations, superparamagnetic iron oxide (SPIO) nanoparticles were conjugated with CREKA and successfully targeted to growing tumors in mice [171]. If the fibrinogen knockout mice were used in the experiment, no

targeting was observed, confirming that the targeting mechanism relies on specific interaction of the peptide unit with clotting proteins. Subsequent studies verified the ability to target clinically approved chemotherapeutic nanoparticles in mice [172]. The effect of changes in the shape of the targeted nanoparticle and the density of targeting peptides has also been carried out [173]. This peptide has also been shown to be effective at targeting nanoparticles to atherosclerosis plaques for diagnosis and therapy [174].

In order to improve the understanding of CREKA and to develop functional analogs, several modeling studies using molecular dynamics have been conducted. Initial modeling of the three-dimensional structure of the peptide in aqueous solutions and on the surface of nanoparticles indicated that the conformation is unchanged by surface attachment via the cysteine residue [175]. Subsequent models indicated the relative stability of the three-dimensional structure of the CREKA unit with the addition of dye molecules or with substitution of protease-resistant arginine analogs [176-177]. While the nature of the interactions of this peptide with fibrin is not well understood, the effectiveness of its targeting ability and its robust three-dimensional structure make it an attractive ligand for the targeting of materials to fibrin.

2.7. Conclusion

Post-surgical adhesions represent a significant clinical complication that affects a large patient population. To address this multifaceted problem, a range of methods were developed. Although use of physical material barriers provides the best results, no single method has proven to be effective in all instances, to date. This failure is most likely due to the complexity of PSA formation, the uniqueness of each surgical procedure and patient, and lack of understanding of the underlying mechanism of PSA etiology and

successful prevention. PSA remains a serious clinical problem. New methodologies to improve material/device performance at a mechanistic level are a necessity for the success of PSA barriers in the future. In addition, novel materials must be designed and formulated to address all pertinent aspects of the PSA formation (e.g., physical, chemical, inflammatory, oxidative, and wound healing) in order to maximize the potential for clinical success. In this regard, biomaterial engineers could make crucial contributions toward eventual elimination of PSA formation.

This dissertation describes the design, synthesis, and evaluation of a series of polymeric biomaterials for use as prophylactic adhesion barriers. Based on a thorough understanding of the underlying biochemistry and pathology of PSA formation, the materials were specifically designed to interrupt the cascade of events that leads to adhesion formation. Applying tools from polymer chemistry, organic chemistry, and analytical chemistry, these materials were synthesized and fully characterized. The function of these materials was evaluated in model systems, and the relationship between their structure and function was assessed using statistical techniques. Finally, the ability of these materials to inhibit PSA formation *in vivo* was evaluated.

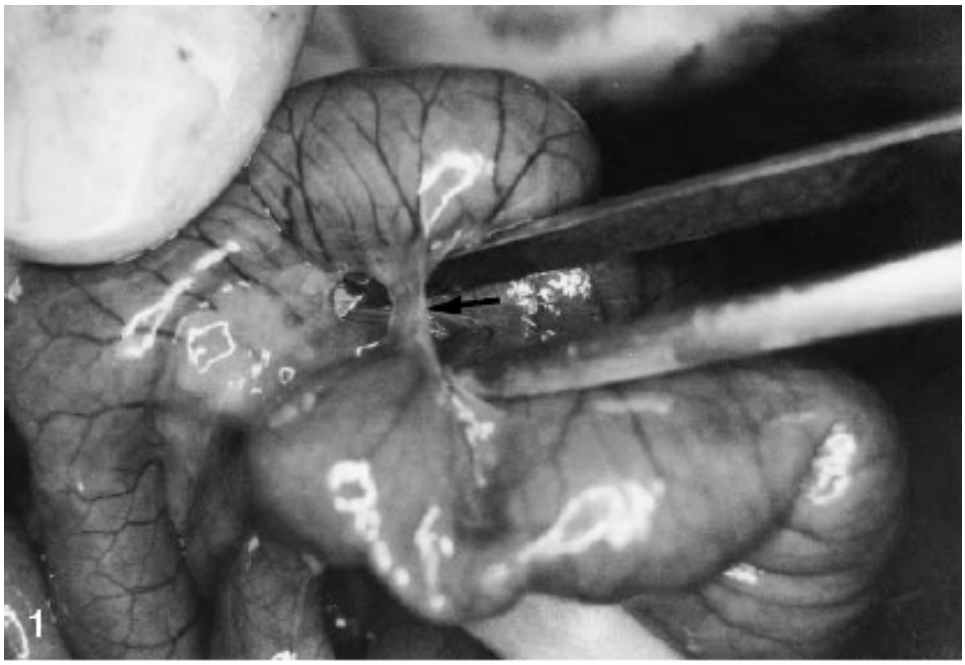

Figure 2-1 An example of intestinal post-surgical adhesion (PSA) formation.
In a rat model, sections of mecum and ileum were abraded using dry gauze until hemorrhage formed. Fourteen days post surgery, adhesion formation was visualized. Figure reproduced with permission from Kutlay, et al. [178].

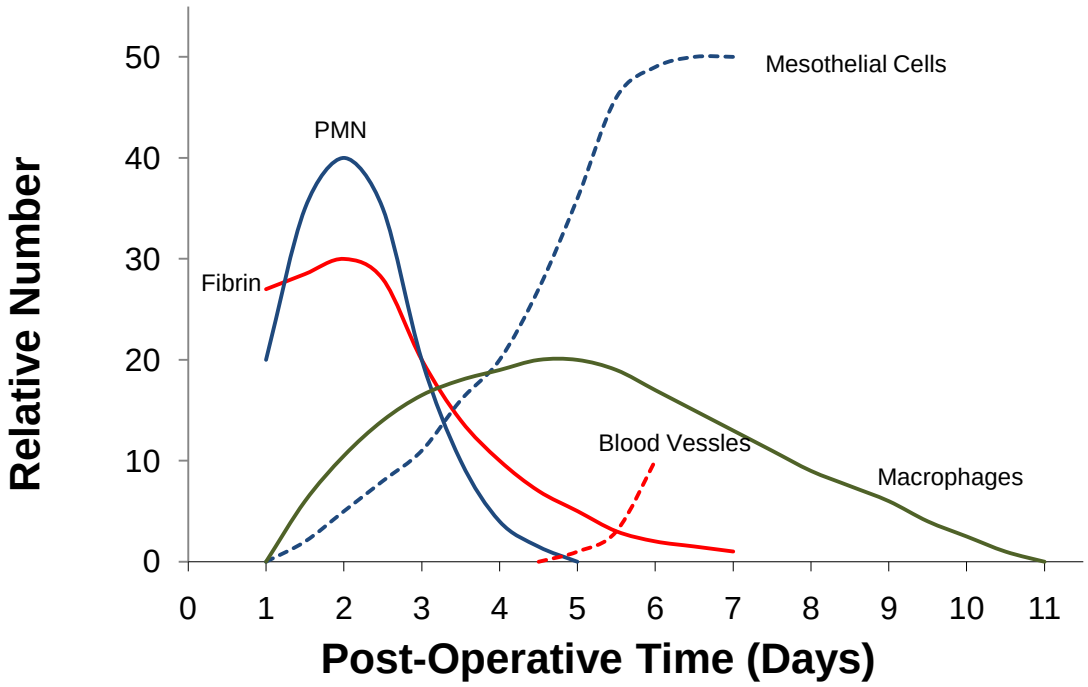

Figure 2-2 Stages and time course of the wound healing process.
Initially, a high concentration of fibrin is observed in the peritoneal fluid. Polymorphoneutrophils PMNs are observed within approximately two days post tissue-trauma, followed by macrophages. Reperitonealization occurs with the appearance of mesothelial cells within the first five days, and vascularization begins within 1 week following tissue damage. Adapted from [126].

Table 2-1 Timeline of events occurring during post-surgical adhesion formation.

1. Damage to the peritoneal mesothelium exposes an acellular, denuded surface, known as the “basement membrane”, which consists primarily of type I collagen, type II collagen, fibronectin, and laminin [6, 8].
2. As the vasculature constricts, homeostasis is obtained and the coagulation cascade begins with the deposition of fibrin [8].
3. The quantities of fluid and plasma proteins increase near the site of injury and an inflammatory exudate develops within the peritoneal fluid [7].
4. The composition of this exudate, initially consisting primarily of neutrophils, changes. If there is no infection, it becomes rich in macrophages over the course of 24 hours [7-8].
5. Epithelial cells are deposited on the surface of the injury by a process called “island implantation” and re-epithelialization of the peritoneal surface proceeds [7].
6. The fibrin gel matrix (FGM), considered the “principal player in adhesion formation,” consists of fibrin, fibronectin, hyaluronic acid, glucosaminoglycans and proteoglycans, and forms 72-108 hours after surgery [7-8].
7. The FGM is remodeled and strengthened, for approximately 1 month [8-9].
8. The FGM is slowly replaced by fibrous collagen molecules and vascularized in a process controlled, at least partially, by macrophages [8].

Table 2-2 Structure of Materials Used for Adhesion Prevention

Hyaluronic Acid (HA)	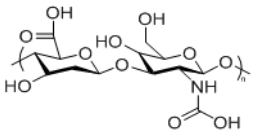
Carboxymethylcellulose (CMC)	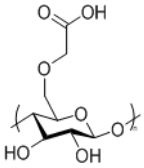
Phospholipid	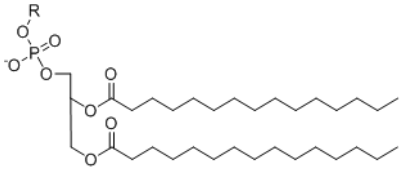
"Adept" Icodextrin	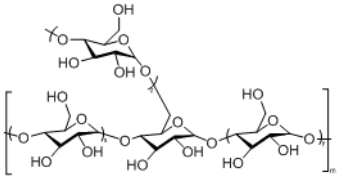
Polyethylene Glycol (PEG)	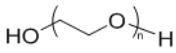
Poly (L-Lysine)	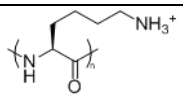
Poly (L-Glutamate)	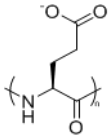
Polyethylene (PE)	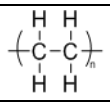
Poly (Tetrafluoroethylene) (PTFE)	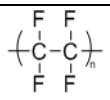
Cellulose	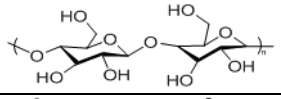
"SprayGel" System	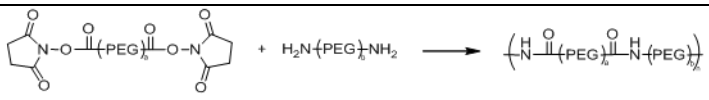

Table 2-3 Summary of Techniques used to Prevent Post Surgical Adhesions

	Technology	Application Method	Biodegradability	Level of Tunable Properties	Level of Success	References
Modification of Surgical Technique	**Non- Suturing of Damaged Peritoneum**	N/A	N/A	N/A	Significant decrease in PSA formation, but adoption of this practice by surgeons problematic	[1-2, 13, 24-26]
	Use of Laparoscopic Procedures	N/A	N/A	N/A	Significant decrease in PSA formation, but: • Application of technique is limited to certain surgeries • Precludes use of many other adhesion-reduction techniques	[34-36]
	Other Technique Changes (Non-powdered gloves, non-use of drainage tubes, increased tissue oxygenation)	N/A	N/A	N/A	Significant decrease in PSA formation, but adoption of this practice by surgeons is problematic	[1-2, 31, 33]
Pharmaceutical Interventions	**Anti-Inflammatories**	IP injection	Yes	Dose, timing, and selection of the therapeutic agent	Moderate success because of the associated risk of side effects	[37-38]
	Antioxidants	IP injection	Yes	Dose can be altered	Very successful. • Vitamin E interrupts several parts of the adhesion formation mechanism.	[45-46]
	Fibrinolytic Agents	IP Injection	Yes	Dose can be altered	Moderately successful but has potential for immunogenic response and reduced hemostasis	[9, 49-50, 52-54]
	Chymase Inhibitors	Oral Delivery	Yes	Dose and timing of the therapeutic agent can be altered	Moderately successful	[59]
Peritoneal Instillates	**Hyaluronic Acid and its Derivatives**	IP injection	Yes	MW and dose of HA can be optimized	Moderately successful	[64-71, 76-77]
	Phospholipids	IP injection	Yes	Dose can be optimized	Very effective. • The zwitterionic nature of the phospholipids allows them to bind onto the epithelial cell membranes and provide lubrication	[79-82]
	Hydroflotation Initiators (“Adept”)	IP Injection	Yes	MW and dose of the starch molecules can be optimized	Moderately successful	[83-89]
	Poly(ethylene glycol)	IP injection	Yes	MW and concentration of PEG solution can be optimized	Moderately successful: • Significant decrease in number and collagen content of PSAs	[4, 90-91]
Adhesion Barriers	**Polytetrafluoroethylene (“Gortex Surgical Membrane”, “Preclude”)**	Film placed directly on the damaged tissue	No	Physical properties of the mesh can be controlled	Moderately successful: • Non-degradable; it remains in site and must be removed with another surgical procedure • Requires suture fixation • Incompatible with laparoscopy	[95, 99-102]
	Oxidized Regenerated Cellulose (“Interceed”)	Film placed directly on the damaged tissue	Yes	MW, degree of oxidation, and the physical properties of the film can be controlled	Moderately successful: • Thrombogenic • Difficult to handle • Incompatible with laparoscopy	[48, 102, 107]
	Cross-Linked Hyaluronic Acid Gel (“Seprafilm”)	Film placed directly on the damaged tissue	Yes	MW and degree of the cross-linking can be optimized	Very successful: • Adheres to the peritoneum • Degrades • Is not procoagulant But causes: • Severe inflammation • Abscess formation • Must be placed directly on the damaged tissue	[102-104]
	***in vivo* Polymerization of Poly(ethylene glycol) (“Spray Gel”)**	*In vivo* spray polymerization	Yes	MW and degree of polymerization can be optimized	Very effective; can be employed with laparoscopic procedures	[105-106, 110]

Table 2-4 Animal Models used to Evaluate Post Surgical Adhesion Prevention Strategies

Tissue(s) Involved	Animal Model	Pros	Cons	References
Abdominal Wall	Mouse	Measure both extent and type of adhesion	Semiquantitative scoring	[33]
	Rat	Quantitative analysis of adhesion area		[93-94]
	Rabbit	Surgical damage carefully controlled	Semiquantitative scoring	[80-81]
Intestinal wall	Rat		Semiquantitative scoring	[111-112]
Intestine / Abdominal Wall	Rabbit	Surgical damage carefully controlled		[82]
	Rabbit		Semiquantitative scoring	[38, 69, 113, 179]
Uterus	Hamster		Semiquantitative scoring	[59]
	Pig	Internal control possible by treating two uterine horns separately	Semiquantitative scoring	[105]
	Rabbit	Internal control possible	Semiquantitative scoring	[31, 97]
	Rat	Internal control possible Quantitative area result		[46, 89, 100]
Uterus Reformation	Mouse	Multiple Adhesion	Semiquantitative scoring	[64]

Table 2-5 Scoring Methodology Employed to Evaluate Post Surgical Adhesion Prevention Strategies

Score	Extent of Adhesion	Severity	Degree
0	None	No adhesions	No adhesions
1	1-25%	Filmy, avascular	Adherent tissue separate with gentle traction
2	26-50%	Vascular and/or opaque	Tissue layer separation requires moderate traction
3	51-75%	Cohesive attachment	Tissue layer separation requires sharp dissection
4	76-100%		

CHAPTER 3. RESEARCH GOALS

3.1. Introduction

In this project, we have developed a series of targeted polymeric biomaterials and investigated their utility as a prophylactic treatment for the prevention of post surgical adhesions. In order to address this real-world problem, the integration of knowledge from numerous fields is required. The molecular design of the final polymer is based on the biological and biochemical environments of interest and the desired mechanical and biomaterial properties. Knowledge of organic chemistry and analytical chemistry facilitates the synthesis and characterization of these materials, and the framework of chemical engineering integrates these varied fields and provides the basis for functional evaluation and enhanced understanding.

By applying a fundamental understanding of the biochemistry, physiology, and pathology of adhesion formation, the materials were specifically designed to meet this clinical need. Using well controlled polymerization chemistry and subsequent functionalization, several structural properties were varied and the affect of this structure was evaluated in numerous *in vitro* models. Finally, the results of these investigations were employed to select a combination of materials to be evaluated *in vivo* in a rabbit model. This methodical, ground up approach, provides unique insight into the relationship between the molecular structure of these materials and their performance as adhesion barriers and increases the likelihood for the development of a viable method to address this clinical need. This approach to biomaterial development and its initial success

should lead to significant additional research into the use of self-assembled systems for PSA prevention and in other applications, including tissue adhesives and oral barriers.

3.2. Objectives and Significance

The following general hypothesis was proposed to direct this research:

Polymeric materials can be designed to assemble in situ by targeting biomarkers of tissue damage and provide protection from the formation of post surgical adhesions.

In order to investigate this hypothesis, the project was conducted in three distinct stages, described below as specific aims, each of which was carried out to test a specific hypothesis.

3.2.1. Specific Aim 1: Design, synthesis, and characterization of polymers to be used for the in situ formation of adhesion barrier.

In order to develop a new material for use as a prophylactic treatment to prevent PSA formation, three stages of synthesis and characterization were addressed:

1. Synthesis of block copolymers incorporating poly(methacrylic acid), reactive methacrylate monomers, and poly(ethylene glycol) functionality with highly-controlled molecular weight and polydispersity.
2. Functionalization of polymers for the addition of cross-linkers and fibrin-specific peptides.

3. Implementation of polymer characterization methods using available tools, including proton nuclear magnetic resonance spectroscopy (^{1}H-NMR), gel permeation chromatography (GPC), and high performance liquid chromatography (HPLC).

3.2.1.1. Hypothesis #1

Group transfer polymerization can synthesize a variety of methacrylic acid based polymers with multiple functionalities and precisely controlled molecular architecture for in vitro evaluation.

3.2.1.2. Significance and Outcomes

Efforts to test this hypothesis are described in **Chapter 4**. As described in this section, we have fully implemented the methodology to perform group transfer polymerization (GTP) in our laboratory. The ability to polymerize various monomers has been established, as has a selective deprotection strategy, allowing multiple functionalities to be added sequentially. Methods to characterize these materials using ^{1}H-NMR, GPC, and HPLC have been realized. We have synthesized diblock copolymers containing functionalized methacrylic acid units with targeting moieties and pendant polyethylene glycol chains. These polymers exhibit precise control of both the molecular weight and polydispersity of individual polymer blocks.

3.2.2. Specific Aim 2: Investigation of non-targeted statistical and block copolymers interactions with model surfaces.

The second phase of this research focused on the evaluation of non-targeted polymeric biomaterials using a variety of *in vitro* test methods. This stage can be divided into three sub-stages:

1. Investigation of the kinetics, thermodynamics, and conformation of non-targeted polymer adsorption to model surfaces.
2. Evaluation of polymeric biomaterials to block non-specific protein adsorption.
3. Reduction of cellular attachment by non-targeted block and statistical copolymers on positively charged self-assembled monolayer surfaces.

3.2.2.1. Hypothesis #2

Non-targeted block copolymers with high charge density will interact more readily with charged model substrates as compared to statistical copolymers. The kinetics and thermodynamics of these interactions and the structure of the resulting surface layer can be characterized by quartz crystal microgravimetry and cellular attachment assays.

3.2.2.2. Significance and Outcomes

The quartz crystal microbalance was proven to be an effective, efficient method to probe the interaction of the polymers of interest with positively charged model surfaces. By fitting a simple adsorption model to the observed adsorption phenomena, it was

possible to quantify the kinetics and equilibrium surface coverage of these materials. This work, described in **Chapter 5**, supported the hypothesis that non-specific protein adsorption can be modulated by varying the structure of the polymer. Finally, depending on the particular molecular architecture employed, these materials also proved effective at reducing the level of cellular attachment to surfaces.

3.2.3. Specific Aim #3: *In vitro* evaluation of targeted copolymers to reduce events leading to fibrin gel propagation and assessment of targeting specificity.

The final aspect of this research project focused on the investigation of targeting in order to enhance the ability of block copolymers to function as desired. This work was carried out in two phases:

1. Investigation of targeted block copolymers to modulate aspects of fibrin gel matrix propagation, including fibrinogen adsorption, fibrin gel propagation, and cellular attachment.
2. Evaluation of interactions of targeting peptides and targeted polymers with fibrin and fibrinogen.

3.2.3.1. Hypothesis #3

Using targeting peptides, block copolymers can be tailored to bind effectively to markers of damaged tissue. Binding to fibrin, these PEG containing polymers will render the growing fibrin gel matrix less susceptible to subsequent fibrinogen deposition and cellular attachment, thereby attenuating propagation of the FGM.

3.2.3.2. Significance and Outcomes

The investigation of hypothesis #3 represents the culmination of the work carried out in the previous investigations. As described in **Chapter 6**, the incorporation of targeting peptides and the careful control of molecular architecture can be used to moderate the propagation of the fibrin gel matrix. The polymers interact strongly with fibrin surfaces and reduce the rate and degree of subsequent fibrinogen deposition. In addition, they provide protection against cellular attachment on model fibrin surfaces.

The investigations described in **Chapter 7** confirm the ability of these targeted materials to interact with fibrin(ogen). Although the effect was less pronounced than anticipated, the molecular architecture of the polymer affects the structure of the fibrin fibrils in the growing fibrin gel matrix. Finally, the targeting peptides, as well as the scramble peptide used as a control, both interact strongly with solution phase fibrinogen and result in a large conformational change in the protein.

CHAPTER 4. POLYMER SYNTHESIS AND CHARACTERIZATION

4.1. Introduction

In order to test the hypothesis that polymeric materials can be employed to assemble *in situ* and provide protection from the formation of post surgical adhesions, we first set out to design the appropriate materials to test. By designing this material from the ground up, we were able to select and tune the biocompatibility of the materials, include desired functionality, and tailor the architecture of the molecules. Employing group transfer polymerization allowed the synthesis of block copolymers containing various functionalities and provided precise control over the molecular weight of the various blocks. To minimize the potential for adverse biological interactions, the selection of materials was limited to those that have previously been shown to exhibit biocompatibility. Specifically, non-toxic and non-immunogenic materials were required. In addition, the potential to incorporate multiple functional groups and to control the molecular weight of the polymerization were desired. Finally, materials were selected that were expected to provide excellent barrier properties and prevent the adsorption of proteins.

Methacrylic acid was selected as the monomer for the polymer backbone for several reasons. First, methacrylate polymers have been employed and have shown excellent biocompatibility in many applications [180-183]. While some studies have employed polyacrylic acid as an adjuvant to heighten the body's immune response to vaccination formulations, the nature of this reaction is believed to stem from the high molecular weight and the large concentration of acidic units employed [184-185]. While

we anticipate that these effects can be modulated by controlling the polymer architecture, they will be investigated in future studies. Finally, methacrylic acid can be readily functionalized with a variety of functional groups, many of which are commercially available or can easily be prepared in the laboratory.

In order to provide resistance to the adsorption of proteins and interrupt subsequent adhesion formation, polyethylene glycol (PEG) was chosen. This polymer has been used in a variety of biomaterials applications in order to provide protection from protein adsorption and from immunological response *in vivo* [118, 134]. Because of its highly hydrophilic nature, water associates strongly with PEG in aqueous environments and the polymer typically exists in a gel state. This structure resembles the extracellular matrix and provides high steric protection in the body [90-91]. Numerous examples can be found employing PEG to create "stealth" drug delivery systems with long circulation times [134, 186-188]. To incorporate PEG into our polymer system, commercially available methoxy polyethylene glycol methacrylate with a PEG chain length of approximately 25 PEG repeat units ($MPEGMA_{1100,}$ Aldrich) was selected for use.

The target molecular weight for polymer synthesis was chosen to meet a variety of requirements. First, it has previously been demonstrated that the maximum reduction in protein adsorption is observed with PEG chains with a molecular weight of 5,000 g/mol [189]. The maximum molecular weight of the polymer was set at 50,000 g/mol to ensure rapid renal clearance of any material entering the bloodstream [134]. The initial polymer synthesized for use in this investigation incorporated a block of t-butyl methacrylate (TBMA) and a block of $MPEGMA_{1100}$; the target molecular weights of these units were each set at 5,000 g/mol.

In order to assess the relationship between polymer structure and function, and to ensure repeatability between synthetic batches, it was necessary to employ a highly controlled polymer synthesis. Group Transfer Polymerization (GTP), shown schematically in **Figure 4-1**, was utilized to synthesize the backbone polymers used in these studies. This technique allows the synthesis of polymers with controlled molecular weight and polydispersity. In addition, statistical and block copolymers can readily be created by reacting multiple monomer units with either simultaneous or sequential monomer addition.

4.2. Materials and Methods

4.2.1. Synthesis and Characterization of Protected Backbone Polymers

Using modifications of previously published reaction schemes, the synthesis was carried out as shown in **Figure 4-2** [190-194]. Solvent was prepared by drying 450 ml THF (Mallinckrodt) over a mixture of sodium (4 g, Aldrich) and benzophenone (8 g, Aldrich) until the purple color characteristic of the dianion was observed. The proton scavenger bis(dimethylamino) methylsilane (ABCR, Gelest) was distilled under vacuum and stored in a freezer under argon prior to use. TBMA (Aldrich) and (M_N = 300, $MPEGMA_{300}$, Aldrich), was passed through an inhibitor removal column, distilled, mixed with ABCR (2 wt%), and stored in a freezer under argon prior to use. $MPEGMA_{1100}$ was dissolved in inhibitor free THF (Aldrich), passed through an inhibitor removal column, and dried under vacuum overnight. This macromer was dissolved in dry, air-free THF to a concentration of 0.4 g/mL, mixed with 2% ABCR, and stored under argon in freezer prior to use. 1-methoxy-1-(trimethylsiloxy)-2-methyl-1-propene (MTS, Gelest), was

vacuum distilled and stored under argon in freezer prior to use. The catalyst, tetrabutyyammonium bibenzoate (TBABB) was prepared as has previously been described and stored under nitrogen prior to use [195]. Prior to polymerization, all glassware was dried overnight at 180 ^{o}C, assembled hot, and flamed under vacuum to remove residual water.

Approximately 10 mg TBABB was added to the reaction flask under inert atmosphere. Approximately 15 mL of dry, air free THF was added to the flask by solvent transfer. The initiator, (MTS, 93.3 mg, 0.53 mmol) was added via syringe under argon and allowed to stir for 15 minutes at room temperature. To form a block copolymer, 1.97 g TBMA (13.9 mmol) was added to the reaction vessel via syringe under argon. No apparent exotherm was observed. The reaction was allowed to proceed under argon for 30 minutes, at which time approximately 5 mL was removed for analysis and quenched with methanol. A solution of the second monomer, $MPEGMA_{1100}$, (5 mL, 1.8 mmol) was then added to the reaction vessel and allowed to react for 90 minutes. The reaction was quenched with methanol, the solvent was removed with vacuum, and the product was dried for 48 hours under vacuum. Based on the stoichiometry, the molecular weights for the TBMA block and the $MPEGMA_{1100}$ block were predicted as 3,700 and 5,900 g/mol, respectively, and the ratio of TBMA blocks to $MPEGMA_{1100}$ was predicted to be 5.1:1.

Block copolymers of $MPEGMA_{300}$ and TMBA were prepared similarly. Additionally, statistical copolymers were synthesized using the same technique, with simultaneous addition of the two monomers. Finally, a homopolymer of TBMA was prepared using the same technique. The resulting polymers were dissolved in deionized

water and purified by triplicate ultrafiltrations with Ultracel Amicon YM membranes with appropriate molecular weight cutoffs and isolated by lypholization.

4.2.2. Deprotection of tert-Butylmethacrylic Acid Group

A modification of a previously described procedure was used to convert the TBMA groups to methacrylic acid groups [194]. As shown in **Figure 4-2**, hydrolysis was carried out by refluxing in 1,4-dioxane (Aldrich) with p-toluenesulfonic acid (PTSA, Aldrich) for 20 – 96 hours. The resulting polymers were purified by triplicate ultrafiltration and isolated by lypholization.

The polymers were characterized by gel permeation chromatography (GPC) and by proton nuclear magnetic resonance spectroscopy (^{1}H-NMR). GPC was carried out using a Shimadzu Prominence High Performance Liquid Chromatography system equipped with a Waters Refractive Index Detector (RID). All analyses were conducted in THF using Waters HR1 and HR2 columns in series with an Agilent PLGel Mixed B column, a flow rate of 1.0 mL/min, and referenced to narrow molecular weight polystyrene standards (Polymer Laboratories). The molecular weight distribution of the polymers was determined using the Shimadzu LabSolutions software.

Proton NMR analysis was conducted by dissolving the polymer in deuterated chloroform (Cambridge Isotopes) and measuring the resonance with a Varian Gemini 200 MHz NMR spectrometer. Mestralab Research's MNova software was employed to analyze the NMR spectra.

4.2.3. Polymer Conjugation with N-Aminoethylmaleimide Crosslinker

Peptide functionalization of polymers was achieved through sulfhydryl directed maleimide chemistry. Maleimide was introduced into the structure of the fully deprotected polymers by the coupling of N-aminoethylmaleimide trifluoroacetic acid (NAEM, Aldrich) [196-197]. This moiety was covalently attached to the polymer via a stable amide linkage, leaving the maleimide group available for subsequent peptide conjugation.

As shown in **Figure 4-3**, the primary amine group of the crosslinker was conjugated to the free acid groups in the polymer chain to form amide bonds using well known diimide chemistry [198-199]. Two equivalents of NAEM, based on the number of free acid groups present, were combined with the polymer (1 equivalent of acid groups) and 1.1 equivalent of N,N'-dicyclohexylcarbodiimide (DCC, Aldrich) and dissolved in acetonitrile (ACN, Fisher). This reaction mixture was stirred at room temperature in the dark for 2 hours. Successful conjugation was indicated by the precipitation of insoluble N,N'-dicyclohexylurea (DCU) precipitate that began to form after approximately 5 minutes of reaction. After reacting for 2 hours, the excess DCC was quenched by adding excess acetic acid (HAc, Fisher) and stirring for 10 minutes. The DCU was then removed by centrifugation, leaving a clear yellow solution.

Excess NAEM was removed from the reaction mixture by repeated aqueous extraction from diethyl ether. Upon dissolution in ether, the reaction mixture formed a cloudy liquid, indicating the insolubility of NAEM in the solvent. The clear ether layer that remained after extraction was evaporated. The white solid product was dissolved in acetone, and the solvent was removed by evaporation. HPLC analysis was conducted on

the Shimadzu Prominence HPLC system to confirm the purity of this product. This analysis was carried out with a Restek Viva C18 5 µm 4.6 x 150 mm HPLC column at a controlled temperature of 40 ^{o}C with an isocratic mobile phase consisting of 90% DI water with 0.1% trifluoroacetic acid (TFA, Aldrich) and 10% methanol (Fisher). This material was stored at -20 ^{o}C for subsequent peptide conjugation.

4.2.4. Conjugation of Peptides to Polymer

Two five unit oligopeptides were incorporated in the crosslinker-conjugated polymers via the specific reaction between the sulfhydryl group on cysteine and the maleimide group on the crosslinker. Both peptide chains included the amino acids alanine (A), arginine (R), cysteine (C), glutamic acid (E), and lysine (K). The first peptide employed, CREKA, was employed to target the polymers to fibrin, while the second peptide, CAERK, was used as a control. Both of these materials were produced specifically for this study by Celtek Biosciences.

The peptide conjugation reaction was carried out at room temperature in a solution containing 50% ACN and 50% PBS as shown in **Figure 4-4**. The NAEM-conjugated polymer was dissolved in this solution, and the desired amount of peptide (3-9 peptides per polymer chain) was added to the solution. This reaction mixture was stirred at room temperature in the dark for five hours. Excess cysteine was added to consume unreacted maleimide groups, and the reaction was allowed to proceed for one hour. After removing the solvent *in vacuo*, approximately 3 mL of acetone was added. Insoluble salts were removed by centrifugation, and the product was isolated by evaporating the solvent with a stream of dry nitrogen.

4.2.5. Purification of Polymer-Peptide Conjugates

HPLC analysis was conducted to assess the purity of the reaction mixtures. As shown in **Figure 4-5**, the reaction mixture contained several products. In order to achieve a pure product for analysis, preparative HPLC was employed to isolate the desired peptide conjugate from the reaction mixture. The Shimadzu Prominence HPLC system was used, with a Shimadzu Viva C18 21.2 x 150 mm column. The isocratic mobile phase consisted of 90% DI water with 0.1% trifluoroacetic acid (TFA, Aldrich) and 10% methanol (Fisher). The polymer conjugate, which eluted around 7 – 10 minutes, was isolated by collecting appropriate fractions, and the solvent was removed *in vacuo*. The purity and identity of the products was confirmed by subsequent HPLC and ^{1}H-NMR analysis.

4.3. Results and Discussion

4.3.1. Polymer Synthesis and Characterization

In order to synthesize the backbone polymers for this study with the desired level of control over the molecular architecture, it was necessary to employ group transfer polymerization. Attempts to use anionic polymerization proved to be ineffective due to the low temperature required. Although the TBMA monomer is readily soluble in THF at -78 ^{o}C, the MPEGMA monomer was insoluble at this temperature. Group transfer polymerization (GTP) overcomes this limitation, as it can be conducted at ambient temperature. While it allows the desired control over the molecular architecture, the use of GTP introduces additional complications into the synthetic scheme. Because GTP is highly susceptible to proton quenching, it is necessary to employ aprotic monomers and

anhydrous reaction conditions. Since it was desired to synthesize polymers with acidic functional groups, synthesis of the polymer backbone was carried out with protected monomers using standard Schlenk techniques to maintain inert reaction conditions. The desired functionality was then introduced into the polymer by deprotection and subsequent conjugation reactions.

A representative the gel permeation chromatogram of the protected polymer is shown in **Figure 4-6**. As shown in **Table 4-1** and **Table 4-2**, the polymers were synthesized with low polydispersity and had molecular weights that were in close agreement with the molecular weights predicted from stoichiometry. Each polymer was analyzed by ^{1}H-NMR in deuterated chloroform to confirm the structure and determine the relative number of PEGMA units to TBMA units. The resulting NMR, shown in **Figure 4-7**, confirms the successful synthesis and purification of the desired polymer. The large peak at • = 3.61 ppm corresponds to the ethyl ether peaks of the PEG chain, while the peak at • = 3.36 ppm represents the three protons on the methyl ether terminus of the PEG chain. The peak at • = 1.40 ppm arises from the t-butyl ether group on the TMBA unit, while the broad peaks at • • 1.1 ppm and • • 1.8 ppm result from the methyl and methylene groups in the polymer backbone. The absence of peaks in the range from 5.5 – 6.5 ppm indicates that no unreacted monomer remains after purification. By comparing the areas of t-butyl ether peak to the area of the methoxy peak, it is possible to determine the ratio of TBMA groups to PEGMA groups in the polymer. Combining this result with the molecular weight data obtained from the GPC, the number of TBMA and PEGMA monomers in each polymer was determined. These results, also summarized in **Table 4-1** and **Table 4-2**, agree well with the predictions based on stoichiometry.

Since the deprotection of the TBMA group results in the formation of methacrylic acid groups along the polymer chain, GPC of this product using the previously described method was not practical. Instead, the degree of TBMA deprotection in the polymer was determined by monitoring the ratio of TBMA to PEGMA using ^{1}H-NMR analysis. **Figure 4-7** shows the resulting spectrum for this deprotection. The decrease in this ratio indicates 80% deprotection of the polymer in this instance. The increase in hydrophilicity of the polymer is also indicated by the presence of residual water at • = 1.5 ppm. As the hydrolysis reaction proceeded from 20 to 96 hours, the extent of hydrolysis increased from 20% to 100%. Analysis of the reaction mixture confirmed that no cleavage of the PEG ester bond occurred during deprotection. Using these results, along with the previously determined molecular weight of the protected polymer, the molecular weight of the deprotected polymer was calculated.

4.3.2. Polymer Conjugation with N-Aminoethylmaleimide Crosslinker

The success of the NAEM conjugation and purification procedure was confirmed by ^{1}H-NMR and by HPLC. As shown in **Figure 4-8**, HPLC analysis confirmed that this purification procedure results in a pure polymer conjugate. The combination of the unconjugated polymer (r.t. = 5.0 min) and the NAEM (r.t. = 2.4 min) resulted in the formation of a new peak (r.t. = 7.7 min). Aqueous extraction from ether resulted in quantitative separation of the excess NAEM (water layer) from the product (ether layer). NMR analysis confirmed the incorporation of the crosslinker into the polymer structure. As shown in **Figure 4-9**, the PEG peak (• = 3.57 ppm) and the polymer backbone peaks (• • 1.2) remain intact. In addition, the • -amide is indicated by the peaks at • = 1.71 and • = 3.75, and the integrity of the reactive maleimide bond (• = 6.75 ppm) is confirmed.

4.3.3. Conjugation of Peptides to Polymer

The peptide-polymer conjugates were successfully purified using preparatory HPLC, as confirmed by analytical HPLC and ^{1}H-NMR analysis. HPLC analysis of the reaction mixture, shown in , the reaction mixture contained numerous products. By collecting the fraction of the preparative HPLC eluent from 7 – 10 min, the purified product was isolated and showed a single analytical HPLC peak (r.t. = 3.9 min). Proton NMR analysis of this product confirmed the successful incorporation of the peptide into the structure. As shown in **Figure 4-9**, the disappearance of the maleimide peak (• = 6.75 ppm) confirms the complete reaction of the crosslinker. Multiple NMR peaks (• = 1.20 – 1.5 ppm and 2.9 ppm) indicates the presence of the peptide in the polymer structure.

Quantitative analysis of the peptide incorporation into the structure was frustrated by the complex NMR spectrum and by the difficulty in making unambiguous peak assignment. Fortunately, by monitoring the progress of the peptide conjugation with HPLC, it is possible to confirm that the peptide is quantitatively incorporated into the polymer structure. **Figure 4-10** shows HPLC chromatograms for the starting materials (CREKA and P1-N) employed for this reaction. As seen in the two chromatograms collected from the reaction at later time points, it is evident that the starting materials are both consumed, and that there is only one product peak. As a result of this rapid, quantitative reaction between the sulfhydryl group on the peptide and the maleimide group on the polymer, it is possible to determine the composition of the resulting polymer based on the stoichiometry of the reactants. The materials employed in the untargeted analysis and targeting studies are summarized in **Table 4-1** and **Table 4-2**, respectively

4.4. Conclusion

The ability to synthesize and characterize functionalized diblock and statistical copolymers for investigation as post-surgical prevention barriers has successfully been demonstrated. The robust synthetic methodology that has been developed allows the rapid synthesis of block and statistical copolymers of methacrylic acid and PEGMA. These materials can be functionalized with targeting peptides. In order to ensure that subsequent tests to ascertain the impact of changes in the molecular structure on material performance, it is important to note that these materials can readily be isolated as pure materials by preparatory HPLC. Using these techniques, we have prepared several materials and initial analysis confirms the strong dependence of function on molecular architecture. These techniques provide readily accessible methods that are capable of avoiding many of the technical challenges that plague functional polymer synthesis.

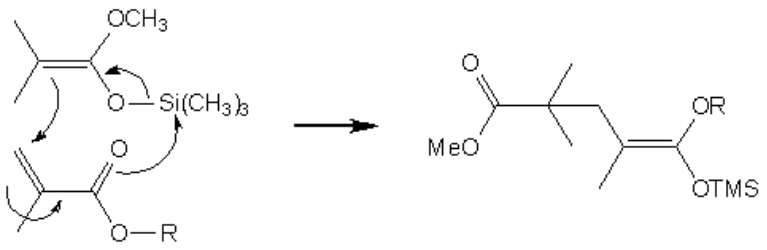

Figure 4-1 Concerted mechanism for group transfer polymerization.
The initiator, 1-methoxy-1-(trimethylsiloxy)-2-methyl-1-propene (MTS) reacts with the protected methacrylic acid group. The trimethylsilyl (TMS) group is transferred from the initiator to the end of the polymer chain. This "living" end propagates the polymerization until the reaction is terminated [200].

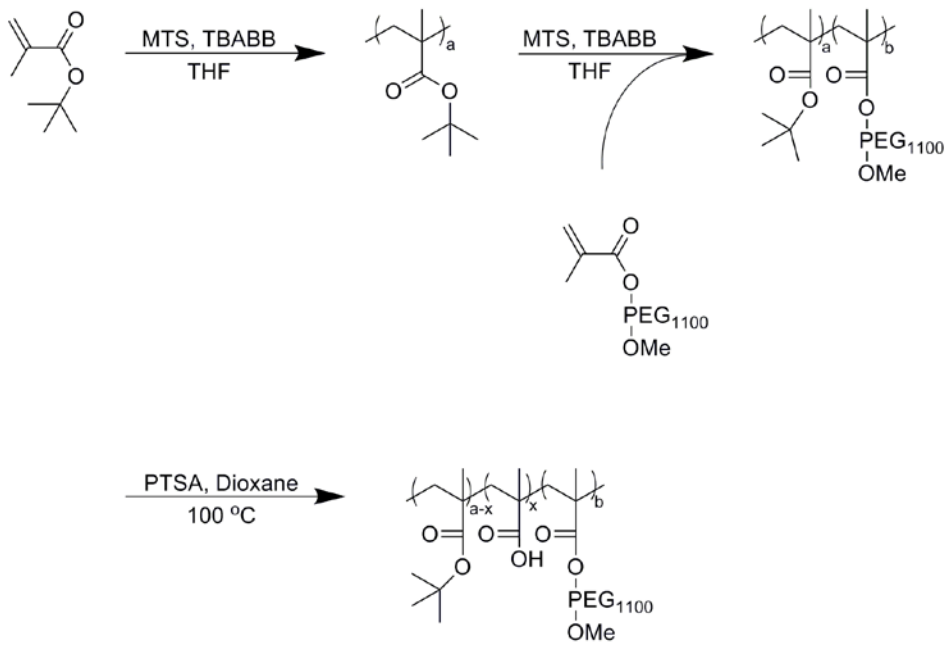

Figure 4-2 Reaction scheme for the synthesis of poly $PEGMA_{1100}$-block-(TBMA-co-MA) by group transfer polymerization.
In the presence of the initiator (MTS) and catalyst (tert-butylammonium bibenzoate, TBABB), tert-butyl methacrylate (TBMA) monomer polymerizes via group transfer polymerization. Subsequent addition of poly(ethylene glycol) methacrylic acid (PEGMA) facilitates block copolymer formation. The MA units are then deprotected by hydrolysis of the t-butyl group in refluxing 1,4-dioxane with p-toluenesulfonic acid (PTSA).

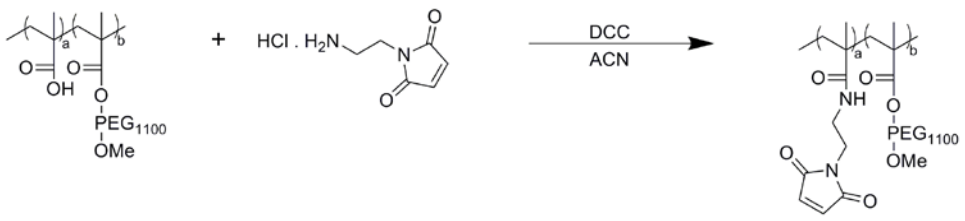

Figure 4-3 Reaction scheme for the conjugation of N-aminoethylmaleimide (NAEM) to deprotected polymer.
Functionalization of copolymer with the crosslinker (NAEM) is conducted in the presence of dicyclohexylcarbodiimide (DCC) in acetonitrile (ACN).

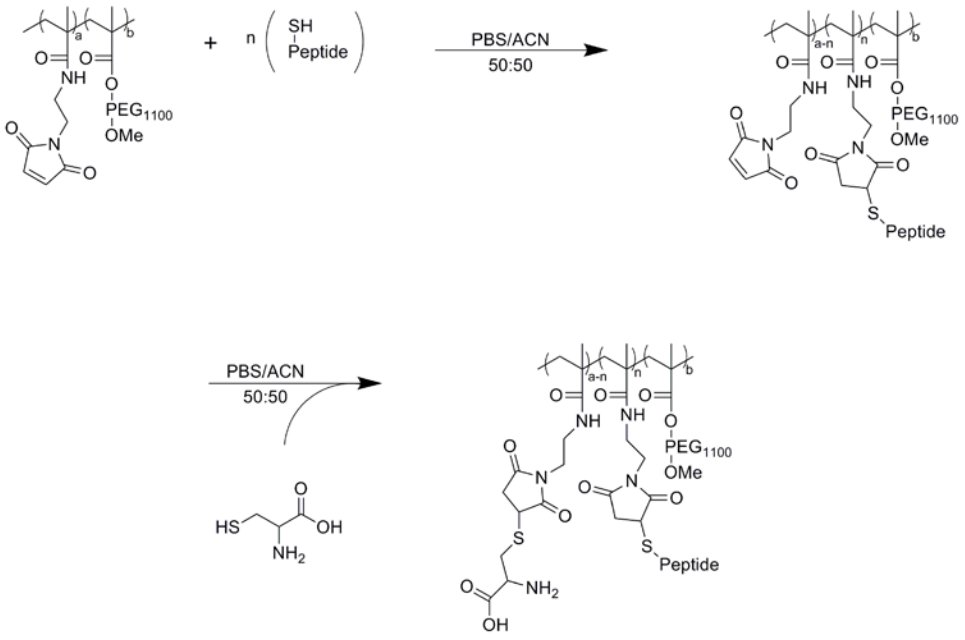

Figure 4-4 Reaction scheme for the conjugation of peptide to NAEM functionalized polymer.
When the crosslinker functionalized polymer is mixed with peptide, the sulfhydryl group on the peptide unit reacts specifically with the maleimide group on the crosslinker in a 50/50 mixture ANC and PBS at pH = 7.4. Unreacted NAEM groups are then quenched by reaction with cysteine groups to prevent subsequent reaction.

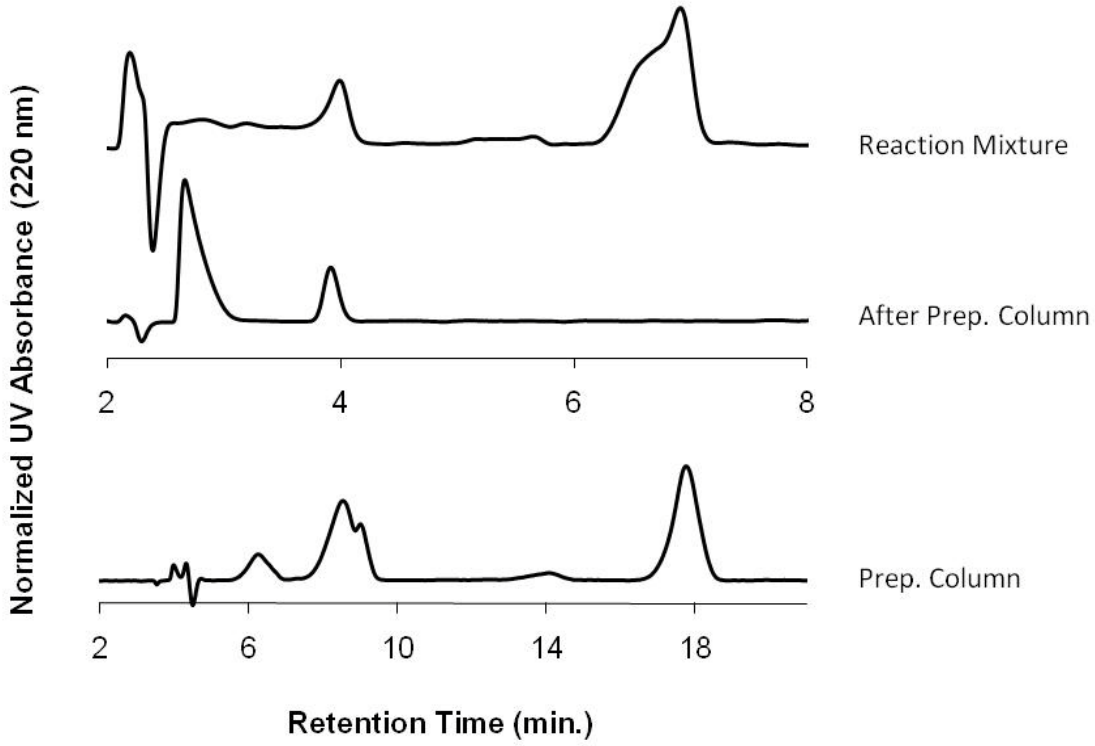

Figure 4-5 HPLC analysis and purification of peptide conjugate.
The HPLC chromatogram for the unpurified reaction mixture (top) indicates a mixture of products and unreacted starting materials. Preparatory HPLC (bottom) was conducted to isolate the desired product (r.t. = 7 – 10 min.). The purified material (middle) shown a single peak for the desired product (r.t. = 3.9 min). The peak at 2.7 min. corresponds to acetone, used as the injection solvent in this analysis.

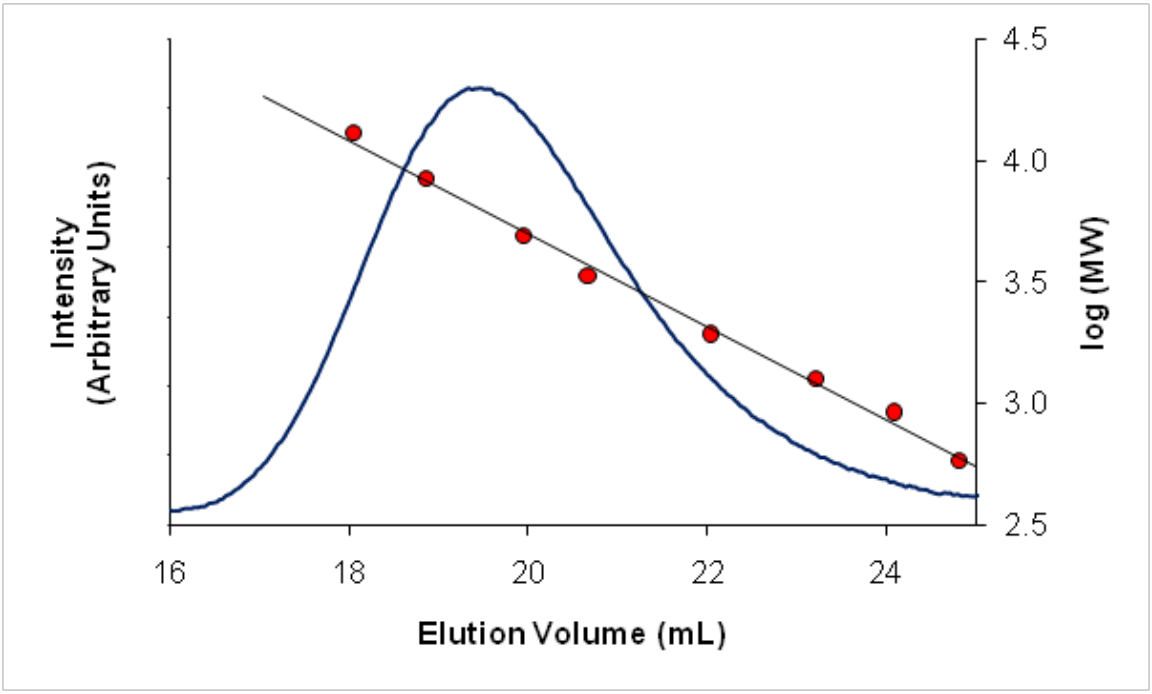

Figure 4-6 Sample GPC chromatogram for P2-Pro.
GPC was conducted and described and referenced to narrow molecular weight distribution polystyrene standards. Triplicate analyses of this material indicate that M_N = 3,120 ± 150 g/mol (M ± SD), M_W = 5,020 ± 280 g/mol, PD = 1.61 ± 0.04.

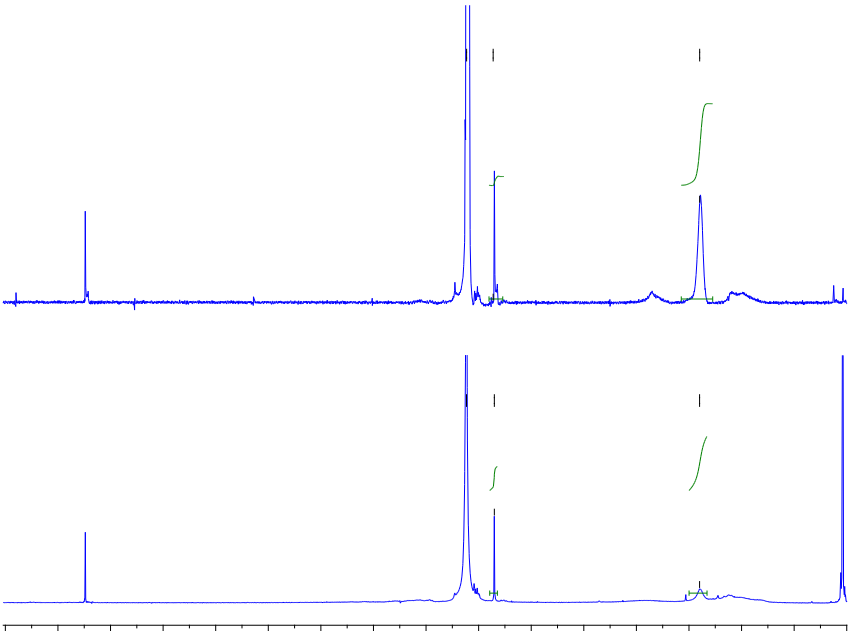

Figure 4-7 ^{1}H-NMR analysis of polymeric product.
Prior to hydrolysis (top), TBMA:PEGMA$_{1100}$= 3.1 based on peaks at δ = 1.4 (t-butyl group) and δ = 3.35 (methyl ether), respectively. Hydrolysis was determined by evaluating the change in peak ratio. The relative change in TBMA intensity (bottom) indicates 80% hydrolysis was achieved. The peak at δ = 1.55 indicates residual water bound to the hydrophilic polymer.

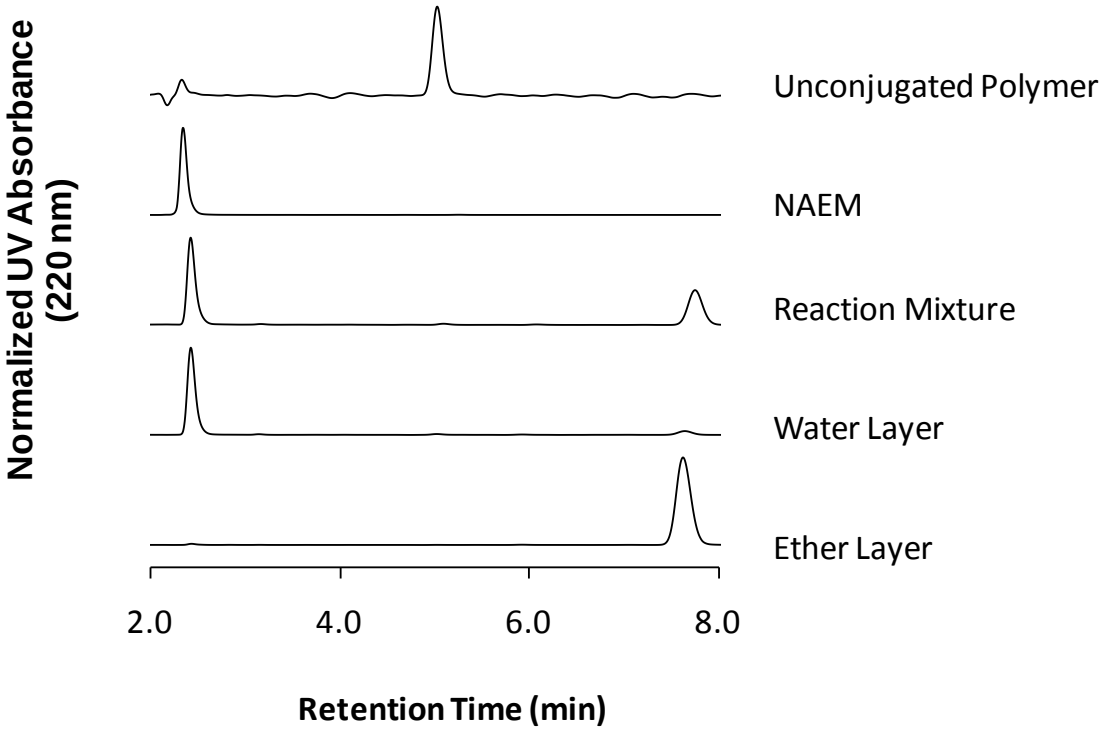

Figure 4-8 N-Aminoethyl Polymer Conjugate Purification.
Conjugation of polymer (r.t. = 5.0 min.) with an excess amount of NAEM (r.t. = 2.4 min) yields a new peak in the chromatogram (r.t. = 7.7 min). Multiple ether/water extractions of the excess NAEM from this reaction mixture results in pure NAEM conjugate in the ether layer.

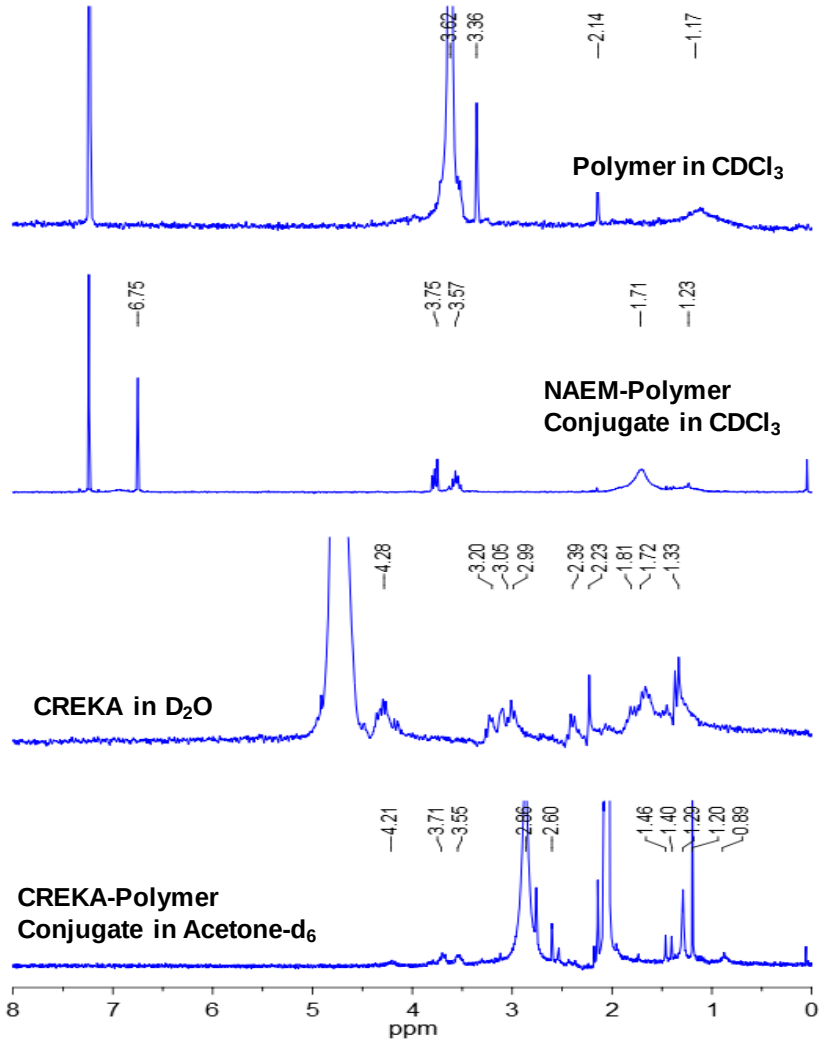

Figure 4-9 [1]H-NMR analysis of unconjugated polymer, NAEM conjugate, and peptide product.

The unconjugated polymer (P1) indicates the presence of methyl and methylene and groups from the methacrylic acid units (broad peak at • = 1.2 ppm). In addition, the ethylene glycol and terminal methoxy peaks are clearly evident at • = 3.5 ppm and • = 3.4 ppm, respectively. Upon conjugation with NAEM, the peaks from the aminoethyl group (• = 1.7 ppm) and the maleimide group (• = 6.75 ppm) appear. Upon addition of the peptide (CREKA) and cysteine, several peaks corresponding to the pentapeptide (• = 1.0 – 1.5 ppm, • = 2.9 ppm) are evident. In addition, the disappearance of the maleimide confirms the reaction with sulfhydryl groups.

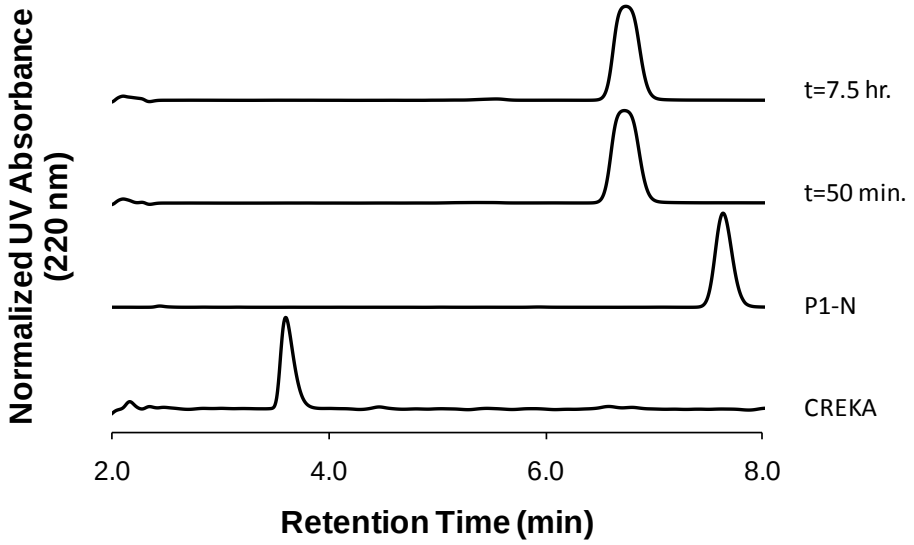

Figure 4-10 HPLC chromatograms of quantitative conjugation reaction between CREKA and NAEM conjugate.
When NAEM functionalized polymer is reacted with peptide (CREKA, r.t. = 3.7 min), a new peak is formed (r.t. = 6.7 min). The peptide is consumed, and only one product peak is observed. This product peak forms within the first hour of reaction and remains unchanged thereafter. These observations indicate the quantitative incorporation of the peptide unit into the polymer.

Table 4-1 Summary of Block and Statistical Copolymers used for Analysis of Untargeted Polymers

Polymer	Polymer Type	TBMA / PEGMA	Degree of Deprotection (NMR)	$M_{N, CAL}$	$M_{N, GPC}$[a]	PD_{GPC}[a]
NP	No Polymer	N/A	-	-	-	-
EPC	Phospholipid (Egg Phosphatidylcholine)	N/A	-	760*	-	-
PAA	Homopolymer	N/A	-	-	-	< 2*
PTBMA	Homopolymer	N/A	0%	4,240	3,960	1.28 (0.01)
PMAA	Homopolymer	N/A	100%	2,570	2,400	1.28
0% B	Block Copolymer	3.1:1	0%	9,320	13,200 (384)	1.13 (0.01)
PTBMA-40	Homopolymer	N/A	40%	3,640	3,380	1.28
50% B	Block Copolymer	3.1:1	50%	8,620	12,500	1.20 (0.04)
80% B	Block Copolymer	3.1:1	80%	8,250	11,700	1.29 (0.01)
0% S	Statistical Copolymer	2.7:1	0%	7,090	11,000 (442)	1.27 (0.05)
80% S	Statistical Copolymer	2.7:1	80%	6,240	10,200	1.28 (0.01)

* Vendor data

Table 4-2 Polymers used for Evaluation of Targeted Polymer Analysis

Polymer Name	Functional Group	Number of Functional Groups	Chain Length	Number of MA Units	Number of PEG Units	MA/PEG Ratio	PEG Chain Length	Molecular Weight
P1-Pro	-	-	18.4	15.9	2.5	6.5	1,100	5,200
P1	-	-	18.4	15.9	2.5	6.5	1,100	4,300
P1-N	NAEM	-	18.4	15.9	2.5	6.5	1,100	6,200
P1-L	CREKA	2.3	18.4	15.9	2.5	6.5	1,100	9,300
P1-H	CREKA	6.7	18.4	15.9	2.5	6.5	1,100	14,400
P1-S	CAERK	2.4	18.4	15.9	2.5	6.5	1,100	9,300
P2-Pro	-	-	18.2	16.0	2.2	7.3	300	3,100
P2	-	-	18.2	16.0	2.2	7.3	300	2,200
P2-N	NAEM	-	18.2	16.0	2.2	7.3	300	4,200
P2-L	CREKA	2.4	18.2	16.0	2.2	7.3	300	7,300
P2-H	CREKA	7.4	18.2	16.0	2.2	7.3	300	12,800
P2-S	CAERK	2.4	18.2	16.0	2.2	7.3	300	7,300
P3-Pro	-	-	30.9	26.7	4.2	6.4	1,100	8,700
P3	-	-	30.9	26.7	4.2	6.4	1,100	7,300
P3-N	NAEM	-	30.9	26.7	4.2	6.4	1,100	10,500
P3-L1	CREKA	2.2	30.9	26.7	4.2	6.4	1,100	14,800
P3-H	CREKA	6.2	30.9	26.7	4.2	6.4	1,100	21,000
P3-S	CAERK	2.2	30.9	26.7	4.2	6.4	1,100	14,800
P4-Pro	-	-	22.1	17.5	4.6	3.8	300	4,300
P4	-	-	22.1	17.5	4.6	3.8	300	3,300
P4-N	NAEM	-	22.1	17.5	4.6	3.8	300	5,400
P4-L	CREKA	2.3	22.1	17.5	4.6	3.8	300	8,700
P4-H	CREKA	7.1	22.1	17.5	4.6	3.8	300	14,200
P4-S	CAERK	2.3	22.1	17.5	4.6	3.8	300	8,600
PMAA-Pro	-	-	18.3	18.3	0.0	N/A	N/A	2,600
PMAA	-	-	18.3	18.3	0.0	N/A	N/A	1,600
PMAA-N	NAEM	-	18.3	18.3	0.0	N/A	N/A	3,800
PMAA-L	CREKA	1.9	18.3	18.3	0.0	N/A	N/A	5,800
PMAA-H	CREKA	5.8	18.3	18.3	0.0	N/A	N/A	10,800
PMAA-S	CAERK	2.0	18.3	18.3	0.0	N/A	N/A	7,800

CHAPTER 5. BLOCKADE OF NON-SPECIFIC PROTEIN ADSORPTION AND CELLULAR ATTACHMENT WITH UNTARGETED POLYMERIC BIOMATERIALS

Based on studies published in:

> John M Medley, Eric J Beane, S K C Sundararaj, Eugene Kaplan, David A Puleo, Thomas D Dziubla. "Block copolymers for the rational design of self-forming postsurgical adhesion barriers." *Acta Biomaterialia,* 2010, 6 (1): p. 72 [5]. Used with permission.

5.1. Introduction

Following abdominal surgery, the internal wound healing process can result in fibrous tissue deposits that connect adjacent tissues, leading to the formation of post-surgical adhesions[1, 2]. While often asymptomatic, these post-surgical adhesions (PSAs) can lead to serious problems, including bowel obstructions, chronic pain, and infertility. In the United States, an estimated 440,000 adhesiolysis surgeries are conducted annually to correct issues arising from the formation of PSAs [3, 4].

Of all the strategies used to prevent PSA formation, physical barriers have been the most successful [5]. While solid barriers are often employed (such as hyaluronic acid derivatives), some success has been demonstrated with liquid materials such as polyethylene glycol (PEG) and phospholipids [4, 6-11]. In order to obtain next generation improvements upon this technology, the limiting factors must be overcome, including (1) inability to identify pro-adhesive sites, (2) general difficulty in barrier application, and (3) limited applicability to laparoscopic surgeries. These pro-adhesive sites are often characterized by denuded basement membrane or other damaged tissues and fibrin exudates, which can contain highly adhesive, positively charged domains. It is

hypothesized that an aqueous polymer solution, which can naturally target these pro-adhesive sites and form a barrier, will inhibit PSA formation. Adhesion formation occurs when the fibrin gel matrix (FGM) bridges apposing tissues and remains in place, providing a scaffold for subsequent scar formation [12-15]. By retarding protein adsorption and cellular attachment at damaged sites, it is believed that the rate of FGM thickening will decrease, while the rate of fibrinolysis will remain unchanged. This should prevent the FGM from remaining in place long enough to promote PSA formation and therefore should allow normal healing to occur at the site of damaged tissues. Although the mechanism of interaction with the damaged tissues is different, investigation of similar materials with a positive charge has shown promising results in the prevention of PSAs [5, 16].

To design a material for testing this hypothesis, it is necessary to develop clear structure-function relationships to optimize polymer barrier performance. In this work, a living polymerization scheme and a data-rich analytical method were developed to obtain these molecular structure-function relationships, allowing for the further development of targetable post-surgical adhesion barriers. Group Transfer Polymerization (GTP) was used to synthesize copolymers of methacrylic acid (MA), t-butylmethacrylate (TBMA), and poly(ethylene glycol-methacrylate) (M_N=1100, $PEGMA_{1100}$) with well controlled structures for investigation as adhesion barriers. The reaction scheme was designed to facilitate precise control of the molecular weight and charge density of the final polymer. Methacrylic acid was selected as the monomer for the polymer backbone due to its demonstrated biocompatibility in a variety of applications and future amenability towards

functionalization [17-20]. PEG was used to inhibit protein-interaction with the adsorbed polymer layer [21-26].

Rapid, quantitative relationships between polymer properties and function were obtained using quartz crystal microgravimetry with dissipation (QCM-D) coupled with kinetic analysis. From this analysis, it was found that these materials adsorb rapidly to charged surfaces and reduce subsequent non-specific protein adsorption. Depending on the molecular architecture and charge density of the polymer, this polymeric material exhibited up to an 81% reduction in bovine serum albumin (BSA) adsorption. The existence of two competing mechanisms for polymer adsorption, as observed in both energy dissipation analysis from the QCM-D and with variable angle spectroscopic ellipsometry (VASE), provides an unanticipated means to control the adsorption of these materials to surfaces. The protective properties of charge-targeted polymers were confirmed with an *in vitro* assay of cell-substrate binding. It is anticipated that further understanding of the adsorption mechanisms will allow the rational development of polymeric biomaterials for the prevention of PSAs.

5.2. Materials and Methods

5.2.1. Quartz Crystal Substrate Preparation

A model surface consisting of amine terminated self-assembled monolayers (SAM) on gold-coated quartz sensor crystals (Q-Sense) was employed for the evaluation of surface adsorption and protein resistance effects. These SAM surfaces were generated immediately prior to testing using a modification of previously described techniques [201-203]. Prior to SAM formation, crystals were cleaned by immersion in an ammonium

peroxide solution for 5 minutes at 70 ^{o}C, rinsed with deionized water, and dried under a stream of inert gas [204]. Immediately after cleaning, the crystals were immersed in vials in alkaline 1 mM 11-amino-1-undecanethiol, purged with argon, sealed, and protected from light. After allowing the SAM formation to proceed overnight, the crystals were removed from the solution, rinsed repeatedly with neutral ethanol and acidic ethanol, and dried with a stream of inert gas.

5.2.2. QCM Analysis

The functional properties of the materials were evaluated by monitoring the sequential adsorption of the polymers and BSA to model surfaces. This technique takes advantage of the fact that the resonant frequency of a quartz crystal varies as mass is adsorbed onto the surface. By monitoring the resonance frequency of the crystal as it is exposed to a series of solutions containing analytes of interest, it is possible to observe the adsorption of nanogram scale changes in mass. All experiments were conducted in a Quartz Crystal Microbalance (Q-Sense E4) using standard Teflon® and Tygon® tubing materials with a flow rate of 250 μL/min. After installing a crystal in the flow module, the sensor crystal was rinsed sequentially with acidic ethanol, neutral ethanol, deionized water, and PBS solution to ensure that all unbound aminothiol was removed from the crystal and to establish a flat baseline (less than 0.25 Hz/min drift). The change in frequency and energy dissipation were measured as a function of time to monitor the adsorption of the polymer from solution (1.0 mg/mL in PBS).

A typical experimental QCM-D curve is presented in **Figure 5-1**. First, a polymer solution was flowed over the crystal surface, resulting in a decrease in resonance frequency until saturation of the surface was achieved. After this saturation point was

obtained, a pure buffer solution was flowed over the crystal to remove the "loosely" bound polymer fraction. To test the barrier function of the adsorbed polymer layer, a solution of BSA was then flowed over the surface until saturation was obtained. Following the saturated binding, a final pure buffer solution was flowed to calculate the amount of BSA strongly adsorbed onto the surface. Using the Sauerbrey model, which neglects viscous effects and assumes that the adsorbed layer is rigid, the mass of adsorbed layer was calculated using Equation (5-1). In this expression, C is a constant characteristic of the Q-Sense E4system (17.7 ng/cm^2 Hz), and n is the number of the harmonic overtone being considered [205]. Since the change in energy dissipation was small in all measurements ($<1*10^{-6}$ per 10 Hz frequency change), the Sauerbrey model was assumed to provide an accurate description of the adsorbed mass for all analyses with the usual caveat that the QCM measurement also includes any water bound or coupled to the surface [206]. A representative curve of specific mass adsorption is shown in **Figure 5-2**.

$$\Delta m = -\frac{C\Delta f}{n} \qquad (5\text{-}1)$$

A simple kinetic model of the adsorption and desorption phenomena was employed to compare the kinetics of the interactions of the materials with model surfaces. If it is assumed that there are a discrete number of uniform surface sites available for reversible adsorption from solution, it is possible to visualize the adsorption phenomenon as shown in **Figure 5-3**. If it is further assumed that no interaction occurs between

adsorbed molecules or between molecules on the surface with molecules in solution, this Langmuir-type adsorption can be described by Equations (5-2) – (5-6):

$$[SA] = \frac{\alpha}{\beta}\left(1 - e^{-\beta t}\right) \quad (5\text{-}2)$$

$$[SA]_{max} = \frac{\alpha}{\beta} \quad (5\text{-}3)$$

$$t_{1/2} = \frac{\ln(2)}{\beta} \quad (5\text{-}4)$$

$$\alpha = k_1[A][S]_0 \quad (5\text{-}5)$$

$$\beta = k_1[A] + k_2 \quad (5\text{-}6)$$

In these expressions, [SA] is the concentration of adsorbate on the surface, $[SA]_{max}$ is the maximum observed concentration observed, $t_{½}$ is the half-life of the adsorption process, [A] is the solution concentration of the adsorbate, $[S]_0$ is the total number of surface sites, and k_1 and k_2 are the kinetic coefficients of adsorption and desorption, respectively. Using a least squares analysis, these equations were fit to the experimental data, and $[SA]_{max}$ and $t_{½}$ were evaluated for each adsorption event. The observed data follow this model very closely for all of the materials examined, with the notable exception of EPC. This material exhibited linear kinetics with no maximum adsorption; as a result, the kinetic half-life was not determined for this material.

Since material was often observed desorbing from the surface after switching back to a buffer solution, this desorption event was also modeled as shown in **Figure 5-4**. Since [A] is equal to zero in this case, this desorption phenomenon is described by Equations (5-7) – (5-8):

$$[SA] = [SA]_{loose}\left(e^{-k_2 t}\right) \quad (5\text{-}7)$$

$$t_{1/2} = \frac{\ln(2)}{k_2} \quad (5\text{-}8)$$

The amount of material strongly bound to the surface, $[SA]_{bound}$, is taken as the difference in the amount initially adsorbed, $[SA]_{max}$, and the amount observed desorbing, $[SA]_{loose}$.

This analysis assumes a perfect laminar flow over the crystal surface. Although the flow chamber was designed to provide a very rapid exchange of solutions with minimal mixing, there is a brief induction period when the observed kinetic rate may be retarded by mixing within the flow cell [207]. At a flow rate of 250 μL/min and a chamber volume of 40 μL, this induction time is 10 seconds. While this limits our ability to obtain absolute kinetics in very fast processes, relative kinetic behavior could still be obtained.

5.2.3. Variable Angle Spectroscopic Ellipsometry

Gold QCM crystals were prepared using the same protocol for SAM formation and polymer adsorption and subjected to variable angle spectroscopic ellipsometry (VASE) using the M-2000V variable angle spectroscopic ellipsometer (J. A. Woolam Co.). Wavelengths from 370 nm to 1700 nm were measured at 45^o to 75^o in 5^o increments. Data was analyzed using the WVASE32® software package in a stepwise fashion. First, a bare gold substrate was analyzed to determine the optical constants (n and k). Then, the amine terminated SAM was measured and the data fitted as a Cauchy film to determine the film thickness. Finally, the polymer samples were measured. Using

the previously fitted valued from the substrate and the SAM layer, the thickness of the polymer layer was fitted as an additional Cauchy layer [208].

5.2.4. Cell Attachment Studies

In order to test the anti-cellular adhesive properties of these materials, a complementary cell culture study was carried out using the mouse mesenchymal D1 cell line (ATCC CRL-12424) in 24-well tissue culture plates. This pluripotent cell line was selected due to its strong adherence to charged surfaces and wound healing components (e.g., collagen I and fibrin) [209-212]. Wells were coated with poly(L-lysine) (250 µL 0.1 mg/mL in sterile PBS) and incubated at room temperature for 2 hours. After rinsing the wells 3 times with sterile PBS, polymer solutions were added (200 µL 1.0 mg/mL in sterile PBS) and incubated at room temperature for 2 hours. The polymer solutions were removed from the wells, and each well was rinsed 3 times with sterile PBS. Finally, each well was seeded with 250,000 cells in Dulbecco's Modified Eagle Medium (DMEM, HyClone Laboratories) containing 10% fetal bovine serum (GIBCO/Invitrogen) and incubated at 37 ^{o}C for two hours. Untreated tissue culture polystyrene (TCP) and PLL-coated TCP were employed, and a minimum of 6 replicates were studied for each material.

After incubation, unattached cells were removed from the wells by rinsing twice with sterile PBS. Representative images of the cells were obtained using an inverted phase contrast microscope. The cells remaining on the surface after rinsing were lysed by sonication in high salt solution (0.05 M NaH_2PO_4, 2 M NaCl, and 2 mM EDTA). DNA contents, measured using Hoechst 33258 stain, were used to quantify the number of cells in each well [213-214]. In short, Hoechst 33258 (final concentration, 0.5 µg/ml, Sigma)

was allowed to react with lysates in the dark for 10 minutes, after which fluorescence was measured ($\bullet_{ex}$ = 356 nm and $\bullet_{em}$ = 458 nm). An exponential calibration curve was prepared using samples with known cell counts (0 – 200,000 cells). After measuring the fluorescence of each well, this calibration was employed to determine the number of cells attached in each well. Sample wells whose fluorescence indicated > 250,000 cells were neglected as spurious measurements, since such readings would correspond to greater than 100% cellular attachment.

5.2.5. Statistical Evaluation

Statistical relevance was determined by performing analysis of variance followed by a Sidak pair wise post-hoc analysis using Minitab 15. Differences at greater than 90% and 95% confidence are reported, with statistical significance being considered at the 95% level.

5.3. Results

5.3.1. Polymer Binding and Release from Amine-terminated SAM Surfaces

Based upon analysis of attachment rates (on rates) of polymer adsorption (**Figure 5-5**), there was no statistical difference among the polymer samples. While the on rates varied greatly between runs, detachment rates (off rates) were much more consistent. As the fraction of acidic groups in the polymer increased from 0% to 80% for the PAA copolymers, polymer adsorption to the charged surface varied from 211 – 468 ng/cm^2 (**Figure 5-6**). A statistically significant maximum in $[SA]_{max}$ was found at a charge density of 50%. The 40% deprotected PTBMA showed significantly less specific mass adsorption that the 50% block copolymer. As PBS was flowed over the surface and

polymer desorption occurred, sample differences between all charged diblock polymers were attenuated. PAA, 40% deprotected PTBMA, and 0% deprotected block copolymer possessed the lowest degree of surface coverage.

There was also a noticeable difference in the mechanism of binding. **Figure 5-7** shows plots of the energy dissipation change (• D) versus the mass adsorbed. The slope of these curves increased with charge density for the PAA copolymers. The final values of the ratio, $\left(\frac{\Delta D}{\Delta m}\right)$), shown in **Figure 5-8**, provide a means to evaluate the conformation of the polymer adsorbed to the surface [207, 215]. A lower value indicates a relatively small amount of energy dissipation per unit mass, while a higher value reflects increasing levels of energy dissipation per unit mass. A low value indicates a relatively rigid, compact adsorbed layer, while a higher value for this ratio indicates an adsorbed layer that extends further away from the surface [207].

5.3.2. Surface Film Thickness

Variable angle spectroscopic ellipsometry was performed to verify the mass absorption trends observed by QCM. The results of the VASE analysis are presented in **Figure 5-9**. By measuring multiple wavelengths and angles, it was possible to probe the surface multiple times and obtain an accurate measurement of the film thickness. The PAA polymer exhibited a thickness of 109.3 Å, while the hydrophobic block copolymer and the EPC film thicknesses were 80.5 Å and 48.4 Å, respectively. The remaining materials showed ellipsometric thicknesses of 1.4 Å to 30.8 Å. Due to the high degree of variance in the data, no statistically significant differences were identified.

5.3.3. Blockade of Protein Adsorption by Diblock Copolymers

Unlike with polymer adsorption, there was a distinct change in kinetics of protein binding among samples (see **Figure 5-10**). The half-life of protein adsorption was lowest for the surfaces with relatively hydrophobic coatings (PMAA, EPC, PTBMA-40) and for the uncoated SAM surface, suggesting the greatest affinity of BSA. The more hydrophilic PMAA copolymers and PAA control possessed the slowest binding rates of all materials tested. There was no statistical difference in the kinetics of the protein adsorption for diblock copolymer coated surfaces. As expected, the uncoated charge surface possessed the greatest degree of protein binding (**Figure 5-11**). Of all test samples, 0% block copolymer possessed the best blocking ability of all tested polymers (**Figure 5-12**). It is possible that the 80% statistical copolymer sample possessed equivalent surface blocking capacity; however, variability in the data makes this analysis inconclusive. As specific and non-specific protein adsorption interactions are integral precursors to the formation of a post-surgical adhesions, it is believed that the ability to delay this event serves as one measure of a material's ability to interrupt PSA formation.

5.3.4. Suppression of Cellular Attachment to PLL Coated Surfaces by Diblock Copolymers

Measurement of cell attachment was used to determine whether previously observed differences in polymer binding to surfaces and protein adsorption to polymers translate to reduced cell-surface interactions. In order to make meaningful comparisons with the QCM data and to mimic the positively charged basement membrane, PLL was used as a control surface. Close observation of the wells revealed significant heterogeneity and pooling of cells in the well edges, suggesting that inadequate washing

was used to remove all unbound cells. Representative images of the wells, taken from the same location in each well, are shown in **Figure 5-13**. TCP and PLL mediated the greatest level of cell attachment, with nearly full surface coverage noted. The PAA, 0% block, EPC, PTBMA-40, and 80% block each appeared to have a slightly lower level cellular attachment than the controls. The 50% block, PMAA, and 80% statistical copolymer treated wells demonstrated a large reduction in the apparent number of cells attached during the 2 hour incubation period.

Quantitative results for cell attachment are shown in **Figure 5-14**. Due to the wide variability contributed by one outlier, no statistically significant differences were observed. Some trends, however, were observed. When copolymers possessed a negative charge, i.e., 50% block, 80% block, and 80% statistical, suppression in cellular attachment, compared to PLL controls, was observed.

5.4. Discussion

In order for a material to be applicable for use as a prophylactic PSA treatment, several requirements must be met. First, the material must be amenable to use within the body, including biodegradability and renal clearance capacity. PEG and PMAA both have well characterized biocompatibility and are not expected to cause adverse biochemical interactions. Using GTP, it is possible to synthesize copolymers of PEG and PMAA with precisely controlled molecular composition. This polymerization technique also facilitates the synthesis of block copolymers to control the spatial orientation of the adsorbing and protective moieties within the molecule. Relying on ester bonds to attach the pendant PEG groups to the PMAA backbone, these materials are designed to be susceptible to both enzymatic and hydrolytic degradation. To ensure ultimate elimination

of the polymer, the maximum molecular weight of the synthesized materials was designed to be less than 50 kDa [134, 216].

The primary method to assess PSA prevention technologies has been through the use of animal models [5, 217]. Since these studies are costly, time consuming, and have ethical implications, it is desirable to test materials *in vitro* prior to initiation of animal studies. QCM-D analysis of polymer and protein interactions with model surfaces provides a data-rich method of analysis, affording data on polymer surface affinity, barrier stability and performance, and absorbed layer rigidity and thickness. The simple amine-terminated SAM model surface allows a reproducible, high throughput method to assess these materials, aiding in the development of the method, and providing a platform for testing the charge based targeting of the diblock poly(methacrylic acid) copolymers. Such a system provides the opportunity for rapid evaluation and optimization during further investigations of potential barrier materials.

The power of this method was realized upon the observation of multiple surface adsorption mechanisms occurring as a result of changes in polymeric charge density. In these experiments, the materials with higher concentrations of acidic groups led to a thicker, more loosely bound layer adsorbed to the substrate. This was likely a result of the negatively charged acid groups strongly interacting with the positively charged surface and the grafted PEG block being forced into a more extended conformation from the surface. As charge density decreased, a second adsorption mechanism was observed. Although the exact nature of the interactions is unknown at this time, it is believed that they result either from hydrogen bonding between the charged surface and PEG chains or from hydrophobic interactions of the uncharged polymer with domains of imperfect SAM

formation that result in the exposure of aminothiol chains to the solution. Both of these proposed mechanisms would result in the development of a more tightly bound polymer layer as multiple points of the polymer chain interact with the surface. This is likely to result in a much more random adsorption to the surface with PEG chains in a less brush-like conformation. The phospholipids, which are expected to form a lamellar structure, also form a loosely bound surface layer.

As has been observed in numerous studies, QCM cannot distinguish between adsorbed polymer mass and polymer mass plus bound water [218-220]. In order to determine the mass of bound water in the adsorbed layer measured by QCM, the values obtained from QCM were compared with the results obtained from VASE. Assuming a nominal polymer density of 1.1 g/cm^3, the amount of water bound in the surface layer can be estimated. The surface layers formed by the most hydrophilic copolymers (50% block, 80% block, and 80% statistical) contain in excess of 90% water. The more hydrophobic materials (PTBMA-40, 0% block copolymer, and EPC) form surface layers with approximately 50% water. These observations support the two mechanisms of surface adsorption and surface conformation. The PAA layer indicated a greater surface mass when measured by ellipsometry and, coupled with the high standard deviation associated with this measurement, suggests a high degree of non-uniformity and variability within the PAA surface film.

The most surprising finding of this work was the performance of the hydrophobic, protected polymers. These materials possessed the lowest degree of polymer binding, but they had the best ability to block subsequent BSA adsorption in the QCM-D analysis. The two competing mechanisms observed during polymer adsorption can explain the

unexpectedly strong performance of the t-butyl protected polymer. While adsorption to the surface via electrostatic interactions was not possible, the multiple points of interaction between the polymer and the surface resulted in a compact layer of strongly bound material. This material occupies sites where BSA binding would potentially occur and therefore effectively prevented nonspecific adsorption of proteins to the surface. Indeed, this result was found to be a unique feature of the QCM-D and not replicated in the cell culture studies, where the 0% hydrolyzed polymer possessed no ability to inhibit cellular attachment to PLL. The complex, multicomponent makeup of cell culture medium compared to BSA-only solutions may explain this apparent discrepancy.

No significant differences were observed between the performances of the statistical and block copolymers. It may be expected that the bifunctional composition of the block copolymer would result in stronger binding to the model surface and an increase in the extended character of the PEG moieties. These differences in polymer architecture, however, have no significant impact on the amount of polymer adsorbed to the model surface or the kinetics of adsorption. This suggests that, when electrostatic forces exist, they dominate polymer-surface interactions. In addition, the fact that the rigidity of the adsorbed layer and its ability to resist protein adsorption was independent of the configuration of the monomeric units comprising the polymer (i.e., block vs. statistical copolymer) suggests that protein-resistant conformation can be achieved without a high relative concentration of PEG units.

It appears that there is a point at which both of these proposed mechanisms contribute significantly to the adsorption of polymer. The 50% deprotected block copolymer exhibited a statistically significant increase for material initially adsorbed to

the surface, but upon rinsing with PBS, this difference was no longer seen. Consideration of this observation and of the protein blockade properties that closely mimic the more highly charged species suggests that, after an initial competition between the two binding mechanisms, a conformation based on charge affinity was obtained. This hypothesis can be tested by varying the pH of the adsorption conditions and determining the relative contributions of the competing mechanisms. It is anticipated that, once more thoroughly understood, these competitive mechanisms may be exploited to provide an additional measure of control over the polymer properties.

The PAA control used in these experiments demonstrated a unique property that results from the absence of PEG groups. While this polymer rapidly formed a strongly bound surface layer, its thickness suggests that, rather than forming a molecular monolayer on the surface, multiple layers of molecules were deposited. The resulting layer inhibited protein adsorption kinetics, as the BSA molecules were forced to permeate this more viscous PAA layer in order to bind to the surface. PMAA and PTBMA-40 form similar surface layers; but, due to their increased hydrophobicity, do not retard the adsorption of BSA.

In cell culture, when in the presence of competing negatively and positively charged serum proteins, which could detach the bound polymer, *in vitro* studies confirmed that the synthetic copolymers can bind to positively charged substrates and significantly reduce cellular attachment. The results of the cell culture studies suggest that the 50% block and 80% statistical copolymer were most effective, while QCM data indicated the largest protein blockade with the 0% block and 80% statistical copolymers. It is believed that this discrepancy results from the nonspecific binding mechanism of the

0% block copolymer to the surface, which is incapable of suppressing cellular attachment in more complex serum-containing solutions. As indicated by the cell attachment studies PMAA, PTBMA-40, PAA and EPC all failed to inhibit cell attachment. Indeed, these materials likely only exchanged the surface charge from positive to negative, and the pluripotent mesenchymal cells can adhere to both of these charges [209, 212]. This result is of paramount importance when designing a material that can suppress tissue adhesion. While the proliferation of cells like the mesenchymal D1 cells are desired in wound healing, they serve as an easy to use reference for strong cell adhesion. By designing a material that can suppress all cells types from attaching to the surface of a damaged organ, it is believe that more time would be allowed for sub surface wound healing to occur, allowing for island implantation and reformation of the epithelial layer without permitting scar tissue bridging. Future in vivo studies will be needed to verify this hypothesis.

5.5. Conclusion

Group transfer polymerization was successfully employed to create block copolymers with varying charge density. The polymers adsorbed strongly to model SAM surfaces via two competing mechanisms; the relative importance of each of these mechanisms is a function of the charge density along the final polymer backbone. The resulting self-formed polymer layer strongly resisted non-specific protein adsorption and may be exploited to develop a new treatment strategy for the prevention of post-surgical adhesions. The control afforded by the polymerization method of these synthetic materials allows their properties to be tailored to optimize their function. Additional investigations will focus on developing a deeper understanding of the mechanism and

thermodynamics of the observed polymer adsorption phenomena as we move to more biologically relevant model surfaces and confirm the relationship observed with appropriate *in vivo* models of surgical adhesion formation.

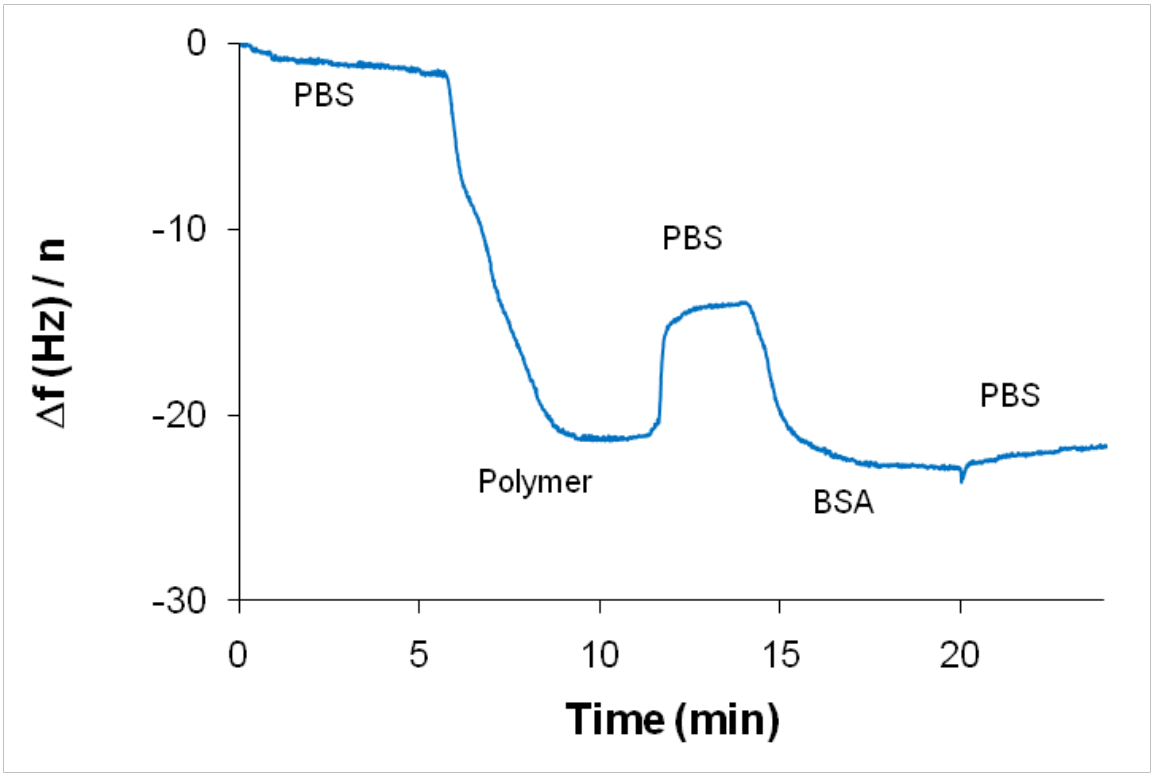

Figure 5-1 Raw data (frequency response) from QCM measurement.

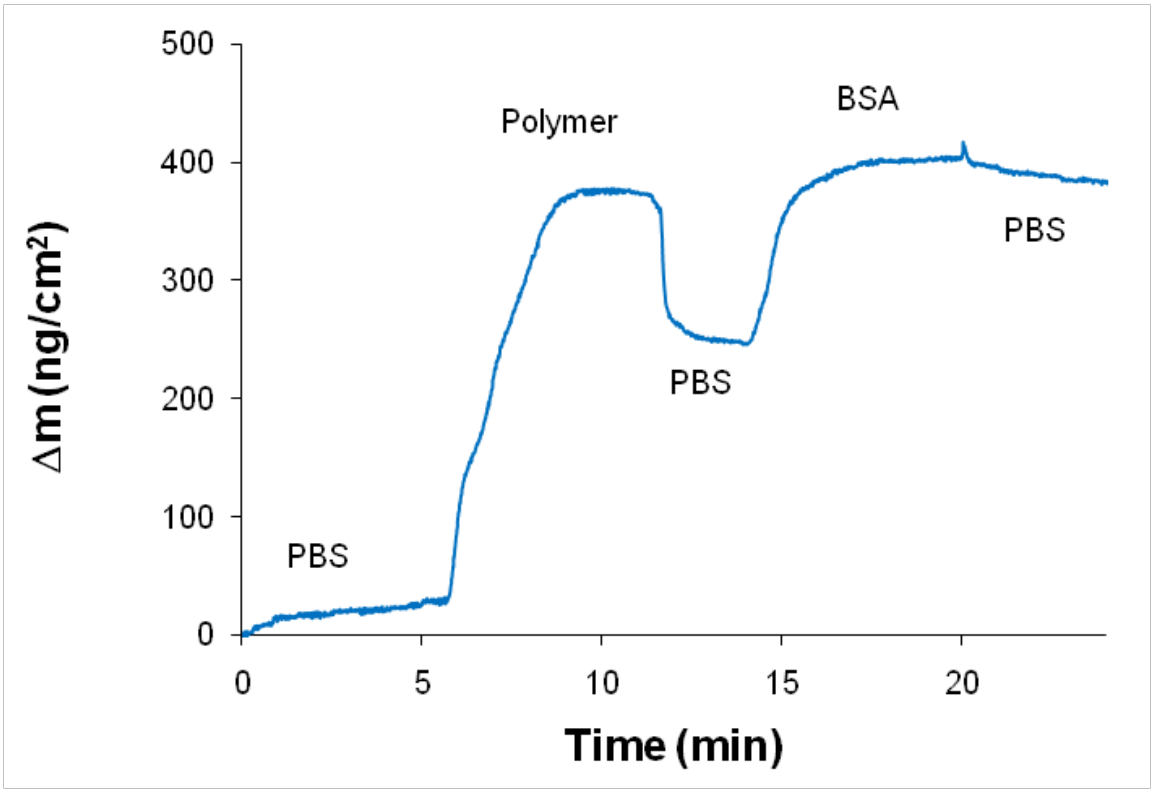

Figure 5-2 Specific mass adsorption based on Sauerbrey model, which assumes a linear fit between frequency response and adsorbed mass.

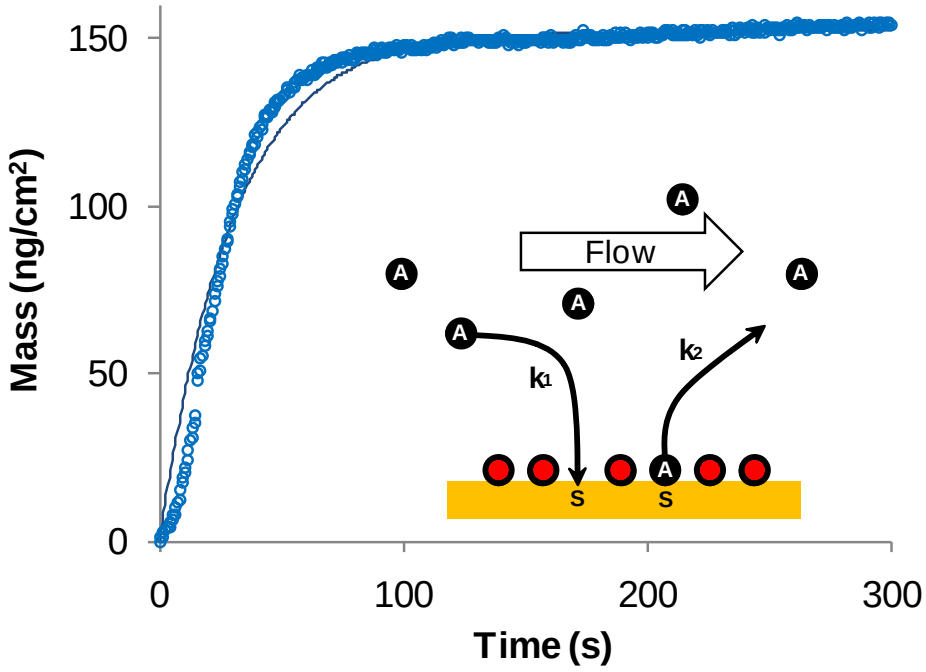

Figure 5-3 Kinetic fit of BSA adsorption to model substrate after preadsorption with 80% block copolymer.
$[SA]_{max}$ = 152.1 ng/cm2 and $t_{½}$ = 20.9 s.

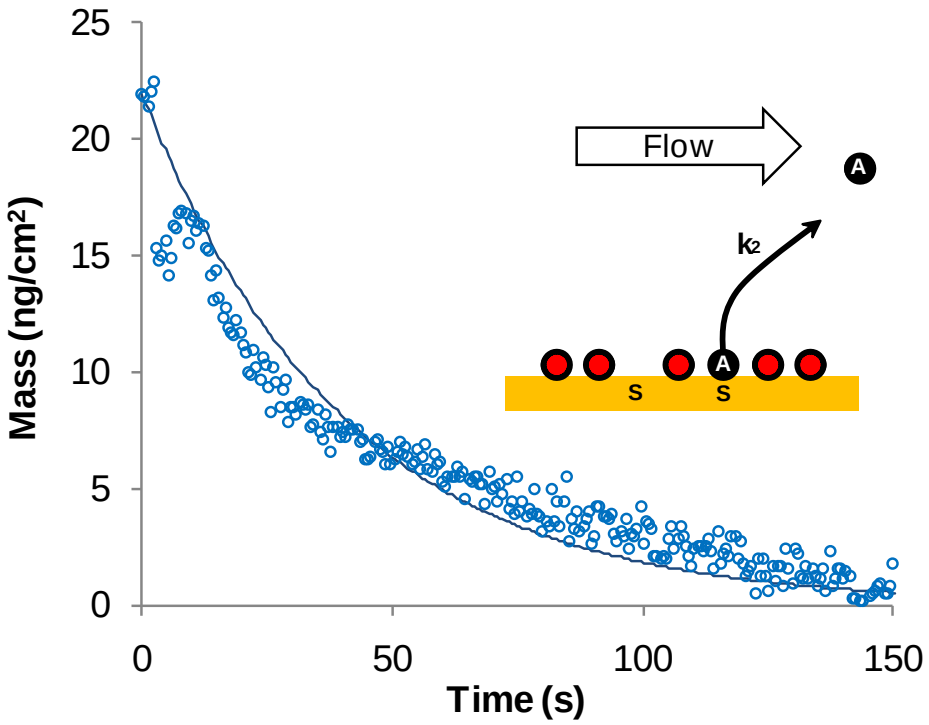

Figure 5-4 Kinetic model fit of BSA desorption from model substrate after preadsorption with 80% block copolymer.
$[SA]_0$ = 21.9 ng/cm^2 and $t_{½}$ = 27.8 s.

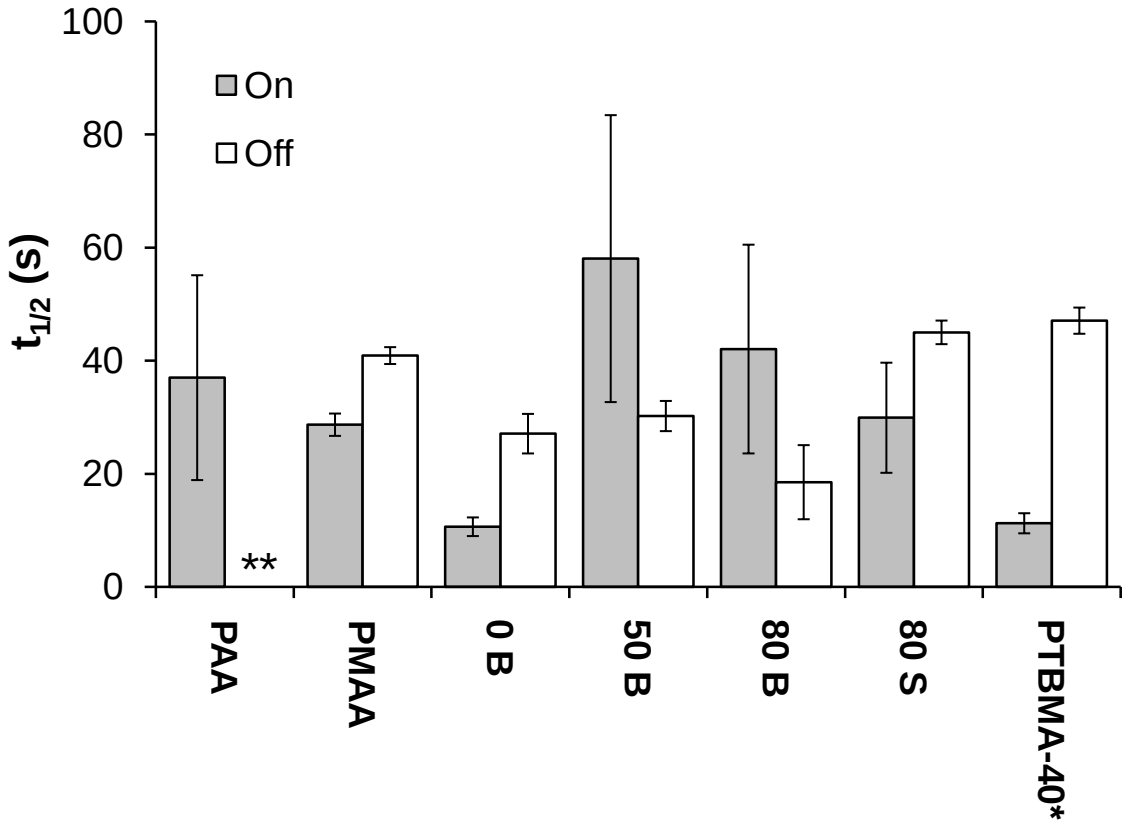

Figure 5-5 Polymer adsorption kinetics.
No significant differences was noted in the half-life for polymer adsorption (grey bars) and desorption (white bars) from solution onto the QCM surface.

* PTBMA-40 was prepared at 1.0 mg/mL, but was only partially soluble. Insoluble material was removed by filtration and the saturated PTBMA-40 solution was used for analysis.

** Insufficient PAA data for meaningful comparison.

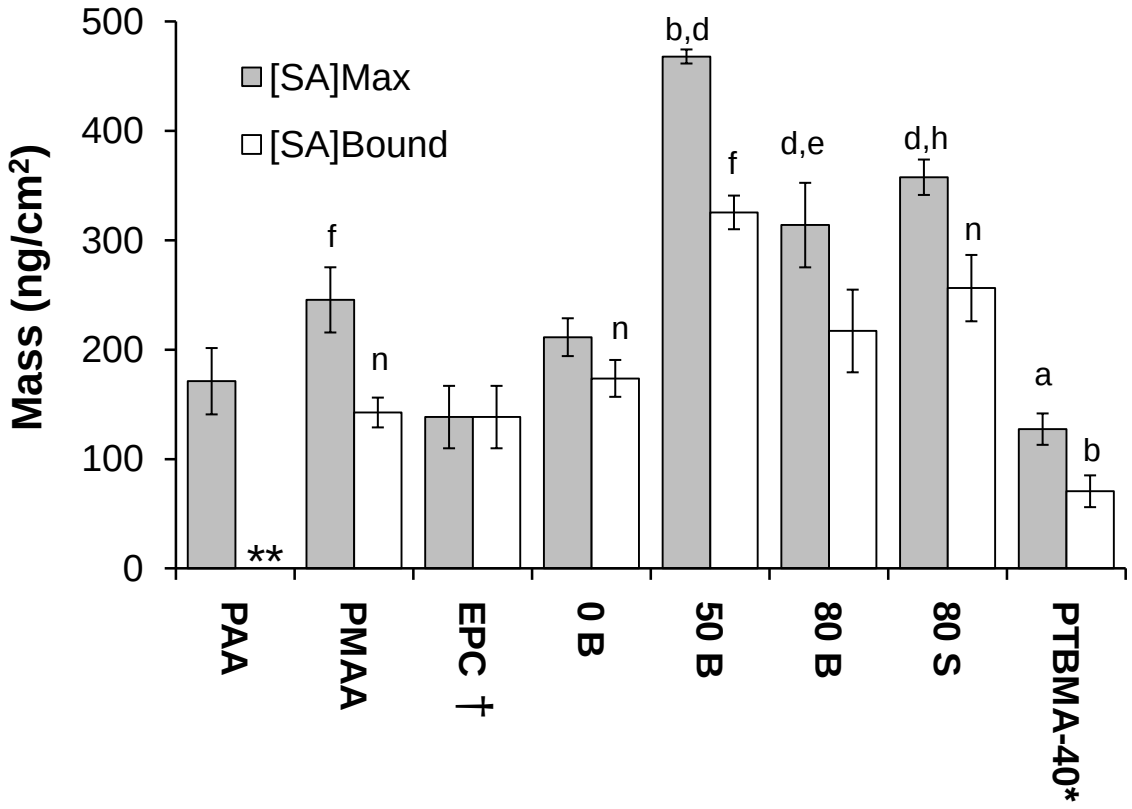

Figure 5-6 Maximum specific mass adsorption, $[SA]_{max}$, and specific mass of tightly bound polymer, $[SA]_{bound}$.

Statistical comparisons are given: 90% confidence compared to 0 B (a), 95% confidence compared to 0 B (b), 95% confidence compared to PTMBA-40 (d), 90% confidence compared to 50 B (e), 95% confidence compared to 50 B (f), 90% confidence compared to PAA (h), and 95% confidence compared to 80 B (n). (n = 3 – 5, M ± SE)

* PTBMA-40 was prepared at 1.0 mg/mL, but was only partially soluble. Insoluble material was removed by filtration and the saturated PTBMA-40 solution was used for analysis.

** Insufficient PAA data for meaningful comparison.

† EPC exhibited linear kinetics with no desorption. The mass reported is the mass adsorbed to the surface after 200 s of adsorption in QCM. Not included in statistical analysis.

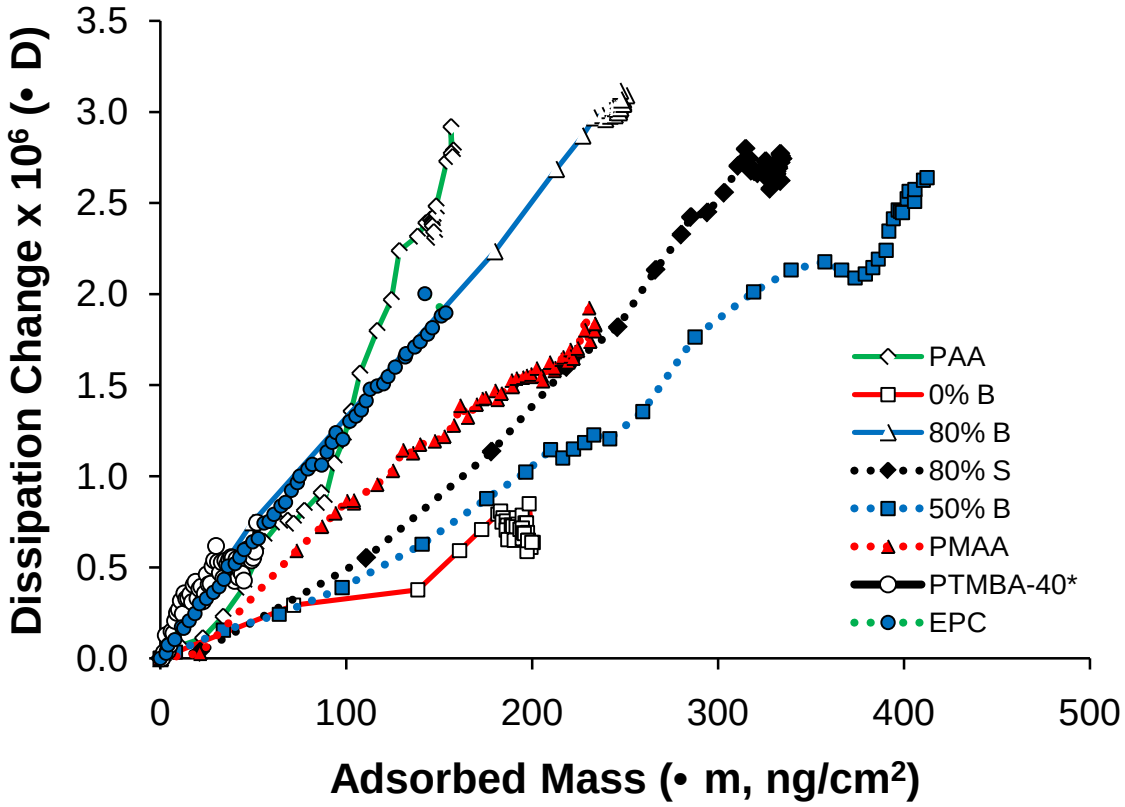

Figure 5-7 Dissipation change as a function of adsorbed mass for polymer adsorption phenomena.
The slope of the curve represents the relative rigidity of the adsorbed layer, with a steeper slope indicating a less rigid adsorbed layer.
* PTBMA-40 was prepared at 1.0 mg/mL, but was only partially soluble. Insoluble material was removed by filtration and the saturated PTBMA-40 solution was used for analysis.

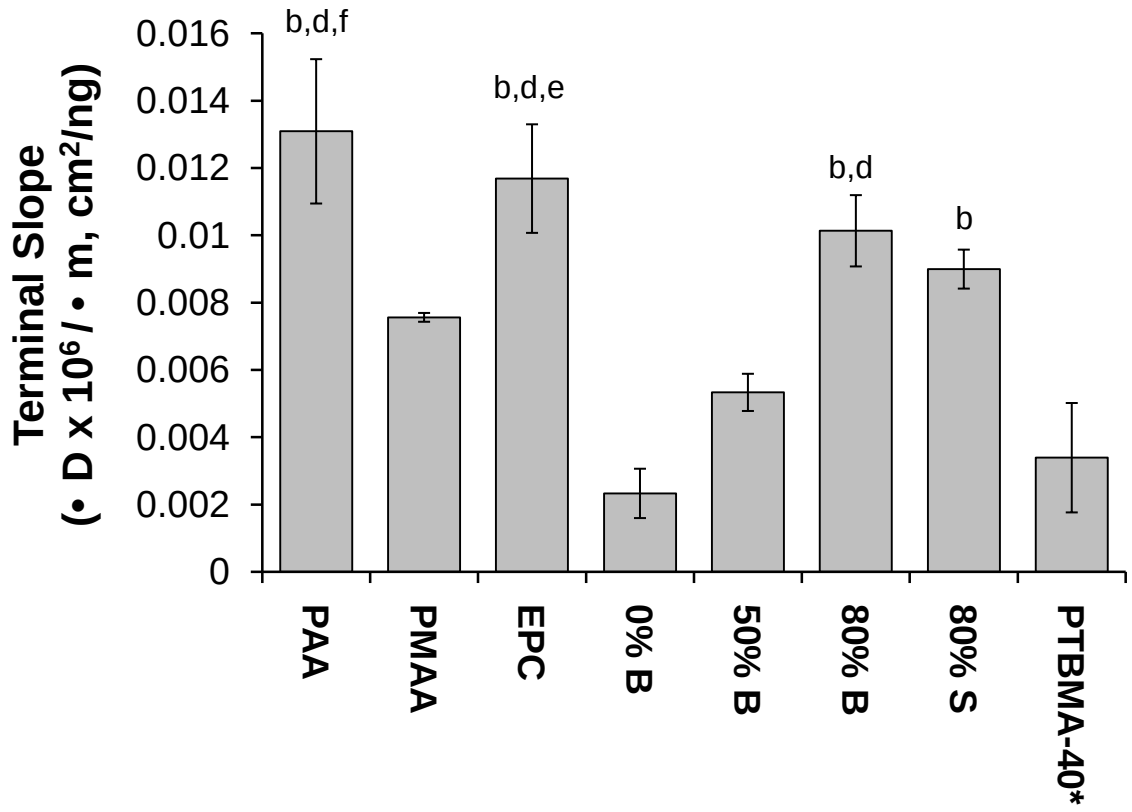

Figure 5-8 Terminal value of the of the energy dissipation change versus adsorbed mass.

The observed trend indicates that, as the charge density along the polymer increases, the polymer extends farther from the surface, indicating a more extended PEG conformation. Statistical comparisons are given: 95% confidence compared to 0 B (b), 95% confidence compared to PTMBA-40 (d), 90% confidence compared to 50 B (e), and 95% confidence compared to 50 B (f). (n = 3, M ± SE)

* PTBMA-40 was prepared at 1.0 mg/mL, but was only partially soluble. Insoluble material was removed by filtration and the saturated PTBMA-40 solution was used for analysis.

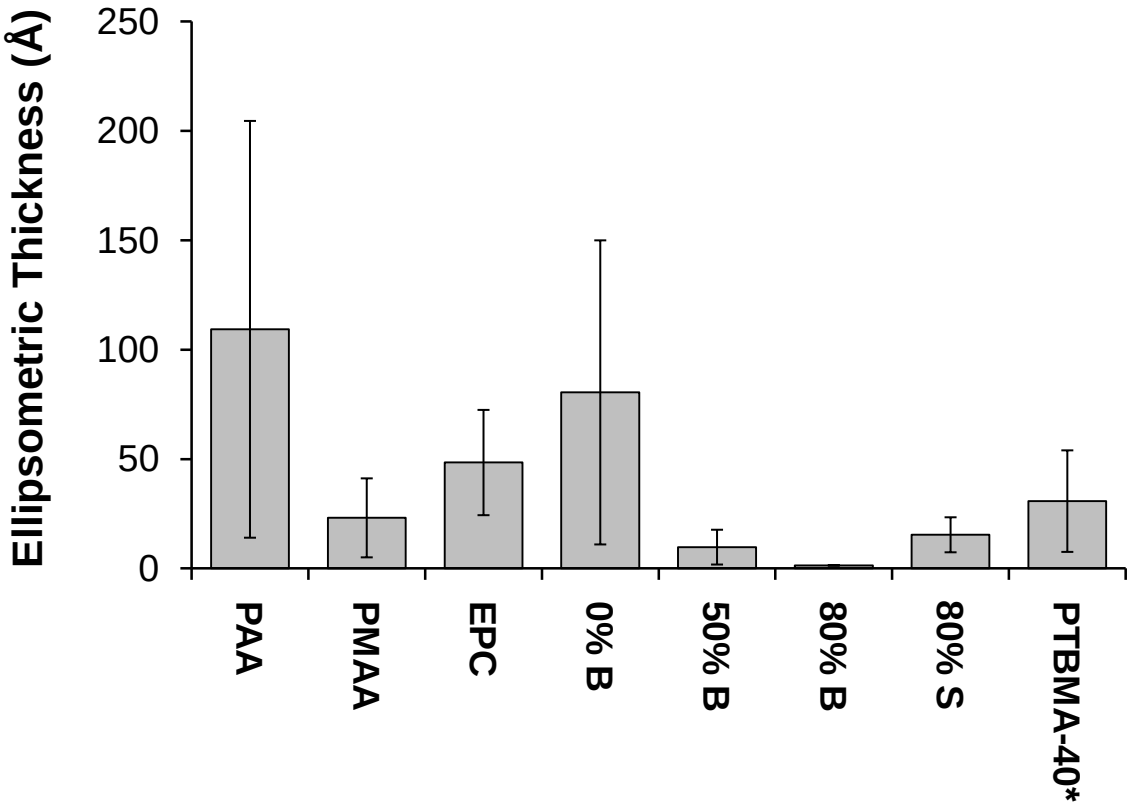

Figure 5-9 Film thickness measured by variable angle spectroscopic ellipsometry. No significant differences were observed.. (n = 2 – 3, M ± SE)

* PTBMA-40 was prepared at 1.0 mg/mL, but was only partially soluble. Insoluble material was removed by filtration and the saturated PTBMA-40 solution was used for analysis.

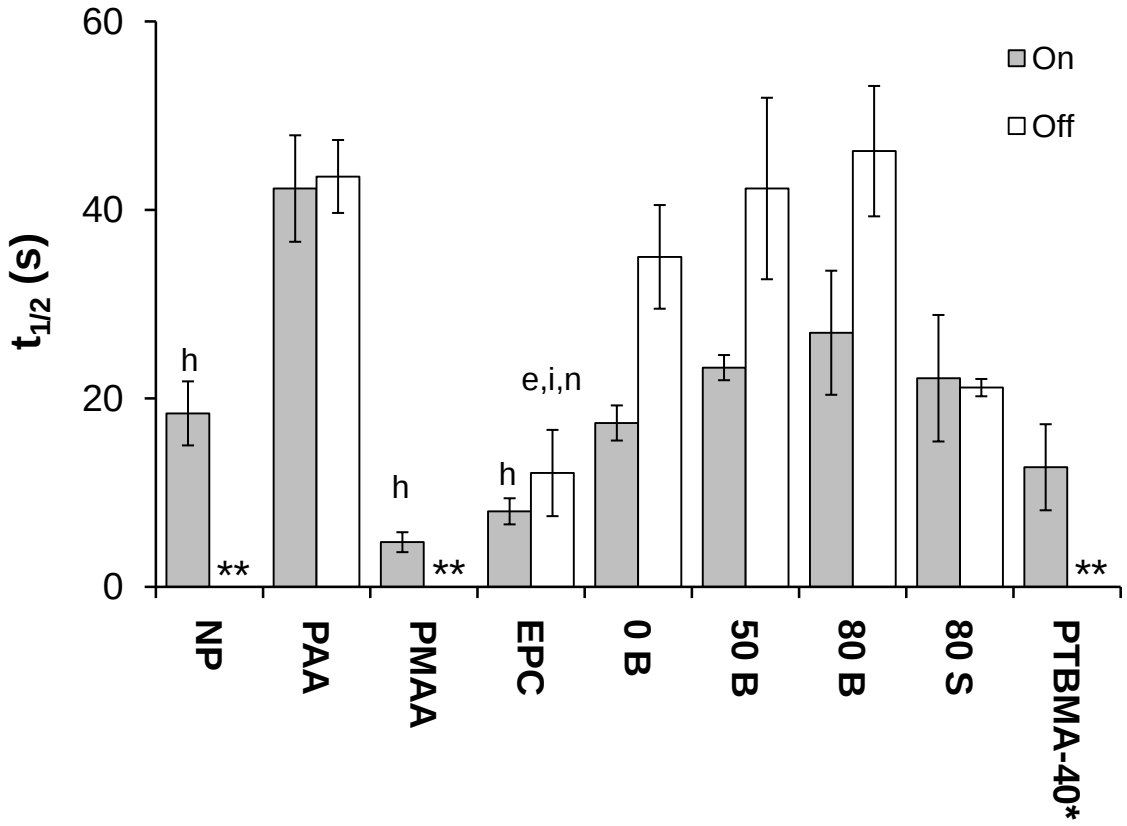

Figure 5-10 Kinetics of BSA adsorption from solution.
Unlike polymer adsorption, half-life for polymer adsorption possessed statistically significant differences suggesting a change in the kinetic accessibility of protein to the material surface. Statistical comparisons are given: 90% confidence compared to 50 B (e), 90% confidence compared to PAA (h), 95% confidence compared to PAA (i), 95% confidence compared to 80B (n). (n = 3 – 5, M ± SE)

* PTBMA-40 was prepared at 1.0 mg/mL, but was only partially soluble. Insoluble material was removed by filtration and the saturated PTBMA-40 solution was used for analysis.

** Insufficient NP, PMAA, and PTBMA-40 data for meaningful comparison.

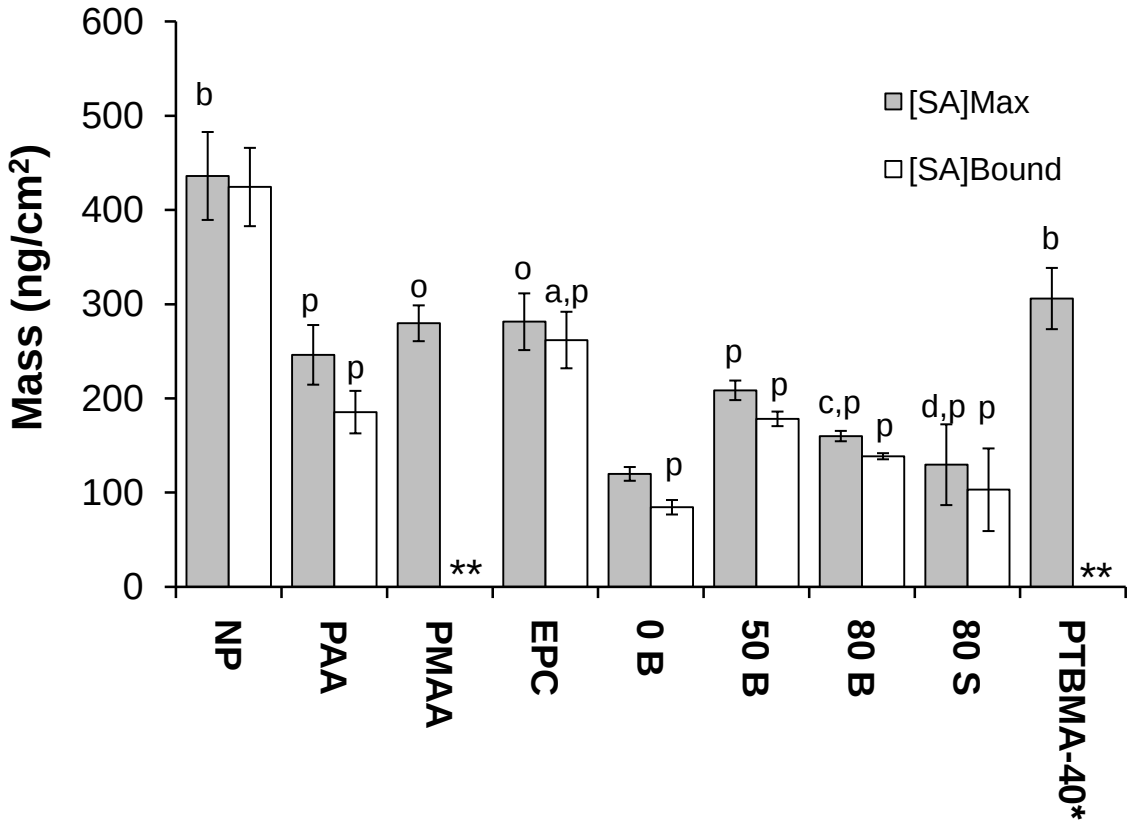

Figure 5-11 Mass of BSA adsorbed from solution.

All polymers possessed an ability to reduce the level of protein adsorption as determined by maximum specific mass adsorption,$[SA]_{max}$, and specific mass of tightly bound polymer,$[SA]_{bound}$.

Best blockage was achieved by the uncharged diblock copolymer. Statistical comparisons are given: 90% confidence compared to 0 B (a), 95% confidence compared to 0 B (b), 95% confidence compared to PTMBA-40 (d), 90% confidence compared to NP (o), and 95% confidence compared to NP (p). (n = 3 – 5, M ± SE)

* PTBMA-40 was prepared at 1.0 mg/mL, but was only partially soluble. Insoluble material was removed by filtration and the saturated PTBMA-40 solution was used for analysis.

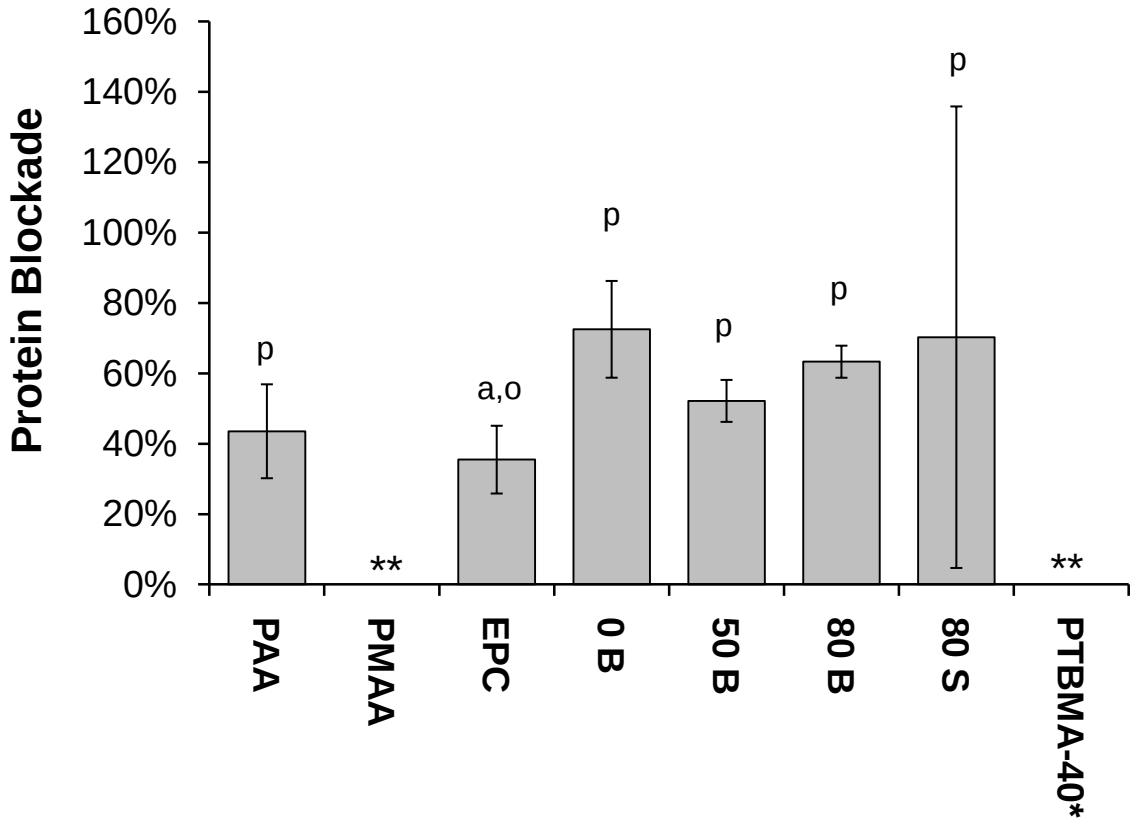

Figure 5-12 Percent protein blockade compared to control.
Statistical comparisons are given: 90% confidence compared to 0 B, 90% confidence compared to NP (o), and 95% confidence compared to NP (p). (n = 3 – 4, M ± SE)

* PTBMA-40 was prepared at 1.0 mg/mL, but was only partially soluble. Insoluble material was removed by filtration and the saturated PTBMA-40 solution was used for analysis.

** Insufficient PMAA and PTBMA-40 data for meaningful comparison.

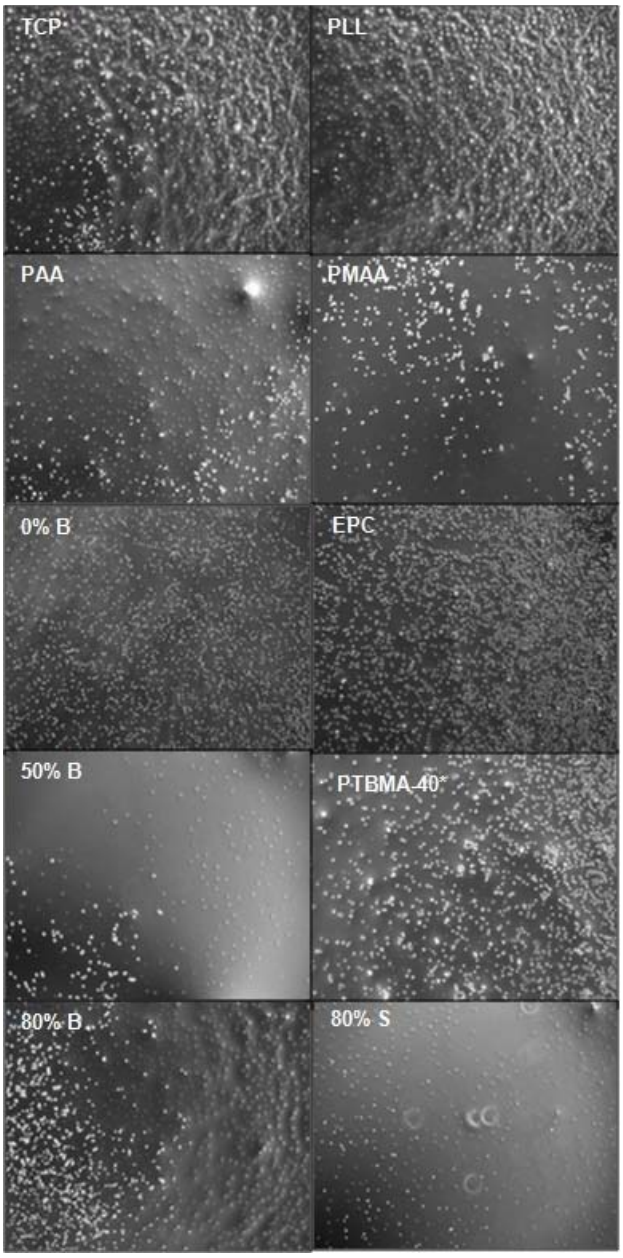

Figure 5-13 Cell attachment to polymer-coated surfaces.
Representative images were obtained after incubating for 2 hours, after which nonadherent cells were removed.

* PTBMA-40 was prepared at 1.0 mg/mL, but was only partially soluble. Insoluble material was removed by filtration and the saturated PTBMA-40 solution was used for analysis.

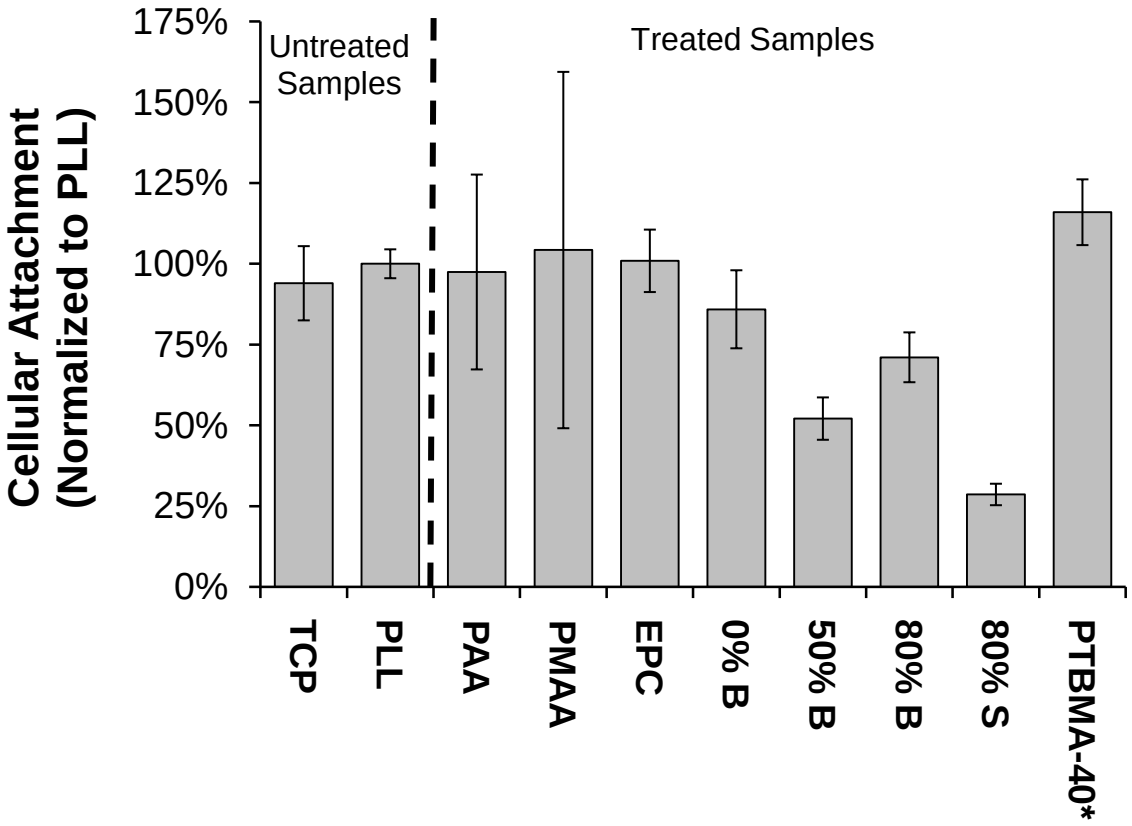

Figure 5-14 Average degree of cellular attachment relative to the PLL control. Cell numbers were determined using a fluorometric DNA assay (n = 4 – 11, M ± SE).

* PTBMA-40 was prepared at 1.0 mg/mL, but was only partially soluble. Insoluble material was removed by filtration and the saturated PTBMA-40 solution was used for analysis.

CHAPTER 6. DISRUPTION OF FIBRIN GEL MATRIX FORMATION BY TARGETED POLYMERS

6.1 Introduction

As has been described, the fibrin gel matrix (FGM) is a critical component in the formation of post surgical adhesions. Consisting primarily of fibrin and a mixture of extracellular matrix components including fibronectin, hyaluronic acid, glucosaminoglycans and proteoglycans, the FGM can bridge apposing tissues in the body and lead to the formation of PSAs [1, 8, 221]. One of the main goals of this research is to develop a material that will interrupt FGM formation and disrupt the cascade of events that leads to PSA formation. In the previous chapter, the ability of synthetic block copolymers to adsorb to charged surfaces and block non-specific protein adsorption was studied.

In order to test these materials in a more biologically relevant manner, this investigation focuses on the ability to target polymers to fibrin coated surfaces and retard the subsequent propagation of the fibrin gel formation. By directing these barrier materials to the site of tissue damage, these targeted materials are expected to provide two unique advantages. First, this approach should facilitate the protection of proadhesive sites that are difficult to identify or are inaccessible. Second, the presence of multiple specific interactions with the damaged tissue, the resulting barriers should provide enhanced durability over non-targeted materials.

It was hypothesized that the molecular structure can be tailored to optimize the adsorption of polymeric biomaterials to pro-adhesive sites on the tissue surface and

attenuate the formation of post surgical adhesions. In order to test this hypothesis, block copolymers were synthesized with highly controlled molecular architectures. Since PEG was incorporated into the polymer structure for its well characterized anti-adhesive properties, the PEG structure in the polymers were varied by using PEGMA monomer (M_N = 300 and M_N = 1,100). In addition, the number of PEG chains in the polymer was varied to study the impact of total PEG content. Finally, the effect of targeting peptides in the polymer structure was investigated by varying both nature and the number of these units in each polymer molecule.

After completion of the experiments, the resulting data set was statistically analyzed to assess the relative importance of these factors in the polymers' ability to target fibrin and to retard various aspects of FGM formation. When statistical differences were observed in the data for an experiment, *post hoc* pairwise Sidak comparisons were used to quantify these differences. Finally, multivariate linear regression was employed to assess the impact of the changes in molecular architecture on the results and to identify the most important factors in the polymer's performance in each test.

In order to exhibit optimum function, the polymer system was designed to assess three functional criteria: binding to damaged tissue, suppression of protein adsorption, and reduction in cellular adhesion. In order to assess these functions, several techniques were employed. Quartz Crystal Microbalance with Dissipation (QCM-D) was used to study the kinetics and blockade of fibrinogen adsorption. The ability to retard the propagation of the FGM was studied using a turbidity assay to assess the kinetics of FGM formation from a fibrin-coated surface. The attachment of cells to polymer-treated fibrin

gels was investigated and quantified using a fluorescent DNA assay to mimic the action of macrophages during the rearrangement and strengthening phase of PSA formation.

6.2. Materials and Methods

6.2.1. Polymers

A total of 20 polymers, as synthesized in **Chapter 4**, were created for this analysis. As shown in **Table 4-2**, these polymer architectures included two levels each for the PEG chain length (M_N = 300 and M_N = 1,100) and the backbone chain length (approximately 24 and approximately 42 monomer units). In addition, the impact of peptide type (fibrin specific CREKA versus CAERK scramble) was investigated. The number of fibrin specific CREKA units per polymer molecule was varied from 2 – 5 peptide units per molecule. Control polymers, consisting of functionalized PMAA units without PEG grafts were included in the analysis. Finally, free peptide (both CREKA and CAERK), as well as a commercially available phospholipid (egg phosphatidycholine, EPC) were used as controls.

6.2.2. Solution Preparation

Polystyrene (PS) solution was prepared by dissolving polystyrene (M_N = 280,000, Fisher, 0.5 wt. %) in toluene (Fisher). Fibrinogen solutions (13.2 mg/ml, 0.50 mg/mL, and 0.10 mg/mL) were prepared in Tris Buffered Saline (TBS, Aldrich). Bovine Serum Albumin (BSA, Fisher, 1.0 mg/mL) solution was prepared in TBS. Thrombin solutions were prepared by diluting a stock thrombin solution (5 U/mL) to the desired concentrations in TBS (2.5 U/mL and 0.1 U/mL). All protein solutions were prepared

each day, prior to use. Polymer solutions were prepared by dissolving purified polymer in TBS to the desired final concentration and were stored at -20 ^{o}C prior to use.

6.2.3. Measurement of Fibrinogen Adsorption to Fibrin Coated Quartz Crystal

Our previously developed quartz crystal microbalance method was used to monitor the ability of targeted polymers to adsorb to fibrin coated samples and to block subsequent fibrinogen adsorption [5]. Shown schematically in **Figure 6-1**, this QCM analysis was carried out in a series of steps. First, polystyrene coated quartz crystals were prepared to promote protein adhesion. A layer of fibrinogen was allowed to adsorb to these crystals and was subsequently activated with thrombin to form a fibrin coated surface. After blocking nonspecific adsorption with BSA, the test material was introduced into the sample chamber. After a rinse step, a second fibrinogen adsorption step was carried out and the ability of the materials to suppress this fibrinogen binding was evaluated.

6.2.3.1. Polystyrene Substrate Preparation

Gold coated AT-cut quartz crystals with a fundamental frequency of 5 MHz obtained from Q-Sense were used as model substrates. These crystals were spin coated with polystyrene (PS) to create a uniform hydrophobic surface for fibrin adsorption using modifications of a previously described procedure [222]. Prior to coating with polystyrene, the crystals were cleaned by soaking in toluene for a minimum of two hours and dried in a stream of inert gas. They were subsequently spin coated with a PS solution at 2,500 RPM for 60 seconds using a Cee® 100 spin coater manufactured by Brewer Scientific and dried at 100 ^{o}C in a vacuum oven overnight. Using the parameters

described in **Chapter 5**, the thickness of the PS layer was measured using variable angle spectroscopic ellipsometry. Five samples were analyzed and the PS layer was determined to be 57.1 ± 8.4 nm. In order to ensure the repeatability of this surface preparation procedure, control QCM experiments with no barrier material were conducted periodically throughout the data acquisition and no notable differences were observed in the rate or level of fibrinogen deposition.

6.2.3.2. QCM-D Analysis of Fibrinogen Deposition

A schematic depiction of the QCM experiment is shown schematically **in Figure 6-1**. The model substrate was first coated with a saturated layer of fibrinogen and activated with thrombin to create a surface bound fibrin layer. After blocking non-specific protein adsorption with BSA, the surface was optionally treated with a solution of the protective polymer. A second fibrinogen adsorption step was then conducted. These experiments were conducted in the Q-Sense E4 at 37 ^{o}C with a flow rate of 50 µL/min. Resonant frequency shift (• f) and energy dissipation (D) values were collected for the fundamental frequency and for odd harmonics (n = 1, 3, 5, 7, 9, 11, and 13) using the low noise setting for the duration of the experiment.

After installing four crystals in parallel and verifying their quality (D < 30 ppm in air), TBS was flowed through the system until a stable baseline was obtained. An experiment was started with TBS flowing and, after 5 minutes, a solution of fibrinogen (0.1 mg/mL) was introduced into the system. After exposing the crystals to fibrinogen for 15 minutes, the system was rinsed with TBS for 5 minutes. Thrombin (0.1 U/mL) was then flowed over the crystals for 10 minutes, followed by an additional 5 minute rinse with TBS. BSA (1.0 mg/mL) was allowed to interact with the surfaces for 10 minutes.

After rinsing again with buffer, a solution containing the analyte of interest (0.10 mg/mL in TBS) was introduced and allowed to flow through the system for 5 minutes. Unbound material was washed away with TBS for 5 minutes. A solution of fibrinogen (0.10 mg/mL in TBS) was then introduced and flowed through the system for 25 minutes. Finally, the QCM was rinsed with of TBS for 20 minutes to facilitate the removal of unbound fibrinogen. As a control, the same procedure was followed without the addition of polymer solution or the subsequent buffer rinse. Each material was evaluated in a minimum of three experiments.

Following each experiment, the QCM flow cells and all tubing were flushed with copious amounts of acidic ethanol (10% acetic acid in ethanol) followed by pure ethanol. The inability to obtain a stable baseline with consistent results without this cleaning process suggests the presence of residual protein or polymer in the system. The effectiveness of this cleaning procedure was verified by performing multiple experiments and confirming that the observed frequency and dissipation shifts were consistent. Finally, a stream of nitrogen was used to dry the QCM-D and the crystals were placed in a bath of toluene to remove the PS coating.

6.2.4. Kinetic Determination of FGM Propagation using Fibrin Turbidity Assay

Previous studies have demonstrated that surface adsorbed fibrin layers formed in this manner retain approximately five active thrombin molecules per fibrinogen molecule after rinsing with buffer solution [223]. These surfaces, then, can react with fibrinogen solutions to form a fibrin gel on the surface. A microplate assay was employed to monitor the reaction of surface bound fibrin with solution phase fibrinogen after treatment with various materials and to investigate the structure of the resulting fibrin gels [224-225].

6.2.4.1. Preparation of Fibrin Gel Substrate

A Costar high binding 96-Well EIA/RIA plate was used to maximize the strength of interaction between the fibrin gel and the microplate. In order to create a stable gel on the surface, fibrinogen (50 µL, 2.0 mg/mL), thrombin (20 µL, 2.5 U/mL), and calcium chloride (10 µL, 100 mM) were added to each well. The resulting gel was allowed to cure for 5 hours at room temperature. Each well was then rinsed twice with 200 µL TBS, and care was taken to avoid removing the fibrin gel from the surface. A solution of each material under investigation (50 µL, 0.10 mg/mL in TBS, n = 4) was added to the wells.

6.2.4.2. Assessment of Fibrin Gel Propagation

After treating each gel with the material under investigation, 150 µL of fibrinogen (0.5 mg/mL in TBS) was added to each well. In order to observe the change in turbidity with time, a Cary Win-UV UV-visible spectrophotometer was used to monitor the UV absorbance at 350 nm for 90 minutes with an average time of 0.5 seconds using a two minute collection interval.

6.2.5. Cellular Attachment to Fibrin Gels

In order to test the anti-cellular adhesive properties of these materials, a complementary cell culture study was carried out using the mouse mesenchymal D1 cell line (ATCC CRL-12424) in 24-well tissue culture plates. This pluripotent cell line was selected due to its strong adherence to charged surfaces and wound healing components (e.g., collagen I and fibrin) [209-212].

6.2.5.1. Preparation of Fibrin Gels for Cell Culture Studies

Stable fibrin gels were created in the well plates for use as a substrate to measure cellular attachment. Tris buffered saline was filtered through a 0.22 μm syringe filter and solutions (13.2 mg/mL fibrinogen, 5 U/mL thrombin, and 100 mM $CaCl_2$) were prepared in a laminar flow hood to minimize microbial contamination. In each well, 152 μL of a fibrinogen solution was subsequently mixed with 40 μL $CaCl_2$ solution and 8 μL thrombin solution to yield a solution that was 10 mg/mL fibrinogen, 20 mM $CaCl_2$, and 0.2 U/mL thrombin. This solution was allowed to gel at room temperature for 1 hour and was then allowed to mature overnight at 4^oC.

6.2.5.2. Cell Culture

After rinsing the wells 3 times with sterile TBS, polymer solutions were added (200 μL, 0.10 mg/mL in sterile TBS) and incubated at 37 ^oC for 90 minutes. The polymer solutions were removed from the wells, and each well was rinsed 3 times with sterile TBS. Each well was then seeded with 250,000 cells in 500 μL Dulbecco's Modified Eagle Medium (DMEM, HyClone Laboratories) containing 10% fetal bovine serum (GIBCO/Invitrogen) and incubated at 37 ^oC for two hours. Untreated tissue culture polystyrene (TCP) fibrin gels with no anti-adhesion barrier were employed as controls, and a minimum of 6 replicates were studied for each material.

After incubation, unattached cells were removed from the wells by rinsing three times with sterile TBS. Representative images of the cells were obtained using an inverted phase contrast microscope. The cells remaining on the surface after rinsing were lysed by sonication in high salt solution (0.05 M NaH_2PO_4, 2 M NaCl, and 2 mM EDTA). DNA contents, measured using Hoechst 33258 stain, were used to quantify the

number of cells in each well [213-214]. In short, Hoechst 33258 (final concentration, 0.5 µg/ml, Sigma) was allowed to react with lysates in the dark for 10 minutes, after which fluorescence was measured ($\bullet_{ex}$ = 356 nm and $\bullet_{em}$ = 458 nm). An exponential calibration curve was prepared using samples with known DNA concentrations (0.16 – 5.0 µg/mL). After measuring the fluorescence of each well, this calibration was employed to determine concentration of DNA in each well. Since the duration of the experiment was not long enough for appreciable cell growth to occur, this value was used as a measure of the number of cells attached in each well.

6.2.6. Statistical Analysis

For comparisons, statistical relevance was determined by performing analysis of variance followed by a Sidak pair wise post-hoc analysis using Minitab 15. Each figure was analyzed separately. Differences at greater than 95% and 99% confidence are reported, with statistical significance being considered at the 95% level. Unless otherwise stated, all values are reported as mean ± standard error.

In order to understand the impact of the molecular architecture on the various performance parameters evaluated, an additional statistical analysis was conducted. This modeling included the 16 block copolymers described in **Table 6-1**. The responses from the QCM analysis, turbidity assay, and cellular attachment study, were included in this analysis. For each response, ANOVA was carried out by fitting a general linear model using the variables of PEG chain length, number of PEG units, number of monomer units in the polymer backbone, peptide type, and number of peptide units per polymer molecule.

For each model, residual plots, including a normal probability plot, a frequency plot, and standardized residual plots were generated. These plots were used to verify the validity of the assumptions made in the general linear model. If the residuals are normally distributed, the normal probability plot is expected to show a linear trend with minor deviations in the tails. In addition, the frequency plot should by symmetrical with approximately 95% of the values within the range of ± 2 [226]. Finally, no apparent bias should be observed in the standardized residual plots [227-229]. In cases where apparent deviations from normality were observed, the analysis was repeated after removal of outliers to ensure that the trends predicted by model were unaffected. Main effects plots were then generated for each model in order to understand the impact of each factor. No outliers were removed from the analysis.

6.3. Results

The studies conducted provided data with a wide range of responses and, in most cases, low variability. If outliers were observed for a given model, they have been identified. The wealth of information that was obtained from these results provides the basis for a thorough understanding of the performance of the materials as a function of the structure of the polymer and the number and composition of the targeting moieties. In addition, the nature of any outliers provides insight into the limitation of the statistical model employed and can be interpreted to provide additional mechanistic information.

6.3.1. QCM Analysis

As can be seen in **Figure 6-2**, the energy dissipation observed with the fibrinogen coated samples (• $D = 4 - 8 \times 10^{-6}$) was much greater than what was seen in SAM

experiments (• D = 0.5 – 3 x 10^{-6}, see **Figure 5-7**). As a result, the approximations employed in the Sauerbrey model are not valid, and the mass adsorbed on the surface could not be accurately determined. Instead, raw frequency response data was employed to extract pseudo-first order parameters for the maximum fibrinogen adsorption and the kinetic rate constant for the two fibrinogen adsorption events.

Since the goal of these studies is to assess the ability of the materials to inhibit the adsorption of fibrinogen to a surface bound fibrin layer, two kinetic parameters are reported. First, the maximum fibrinogen adsorption observed in the second fibrinogen adsorption step was determined using a least squares analysis in Excel®. This value was then normalized to the first fibrinogen response and is reported as the ratio, $\left(\frac{Fg_2}{Fg_1}\right)$. In addition, the pseudo-first order kinetic half-life ($t_{½,Fib}$) of the second fibrinogen adsorption step was determined using a least squares analysis in Excel®.

The data in **Figure 6-3** – **Figure 6-5** present the frequency response for the materials studied. The mass of fibrinogen adsorbed in the second step was found to be dependent upon the nature of the barrier material employed. The ratio for the control samples with no polymer ($\frac{Fg_2}{Fg_1}$ = 0.54 ± 0.05), is shown on the figures as a horizontal line for reference. Statistical differences are indicated on the graphs. The P3 polymer conjugate with the high level of peptide conjugation (P3-H), which appears to be missing from the data, exhibited complete suppression of the second fibrinogen step in three experiments. As a result, all frequency responses for this material are reported as zero. Several other materials, including the peptide controls and the P4 conjugates and the PMAA conjugates PMAA-L and PMAA-S, exhibited significant levels of inhibition of the fibrinogen adsorption ratio. Several of the unconjugated polymers (PMAA, P2, and

P4) increased the second fibrinogen adsorption ratio dramatically (116%, 384%, and 195%, respectively). The low level peptide conjugates of the long PEG chain polymers (P1-L and P3-L) failed to demonstrate suppression of fibrinogen adsorption.

From the residual plots for fibrinogen adsorption, shown in **Figure 6-6**, it is seen that, with the exception of two notable outliers (P2 and P4), the normal probability plot is linear and that the residuals are normally distributed. The main effects plots, shown in **Figure 6-7**, indicate that the fibrinogen ratio decreases with increasing chain length and with increasing PEG chain length. The number of PEG chains per molecule does not show any clear trend. The two peptides reduce the value for the fibrinogen ratio, as does an increase in the number of peptides conjugated to the polymer.

The results of the kinetic analysis for the second fibrinogen adsorption step are presented in **Figure 6-8 – Figure 6-10**. The half-life for the control samples without polymer adsorption ($t_{½}$ = 530 ± 90 s) is shown on these graphs for reference. Since no fibrinogen was observed adsorbing to the surface for PS-3, no value is reported for this material. While there are differences among the materials tested, only PMAA ($t_{½}$ = 1330 ± 160 s) and P2 ($t_{½}$ = 2000 ± 280 s), demonstrated a significant difference in the kinetics of fibrinogen absorption from the control.

The residual plots for the kinetics of fibrinogen adsorption, shown in **Figure 6-11**, confirm that, with the exception of 2 outliers (both P2), the normal probability plot is linear and the residuals are normally distributed. The main effects plots, shown in **Figure 6-12**, indicate that the rate of fibrinogen adsorption is not a strong function of chain length or of the number of PEG chains. The kinetics slow with increasing PEG chain length The two peptides appear to reduce the rate of fibrinogen deposition, as does an

increase in the number of peptides conjugated to the polymer. Because of the relatively thick fibrin surface film and the large size of fibrinogen compared to BSA, the fibrinogen adsorption kinetics are slower that the BSA adsorption kinetics studied in **Chapter 5** by an order of magnitude.

6.3.2. Fibrin Turbidity Assay

In order to assess the ability of the polymers to block the surface growth of the fibrin matrix, a kinetic assay was performed using the data obtained from spectrophotometry. After subtracting the initial absorbance values due to the preexisting fibrin layer in the microplate wells, the increase in turbidity could readily be observed. The rate of turbidity increase was approximated by fitting the initial data with a linear equation and determining the slope of the resulting line. As shown by the data in **Figure 6-13 – Figure 6-15**, the value of this rate varies with the structure of the barrier material. The TBS control exhibited a value of 0.0039 ± 0.0007 min^{-1}. There were no significant differences observed between the samples and the controls. Some statistically significant differences, however, were observed among the polymer samples.

The residual plots for the kinetics of fibrinogen propagation, shown in **Figure 6-16**, confirm that the normal probability plot is linear and the residuals are normally distributed. The main effects plots, **Figure 6-17**, indicate that the rate of fibrinogen propagation is not a strong function of chain length or number of PEG chains. The kinetics slow with increasing PEG chain length and with an increasing number of peptides conjugated to the structure. The CREKA peptide appears to reduce the rate of fibrinogen deposition, while the impact of the CAERK scramble is much less pronounced.

6.3.3. Cellular Attachment

The results of the cellular attachment study, shown in **Figure 6-18** – **Figure 6-20**, indicate that many of the materials significantly reduced the attachment of cells to the model fibrin surface. All of the PMAA polymers result in a significant reduction of cellular attachment, while the majority of the long PEG chain polymers show an effect. There were no significant differences observed with the short PEG chain polymers. As shown in **Figure 6-21**, images taken of the wells indicate that the cells were not uniformly distributed on the fibrin surface. This artifact of the cell loading procedure made accurate visual comparisons of the cells impossible. A comparison of the TCP versus the fibrin control wells, however, is very instructive. The fibrin control showed normalized cellular attachment of 1.00 ± 0.09, while the TCP control had cellular attachment values of 0.30 ± 0.09. This difference, also evident in the images in **Figure 6-21**, results from the greatly enhanced surface area created by the three-dimensional network of the fibrin gel.

The residual plots for the cellular attachment to the fibrin substrate are shown in **Figure 6-22**. With the exception of 1 outlier, the normal probability plot is linear and the residuals are normally distributed. The main effects plots, shown in **Figure 6-23**, suggest that the degree of cellular attachment is not function of the number of PEG units, PEG chain length, or the number of peptide units in the structure. The presence of peptide, both CREKA and CAERK, appears to promote cellular attachment. While no clear trend is evident in the performance as a function of polymer chain length, the longest polymer appears to provide enhanced resistance to cellular attachment.

6.4. Discussion

The quartz crystal microbalance proved to be a very informative means to study the fibrinogen adsorption. Unlike the previous study (see **Chapter 5**), it was impossible to quantify the rate or degree of polymer adsorption to the model surfaces. The presence of the water-rich surface layer of fibrinogen resulted in high levels of energy dissipation and is probably responsible for this inability to discern the adsorption of these barrier materials. As has previously been described, the level of the second fibrinogen adsorption was normalized and reported as the ratio of the second fibrinogen adsorption step to the first ($\frac{\mathrm{Fg}\,2}{\mathrm{Fg}\,1}$). This technique was employed in order to eliminate the effect of the variability observed in the first fibrinogen adsorption step that resulted from a degraded frequency response as QCM crystals were repeatedly reused.

Numerous properties of targeted block copolymers have been investigated to assess their ability to interrupt the physiological processes that lead to the formation of an extended gel matrix. Since this FGM formation is a prerequisite to the formation of post surgical adhesions, it is believed that the finding from these studies will be readily extended to understand the impact on material properties to the ability to reduce PSA formation. A summary of the effects of molecular architecture on these functional properties, summarized in **Table 6-2**, reveals several important relationships that provide insight into the mechanism of action.

The ratio of fibrinogen adsorption in the QCM-D was studied to monitor the ability of these materials to reduce the affinity of surfaces for fibrinogen. It was anticipated that longer PEG chains, longer polymer chains, larger PEG chain density, and a larger density of targeted peptide units would provide increased protection against the

adsorption of fibrinogen to surface bound fibrin layers. This prediction was confirmed in most cases; in fact, the high molecular weight polymer with long PEG chains and a high level of CREKA (P3-H) resulted in the complete suppression of this second fibrin adsorption step. Compared to the rest of the polymer architectures, this structure appears to represent an optimum balance of surface affinity (due to the high peptide content) and protective ability (due to the long PEG chains). The difference observed between the short polymer chain and long polymer chain is also notable. The shorter polymer chains are much less effective at inhibiting fibrinogen adsorption, potentially as a result of the action of the PEG groups on the peptide units. The long PEG chains can articulate and form a hydration shell of approximately the same dimensions as the shorter polymer and shield the attached peptide units from interacting strongly with the fibrin surface. The longer polymer chains extend past this shell and present readily available peptide units to the active surface.

The rate of fibrinogen adsorption, while similar for most of the materials, appears to be slowed for the PMAA and P2 polymers. It is possible that this apparent reduction in rate is an artifact of mass transfer limitations related to the very high level of fibrinogen adsorbed for these materials.

Most of the polymers appear to slow the kinetics of fibrin propagation. Unfortunately, due to the wide degree of variability in the data, very few statistically significant differences were observed in this rate. The phospholipid (EPC), on the other hand, appears to enhance the rate of fibrin propagation. This probably results from the simultaneous growth of phospholipid lamella within the fibrin gel matrix structure. Since

both of these structures can scatter light, such a mechanism would lead to the more rapid turbidity increase.

Cellular attachment studies resulted in several interesting observations. As a result of their highly negative charge, the PMAA polymers were surprisingly effective at reducing the observed cellular attachment. While few statistically significant differences were observed in the level of cellular attachment, all of the materials appear to reduce this response compared to the untreated fibrin control. It can be deduced, then, that all of the materials adsorb to the fibrin gel surface and can reduce cellular attachment through either steric hindrance or charge based repulsion.

Using statistical analysis, it is possible to develop a better understanding of the relationships between the molecular structure and the performance in these experiments. The trends seen in the factor plots can be used to inform decisions about the development of subsequent materials and can serve as the basis for additional mechanistic understanding. Finally, these statistical techniques allow for the identification of potential outliers that may lead to additional understanding of the mechanism or experimental design.

The results obtained from the QCM experiments reveal several trends in the ability of these materials to suppress this fibrinogen adsorption. The trends are summarized in **Table 6-2**. Based on the summary data, it is possible to identify several attributes of the polymer architecture that are important for the attenuation of post surgical adhesion formation. The length of the PEG chains appears to be an important determinants of performance for the materials. Neither the number of PEG chains in each polymer molecule nor the polymer chain length appear to be major factors in assessing

the performance. The largest impact on performance appears to arise from the peptide units. While the number of peptide units appears to be very important, the most unexpected results were observed when assessing the impact of the peptide type on material performance.

For many of the experiments, the number of peptide units conjugated to the polymer is a strong predictor of the material's performance. In most instances, however, the impact of the nature of the peptide was much less pronounces. This result was particularly surprising since CREKA has been shown to be an excellent targeting moiety for protein clots [171-173, 177]. CAERK, on the other hand, was not anticipated to show a high affinity for fibrinogen. While polymers conjugated with CREKA and CAERK both inhibit the degree and rate of subsequent fibrinogen adsorption and reduce the level of cellular attachment to model surfaces, the CREKA-based materials are much more effective at reducing the propagation of fibrin from a surface. These effects may be attributable to differences in the precise nature of the binding epitopes for the two peptide units. Both peptides exhibit an affinity for fibrin and can direct polymeric materials to associate with the fibrin-coated surfaces form barriers to subsequent protein adsorption and cellular attachment. The relative ineffectiveness of the CAERK materials at reducing fibrin polymerization from surfaces suggests that this peptide unit competes less effectively for the binding sites where subsequent fibrinogen polymerization occurs.

The effect of PEG chain length in each of the experiments indicates that longer polyethylene glycol units are more likely to result in a material likely to interrupt the PSA formation process. Longer PEG chains have been shown to result in increasing resistance to protein adsorption, so this result agrees with previously reported observations. The

relationship between an increase in the PEG length and a decrease in the degree and kinetics of fibrinogen adsorption is likely a result of the increasing thickness of the hydrated PEG layer with longer PEG chains. As this layer becomes thicker, not only does the affinity of fibrinogen for the surface layer decrease, but mass transport limitations through this hydrated layer suppress the rate of surface adsorption.

A similar mechanism also explains the ability of the long PEG chain materials to protect surfaces from cellular attachment and to retard the propagation of the fibrin gel matrix. The decrease in cellular attachment results from the inability of proteins to attach to thick, hydrated PEG layers. The decrease in the rate of fibrin propagation may arise from an increase in mass transport limitations due to hydrated PEG layer. In order for the solution phase fibrinogen to polymerize and form a fibrin gel, it must be activated with the surface bound thrombin. If this thrombin is coated with the PEG containing polymer, the fibrinogen must diffuse through this layer to the active site. Longer PEG chains, then, can inhibit the rate of fibrin gel propagation from the model surface more effectively than shorter PEG chains.

Surprisingly, the number of polyethylene glycol chains per polymer molecule does not appear to impact the fibrinogen blocking ability of the materials. Although the level of polymer adsorption could not be directly observed in these experiments, this lack of dependence on the concentration of PEG chains may result from the formation of a surface layer with complete PEG coverage. Once this level of surface saturation is achieved, further adsorption of polymers to the surface is unlikely. This knowledge may provide a means of tailoring the durability of the surface films formed by these materials. Since the desorption of polymers from surfaces should be first order with respect to the

number of polymer chains on a surface, having a larger number of chains on the surface may lead to longer lasting surface protection. Since the number of surface bound polymer molecules appears to be indirectly related to the number of PEG chains per molecule, it may be possible to create longer lasting surface films with similar performance properties by forming polymers with a low number of PEG chains per molecule.

6.5. Conclusion

The techniques employed in this study allowed for a thorough investigation of the relationship between the structure and function for a series of targeted block copolymers. By systematically varying multiple aspects of the molecular architecture and employing statistical analysis to study these structure-function relationships, the complex nature of these materials to inhibit FMG propagation were successfully probed. As was anticipated, the function of these materials was highly dependent on the molecular architecture of the polymer.

As expected, longer PEG chains tend to inhibit all of the potential pathways of PSA that were modeled. While the number of PEG chains in each polymer molecule did not appreciably affect the performance, the impact of the number of peptide units was dramatic. In addition, the subtle differences in the performance of the two peptides support the hypothesis that targeting can be used to direct the performance of materials to interrupt the formation of the fibrin gel matrix and prevent the formation of post surgical adhesions. Although the CREKA functionalized polymers functioned very well in all tests, the CAERK scramble signaled similar efficacy in many cases. This observation suggests that CAERK may also be an effective targeting unit for the fibrin molecule. The relationships between the molecular architecture and performance provide valuable

insight and form a knowledge base that can be used to inform future investigations of biomaterials for PSA prevention.

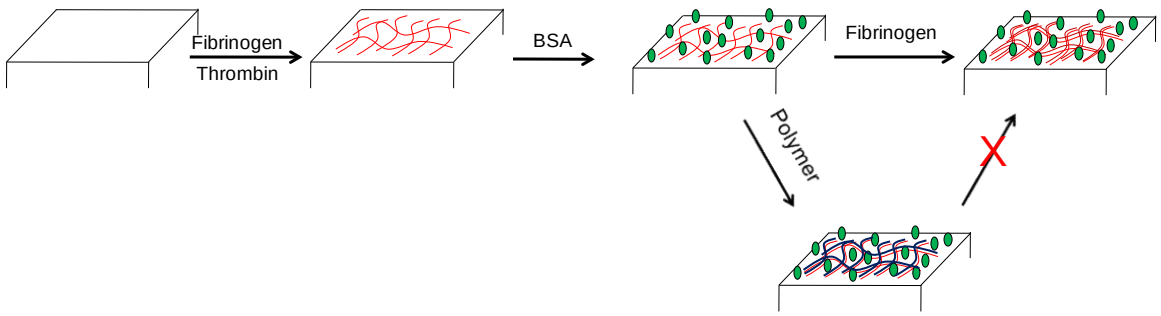

Figure 6-1 Schematic representation of proposed fibrin blockade mechanism in QCM analysis.
A surface-bound fibrin film is first generated by adsorption to the polystyrene surface and activation with fibrinogen. After blocking uncoated surface sites with BSA, a second fibrinogen adsorption step is carried out, and a large amount of fibrinogen is observed adsorbing to the surface. If the initial fibrin layer is treated with a polymeric adhesive barrier material, the amount of fibrinogen adsorbed in this second step can be greatly reduced.

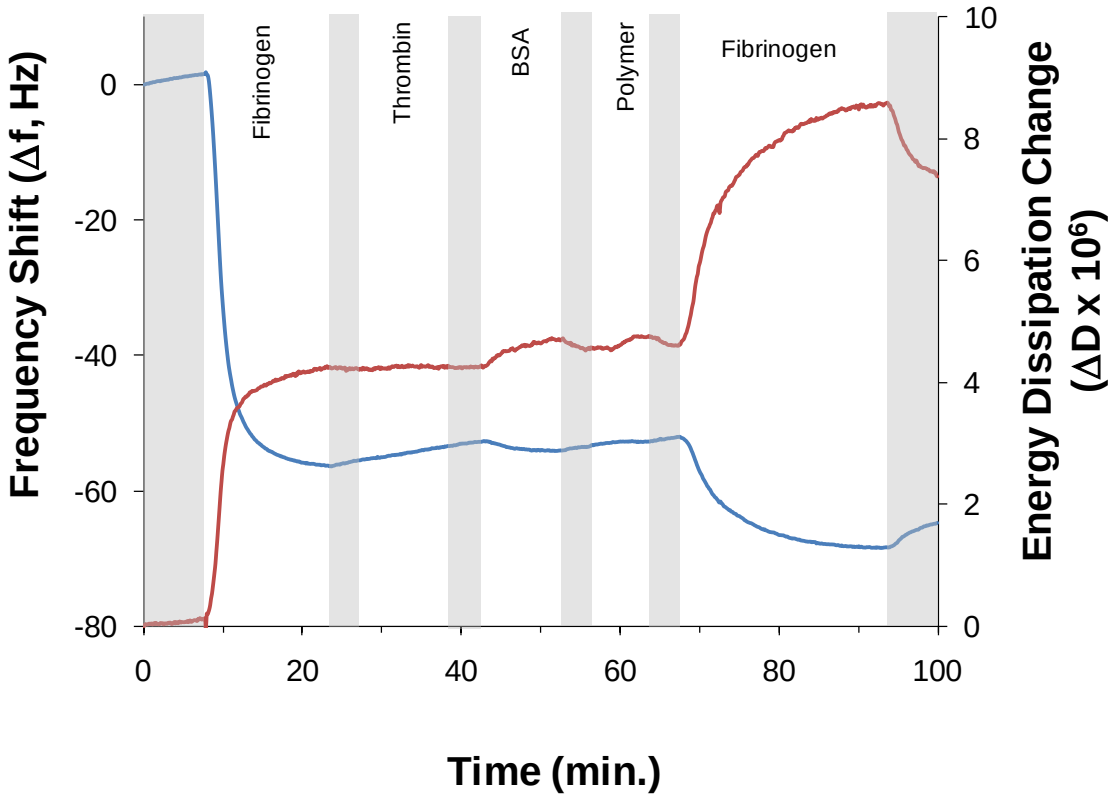

Figure 6-2 Representative QCM sensorgram of fibrinogen suppression study. After establishing a baseline in tris buffered saline (TBS), fibrinogen, thrombin, bovine serum albumin (BSA), polymer, and fibrinogen solutions were introduced into the system sequentially. As indicated by the shaded regions, a TBS wash was employed between solution introductions. The frequency shift (Δf, blue) and energy dissipation change (ΔD, red) were monitored continuously throughout the experiment.

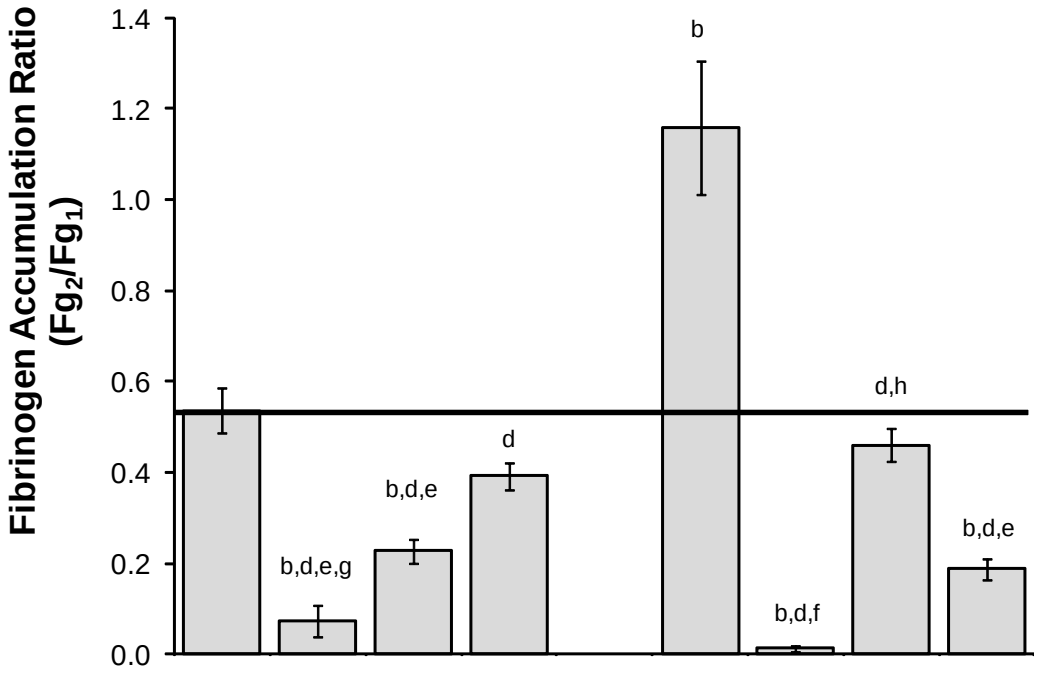

Polymer Chain Length	N/A				18.3			
Peptide Type	N/A	CREKA	CAERK	N/A	N/A	CREKA		CAERK
Number of Peptide Units	-	-	-	-	0	1.9	5.8	2.0
Code	NP	CREKA	CAERK	EPC	PMAA	PMAA-L	PMAA-H	PMAA-S

Figure 6-3 Fibrinogen adsorption ratio for controls and PMAA polymers.
Values (M ± SE) represent the mass ratio seen in the final and initial fibrinogen adsorption steps. The horizontal bar represents the ratio observed for the control samples with no polymer treatment. Statistically significant differences are reported: 99% compared to no polymer (b), 99% compared to PMAA (d), 95% compared to PMAA-H (e), 99% compared to PMAA-H (f), 95% compared to EPC (g), and 99% compared to EPC (h).

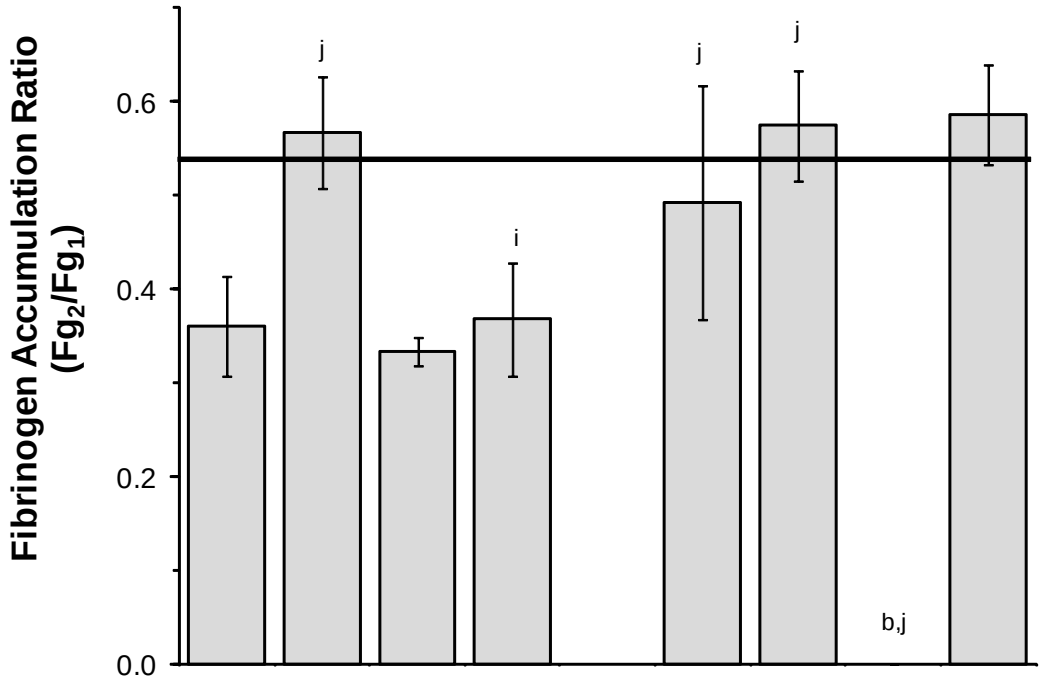

Polymer Chain Length	18.4				30.9			
Peptide Type	N/A	CREKA		CAERK	N/A	CREKA		CAERK
Number of Peptide Units	0	2.3	6.7	2.4	0	2.2	6.6	2.2
Code	P1	P1-L	P1-H	P1-S	P3	P3-L	P3-H	P3-S

Figure 6-4 Fibrinogen adsorption ratio for long (M_N = 1,100) PEG chain polymers. Values (M ± SE) represent the mass ratio seen in the final and initial fibrinogen adsorption steps. The horizontal bar represents the ratio observed for the control samples with no polymer treatment. No absorption was observed for P3-H in the second adsorption step. Statistically significant differences are reported: 99% compared to no polymer (b), 95% compared to P3-H (i), and 99% compared to P3-H (j).

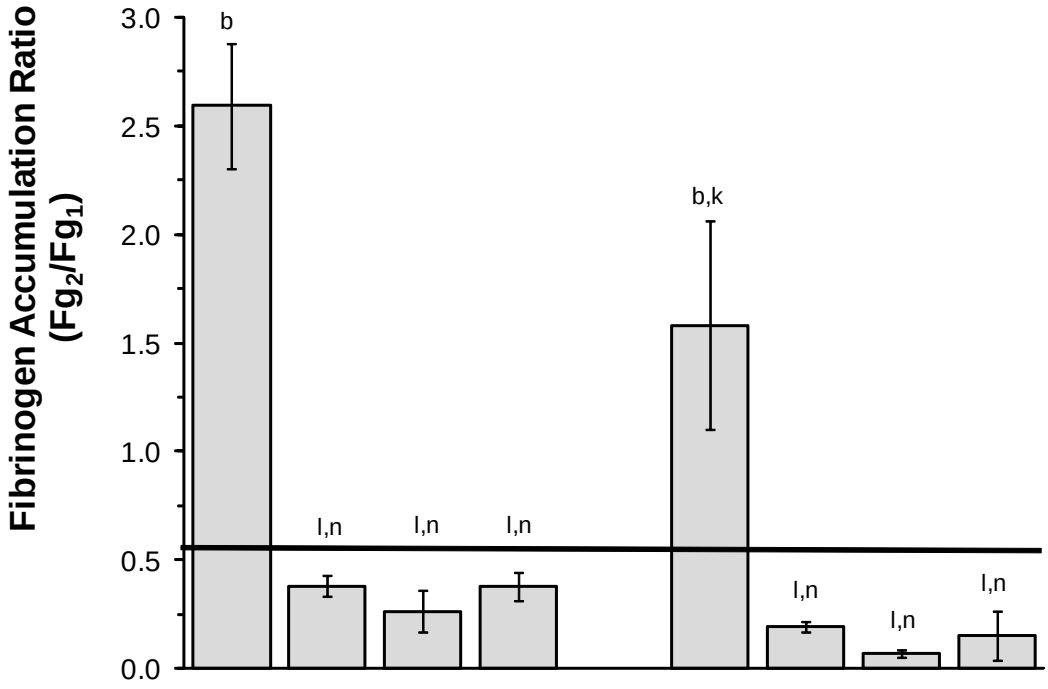

Polymer Chain Length	18.2				22.1			
Peptide Type	N/A	CREKA		CAERK	N/A	CREKA		CAERK
Number of Peptide Units	0	2.4	7.4	2.4	0	2.3	7.1	2.3
Code	P2	P2-L	P2-H	P2-S	P4	P4-L	P4-H	P4-S

Figure 6-5 Fibrinogen adsorption ratio for short PEG (M_N = 300) chain polymers. Values (M ± SE) represent the mass ratio seen in the final and initial fibrinogen adsorption steps. The horizontal bar represents the ratio observed for the control samples with no polymer treatment. Statistically significant differences are reported: 99% compared to no polymer (b), 95% compared to P2 (k), 99% compared to P2 (l), and 99% compared to P4 (n).

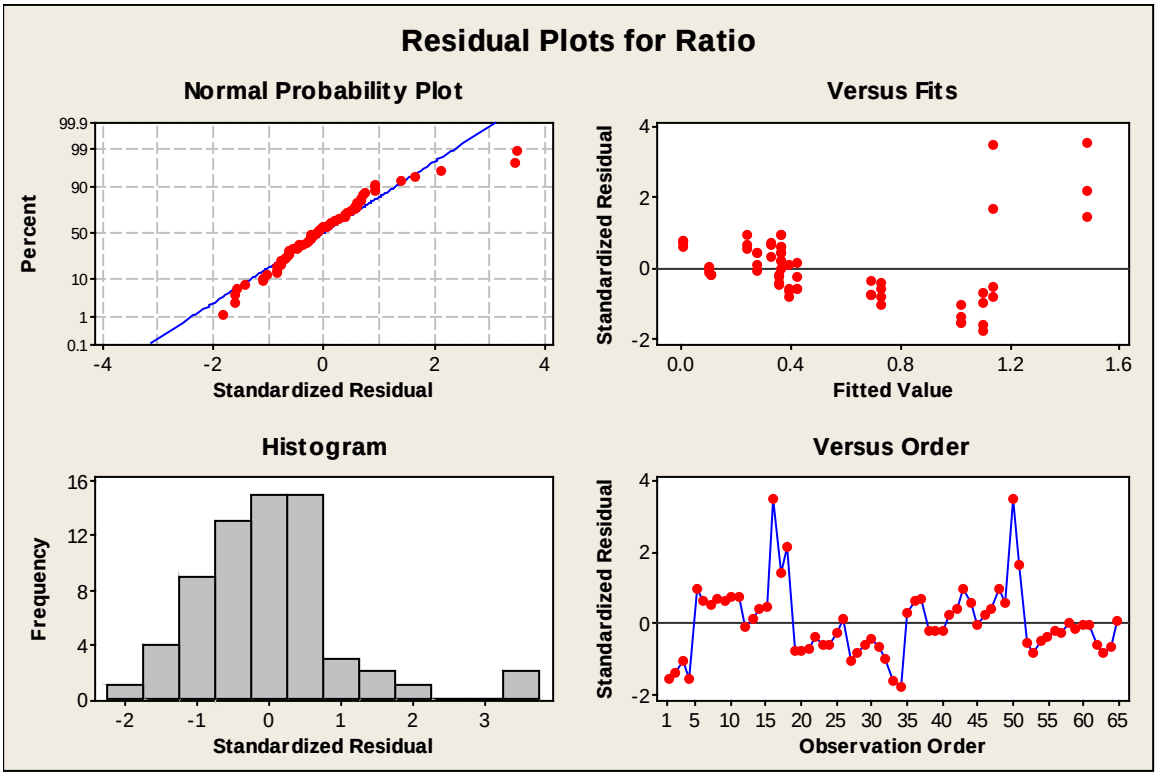

Figure 6-6 Residual plots for fibrinogen adsorption ratio.
The validity of the general linear model used for the ANOVA for the fibrinogen adsorption ratio is confirmed by the residual plots. The linearity of the normal probability plot and random distribution observed in the standardized residual plots indicate a lack of bias in the model fit. The histogram of standardized residuals indicates a normal distribution of residuals. In addition, the vast majority of the residuals are within the expected range of ± 2 standard deviations. The two outliers with standardized residuals above 3 result from the wide variability in the data for the short PEG chain polymers without peptide conjugation (P2 and P4).

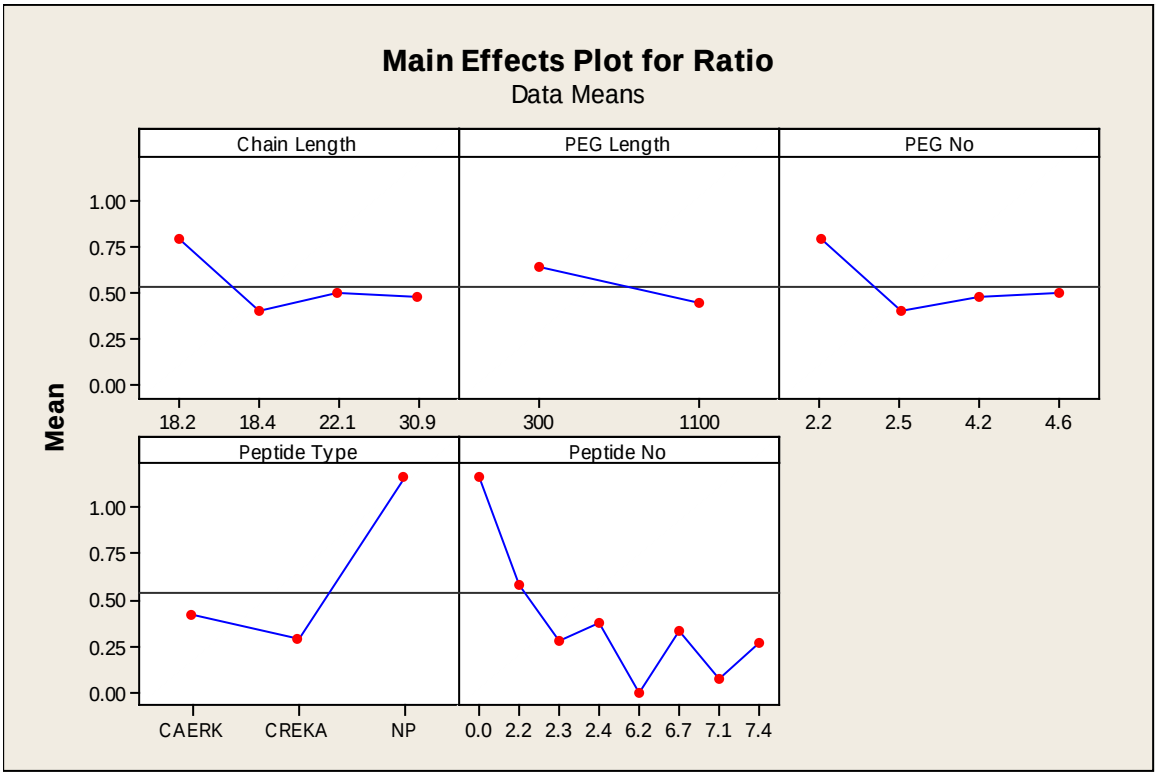

Figure 6-7 Main effects plot for fibrinogen adsorption ratio.

The main effects plots for the ratio of fibrinogen adsorption provide insight into the importance of the various aspects of polymer architecture that were investigated. As indicated by the strong dependence of the response to the number of peptide units (Peptide No) and the peptide type, these two factors have the most influence on the performance in this experiment. The existence of peptide units in the polymer is of critical importance, while the impact of peptide type is unclear. More peptide units lead to a decrease in the observed fibrinogen ratio. Increases PEG length decrease the fibrinogen adsorption ratio, while no statistically significant trend is evident with changes in the number of PEG groups in each polymer molecule or in the overall chain length.

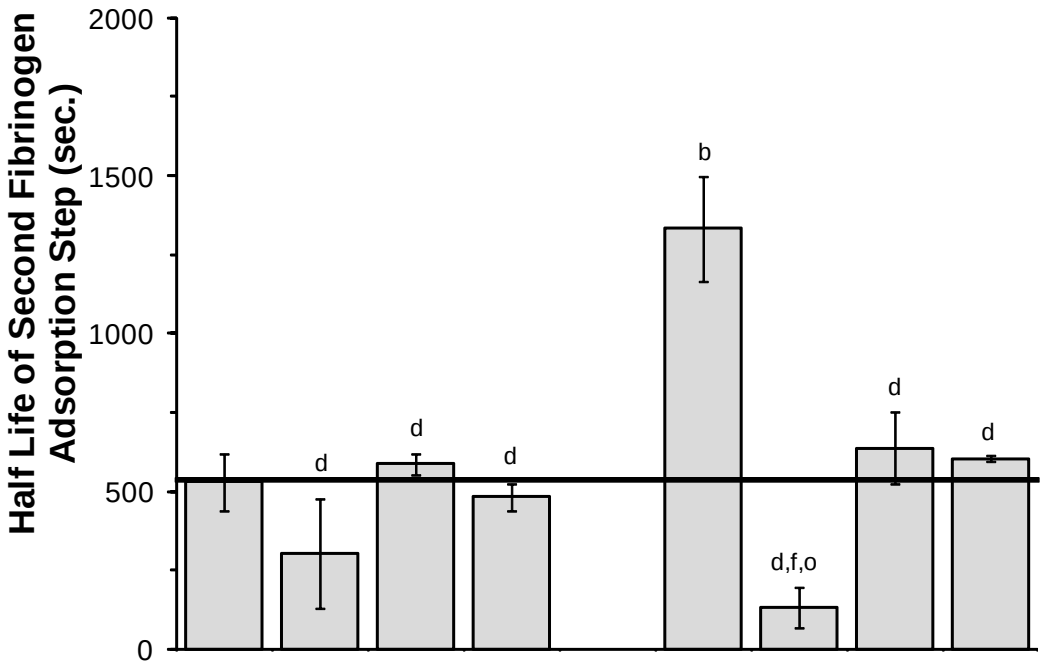

Polymer Chain Length	N/A				18.3			
Peptide Type	N/A	CREKA	CAERK	N/A	N/A	CREKA		CAERK
Number of Peptide Units	-	-	-	-	0	1.9	5.8	2.0
Code	NP	CREKA	CAERK	EPC	PMAA	PMAA-L	PMAA-H	PMAA-S

Figure 6-8 Fibrinogen adsorption kinetics for controls and PMAA polymers. Values (M ± SE) represent the kinetic half-life seen in the second fibrinogen adsorption step. The horizontal bar represents the half-life observed for the control samples with no polymer treatment. Statistically significant differences are reported: 99% compared to no polymer (b), 99% compared to PMAA (d), 99% compared to PMAA-H (f), and 95% compared to CAERK (o).

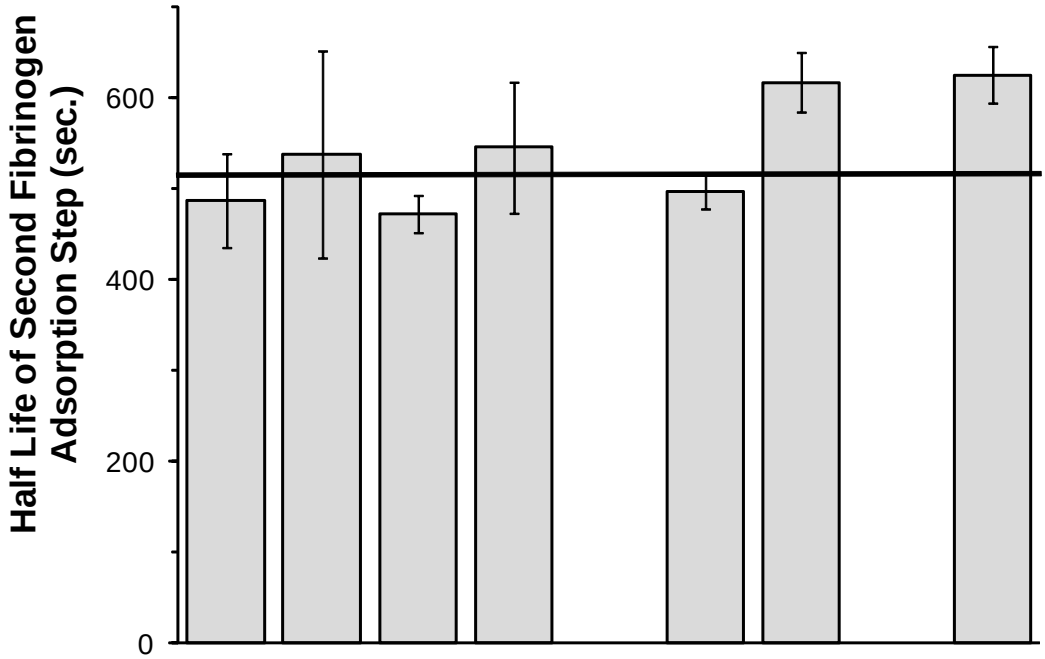

Polymer Chain Length	18.4				30.9			
Peptide Type	N/A	CREKA		CAERK	N/A	CREKA		CAERK
Number of Peptide Units	0	2.3	6.7	2.4	0	2.2	6.6	2.2
Code	P1	P1-L	P1-H	P1-S	P3	P3-L	P3-H	P3-S

Figure 6-9 Fibrinogen adsorption kinetics for long PEG chain (M_N = 1,100) polymers.
Values (M ± SE) represent the kinetic half-life seen in the second fibrinogen adsorption step. The horizontal bar represents the half-life observed for the control samples with no polymer treatment. No statistically significant differences were observed.

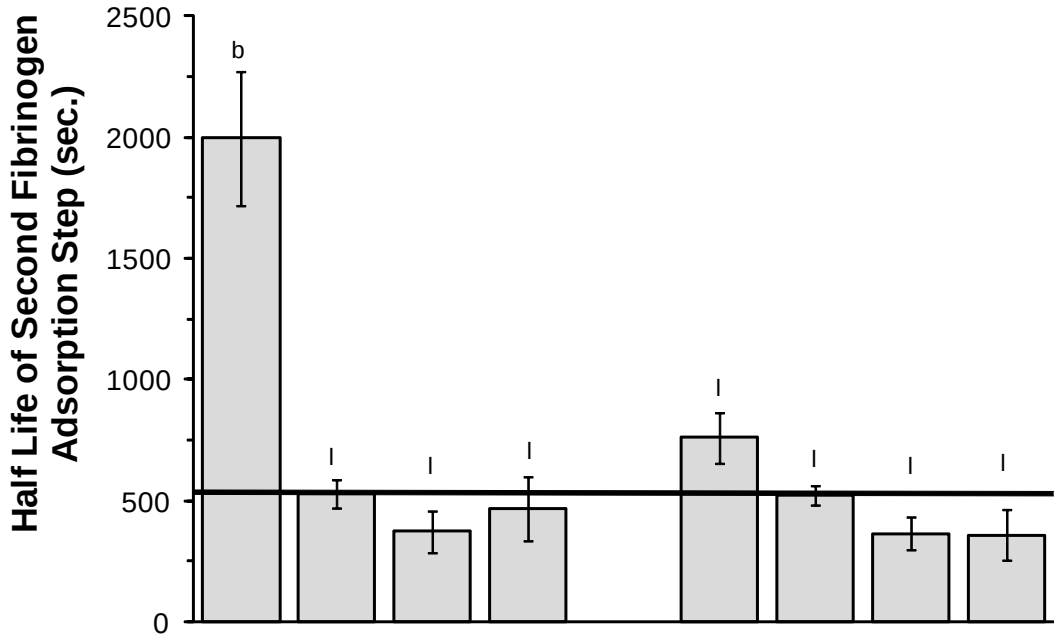

Polymer Chain Length	18.2				22.1			
Peptide Type	N/A	CREKA		CAERK	N/A	CREKA		CAERK
Number of Peptide Units	0	2.4	7.4	2.4	0	2.3	7.1	2.3
Code	P2	P2-L	P2-H	P2-S	P4	P4-L	P4-H	P4-S

Figure 6-10 Fibrinogen adsorption kinetics for short PEG chain (M_N = 300) polymers. Values (M ± SE) represent the kinetic half-life seen in the second fibrinogen adsorption step. The horizontal bar represents the half-life observed for the control samples with no polymer treatment. Statistically significant differences are reported: 99% compared to no polymer (b), and 99% compared to P2 (l).

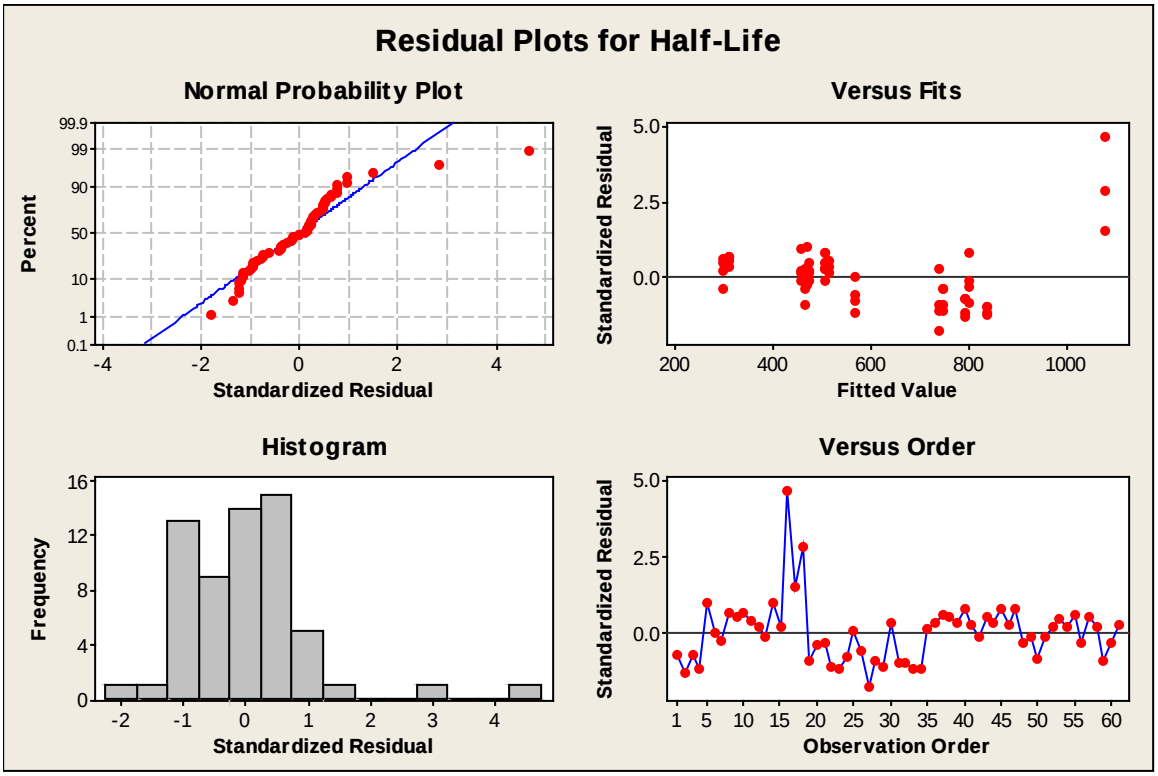

Figure 6-11 Residual plots for the kinetic half-life of the second fibrinogen adsorption step in QCM experiments.

The validity of the general linear model used for the ANOVA for the half-life of the second fibrinogen adsorption step is supported by the residual plots. There are, however, two apparent outliers, both for the short PEG chain polymer with no peptide (P2). With the exception of these outliers, the linearity of the normal probability plot and random distribution observed in the standardized residual plots indicate a lack of bias in the model fit. The histogram of standardized residuals suggests a normal distribution of residuals. Excepting the two outliers, all of the residuals are within the expected range of ± 2 standard deviations.

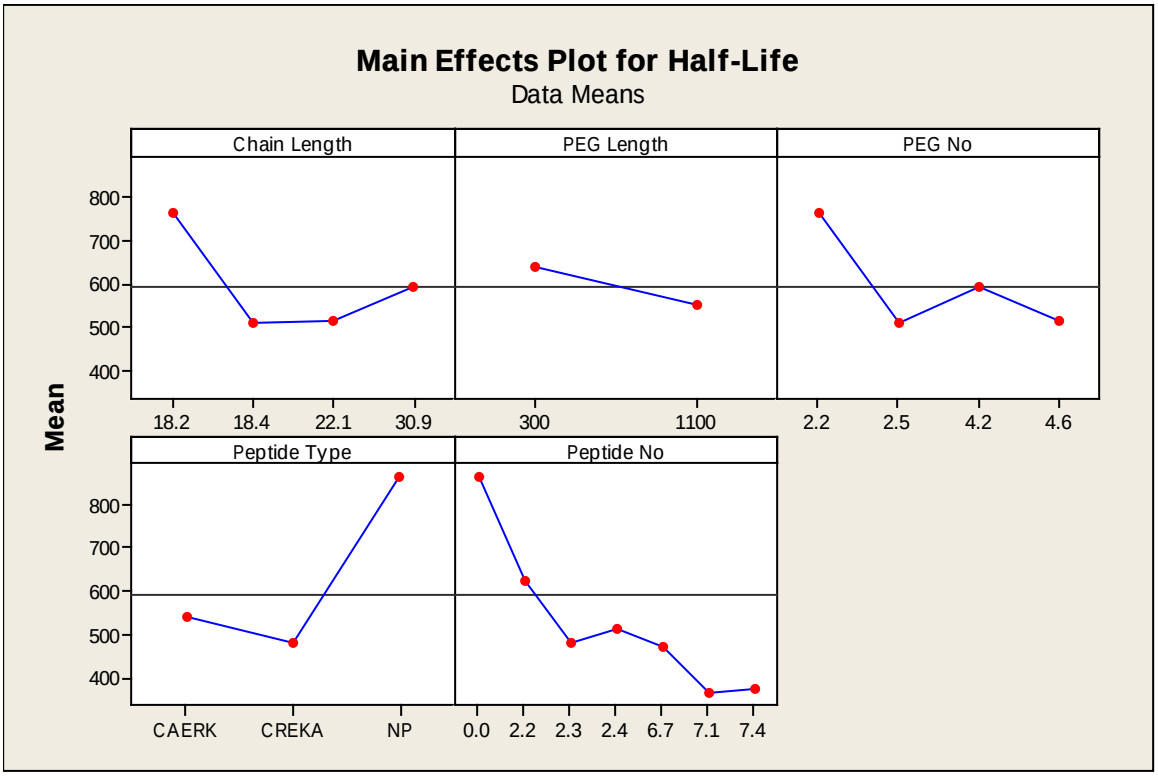

Figure 6-12 Main effects plots for the kinetic half-life of second fibrinogen adsorption step.

The main effects plots for the half-life of the second fibrinogen adsorption step provide insight into the importance of the various aspects of polymer architecture that were investigated. As indicated by the strong dependence of the response to the peptide type this factor has the largest influence on the performance in this experiment. The presence of peptide units in the polymer is of critical importance, while the impact of peptide type is unclear. Increases in PEG length and in the number of PEG units appear to decrease rate of fibrinogen deposition. No statistically significant trend is evident with changes in the overall chain length of the polymer or with the number of peptide units.

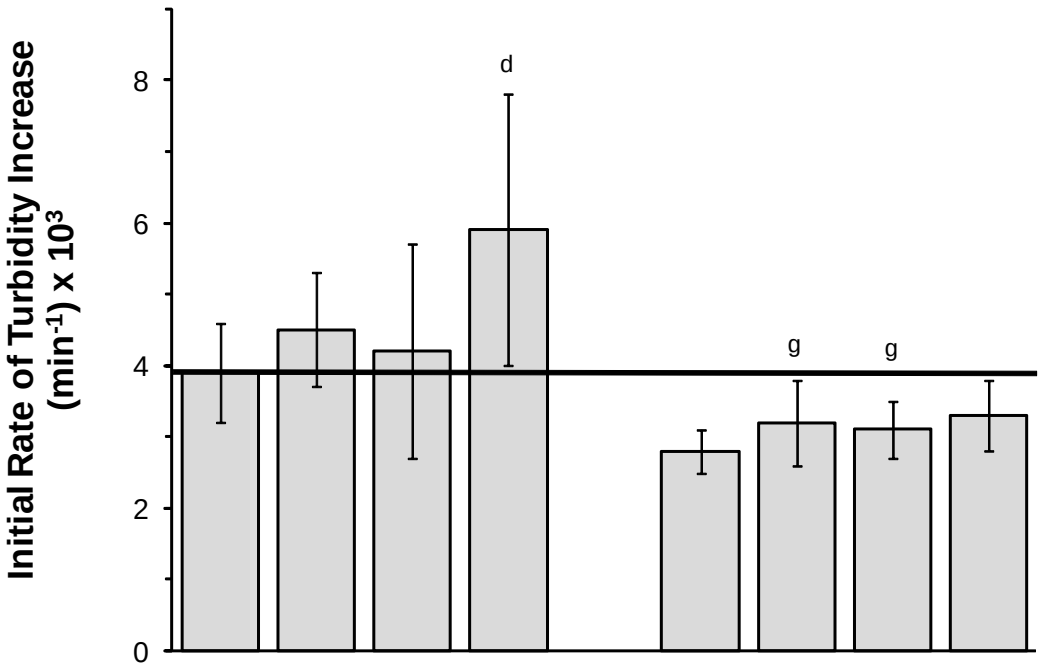

Polymer Chain Length	N/A				18.3			
Peptide Type	N/A	CREKA	CAERK	N/A	N/A	CREKA		CAERK
Number of Peptide Units	-	-	-	-	0	1.9	5.8	2.0
Code	NP	CREKA	CAERK	EPC	PMAA	PMAA-L	PMAA-H	PMAA-S

Figure 6-13 Kinetic analysis of fibrin gel propagation from fibrin surface for controls and PMAA polymers.
Values (M ± SE) represent the initial rate of turbidity increase observed during fibrin propagation. The horizontal bar represents the half-life observed for the control samples with no polymer treatment. Statistically significant differences are reported: 99% compared to PMAA (d), and 95% compared to EPC (g).

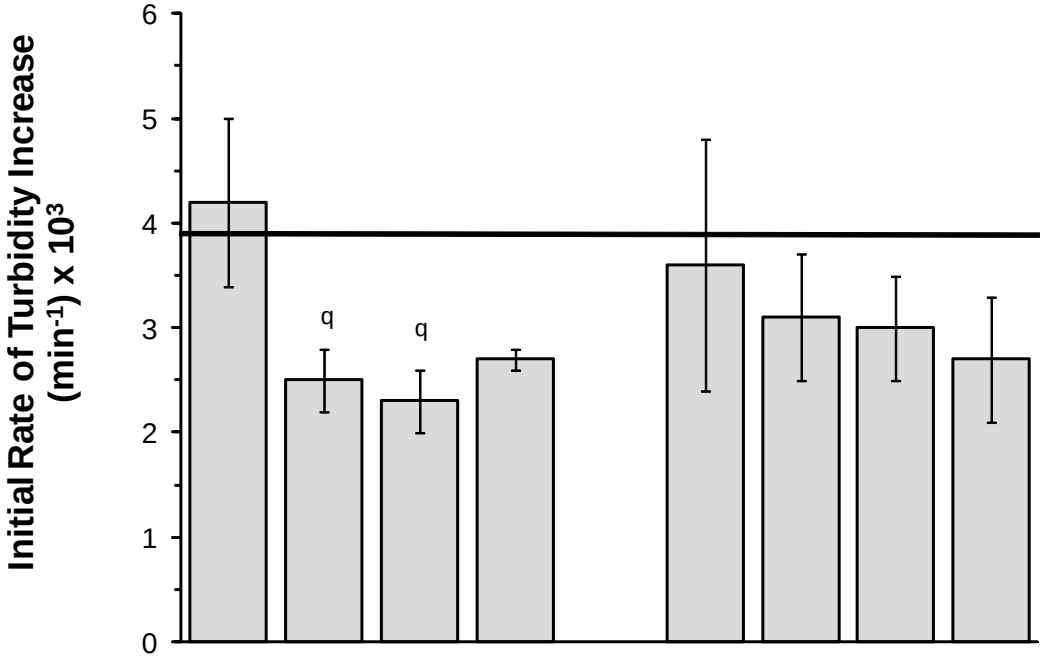

Polymer Chain Length	18.4				30.9			
Peptide Type	N/A	CREKA		CAERK	N/A	CREKA		CAERK
Number of Peptide Units	0	2.3	6.7	2.4	0	2.2	6.6	2.2
Code	P1	P1-L	P1-H	P1-S	P3	P3-L	P3-H	P3-S

Figure 6-14 Kinetic analysis of fibrin gel propagation from fibrin surface for long PEG chain (M_N = 1,100) polymers.
Values (M ± SE) represent the initial rate of turbidity increase observed during fibrin propagation. The horizontal bar represents the half-life observed for the control samples with no polymer treatment. Statistically significant differences are reported: 95% compared to P1 (q).

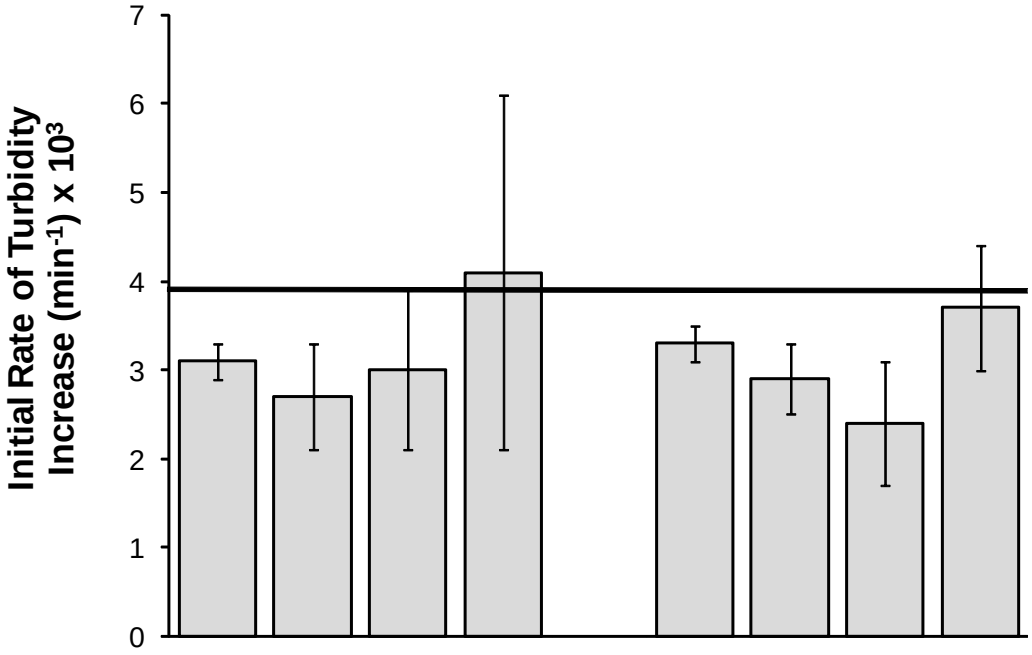

Polymer Chain Length	18.2				22.1			
Peptide Type	N/A	CREKA		CAERK	N/A	CREKA		CAERK
Number of Peptide Units	0	2.4	7.4	2.4	0	2.3	7.1	2.3
Code	P2	P2-L	P2-H	P2-S	P4	P4-L	P4-H	P4-S

Figure 6-15 Kinetic analysis of fibrin gel propagation from fibrin surface for short PEG chain (M_N = 300) polymers.
Values (M ± SE) represent the initial rate of turbidity increase observed during fibrin propagation. The horizontal bar represents the half-life observed for the control samples with no polymer treatment. No statistically significant differences were observed.

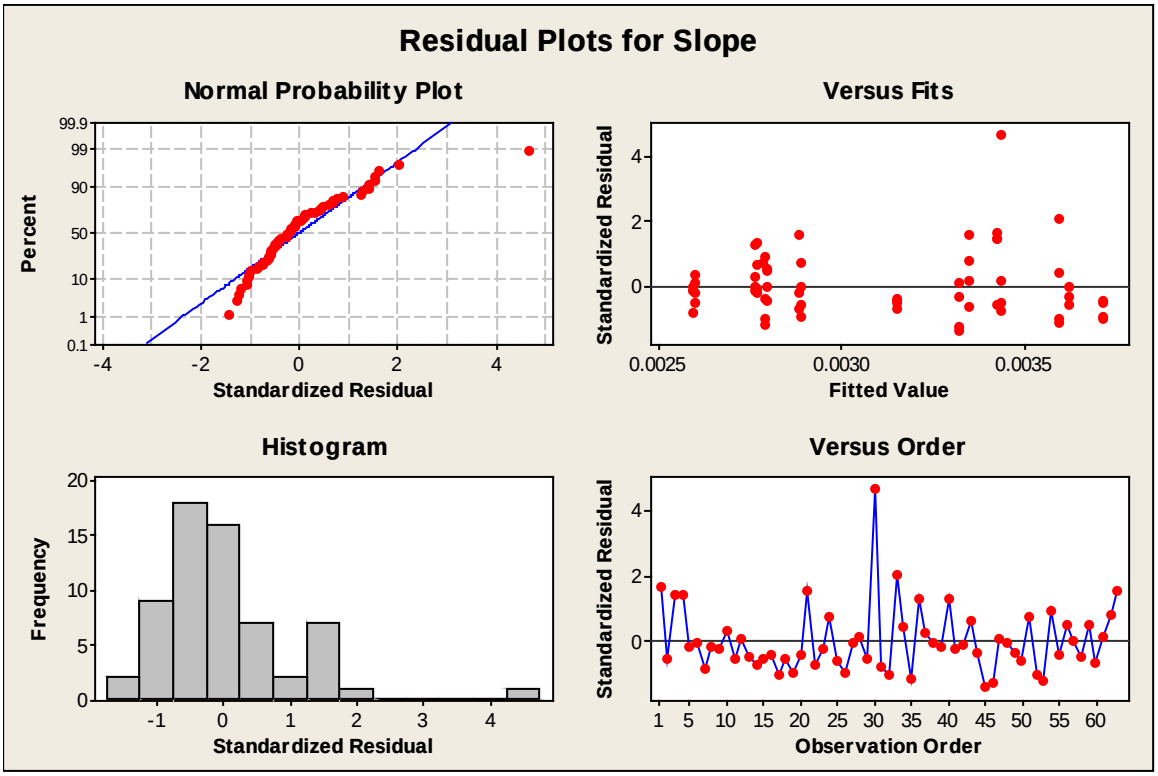

Figure 6-16 Residual plots for kinetic analysis of fibrin gel propagation from fibrin surface.

The validity of the general linear model used for the ANOVA for the kinetic analysis of fibrin gel propagation is supported by the residual plots. There is, however, one apparent outlier, that results from the short PEG chain polymer with no peptide (P2). With the exception of this outlier, the linearity of the normal probability plot and random distribution observed in the standardized residual plots indicate a lack of bias in the model fit. The histogram of standardized residuals suggests a normal distribution of residuals. Excepting the outlier, all of the residuals are within the expected range of ± 2 standard deviations.

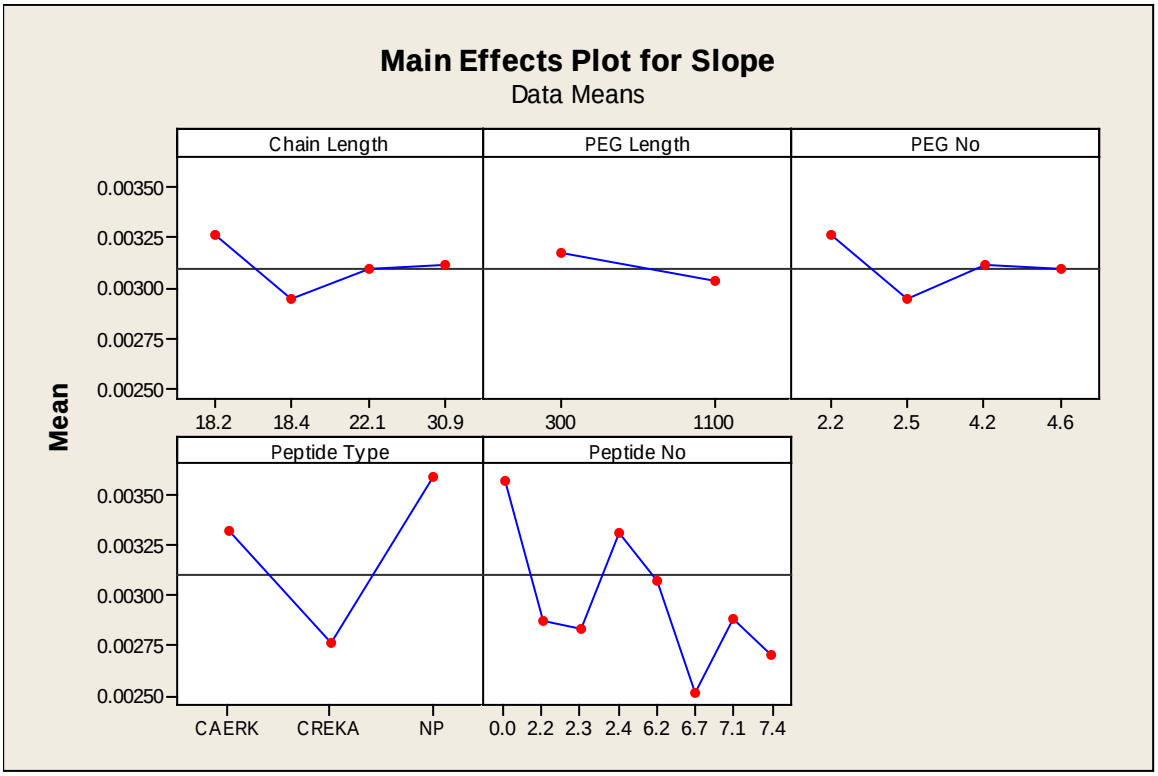

Figure 6-17 Main effects plots for the kinetics of fibrin propagation.

The main effects plots for the kinetics of fibrin propagation provide insight into the importance of the various aspects of polymer architecture that were investigated. As indicated by the strong dependence of the response to the number of peptide units (Peptide No) and the peptide type, these two factors have the largest influence on the performance in this experiment. The type of peptide units in the polymer is of critical importance. No statistically significant trends were observed with changes in the number of peptide units, PEG chain length, or overall chain length.

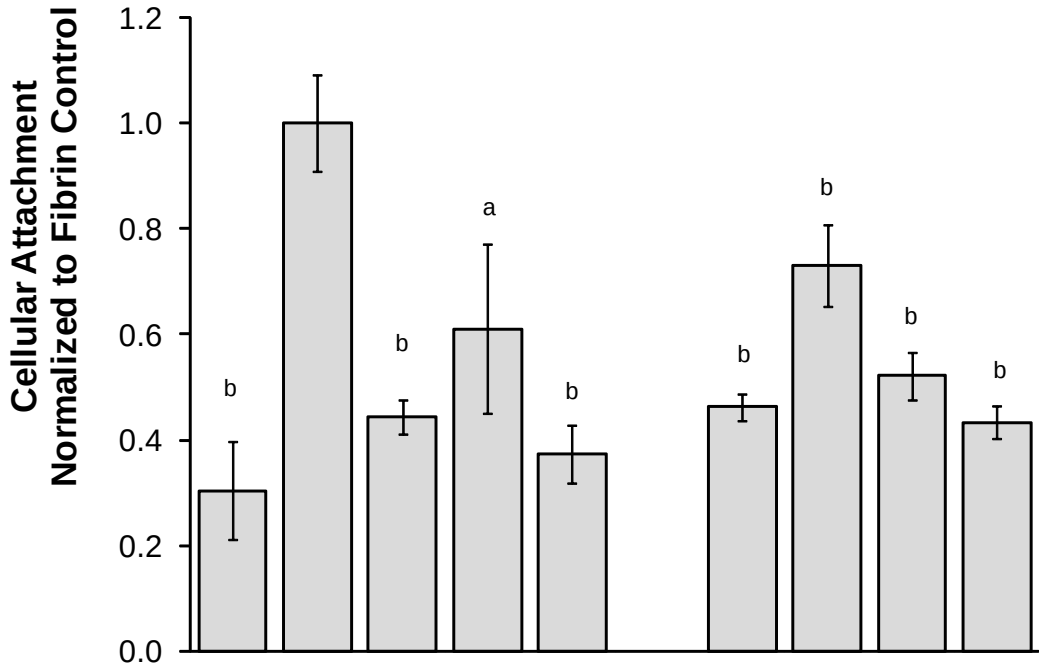

Polymer Chain Length	N/A					18.3			
Peptide Type	N/A	N/A	N/A	CREKA	CAERK	N/A	CREKA		CAERK
Number of Peptide Units	-		-	-	-	0	1.9	5.8	2.0
Code	TCP	Fibrin	EPC	CREKA	CAERK	PMAA	PMAA-L	PMAA-H	PMAA-S

Figure 6-18 Normalized cellular attachment data for controls and PMAA polymers. Values (M ± SE) represent the degree of cellular attachment, based on DNA assay, normalized to fibrin controls. Statistically significant differences are reported: 95% compared to no polymer (a), and 99% compared to no polymer (b).

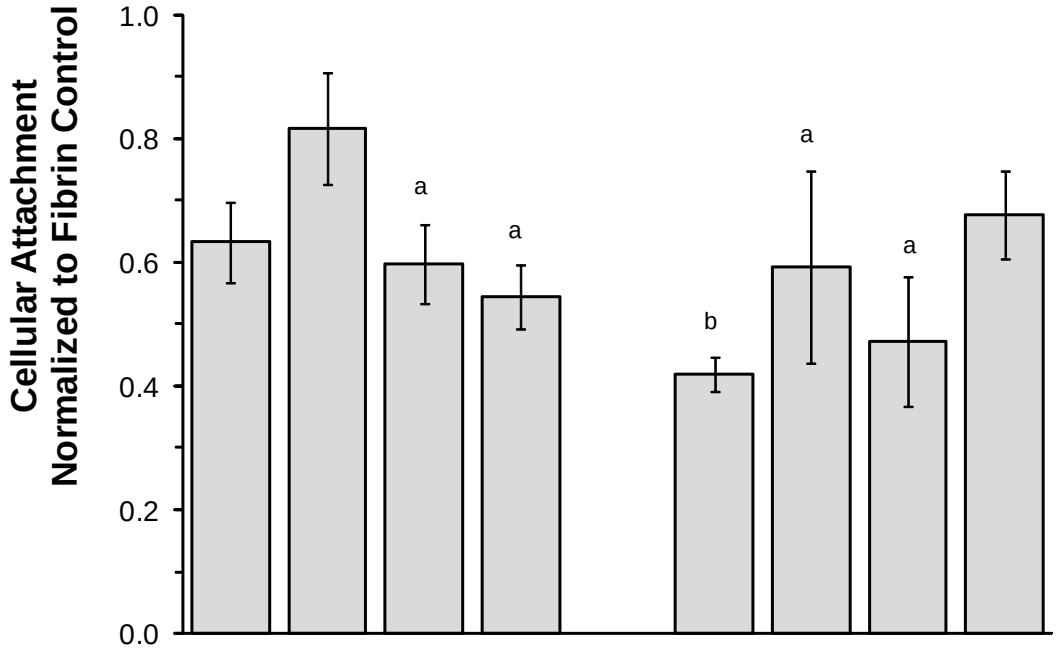

Polymer Chain Length	18.4				30.9			
Peptide Type	N/A	CREKA		CAERK	N/A	CREKA		CAERK
Number of Peptide Units	0	2.3	6.7	2.4	0	2.2	6.6	2.2
Code	P1	P1-L	P1-H	P1-S	P3	P3-L	P3-H	P3-S

Figure 6-19 Normalized cellular attachment data for long PEG chain (M_N = 1,100) polymers.
Values (M ± SE) represent the degree of cellular attachment, based on DNA assay, normalized to fibrin controls. Statistically significant differences are reported: 95% compared to no polymer (a), and 99% compared to no polymer (b).

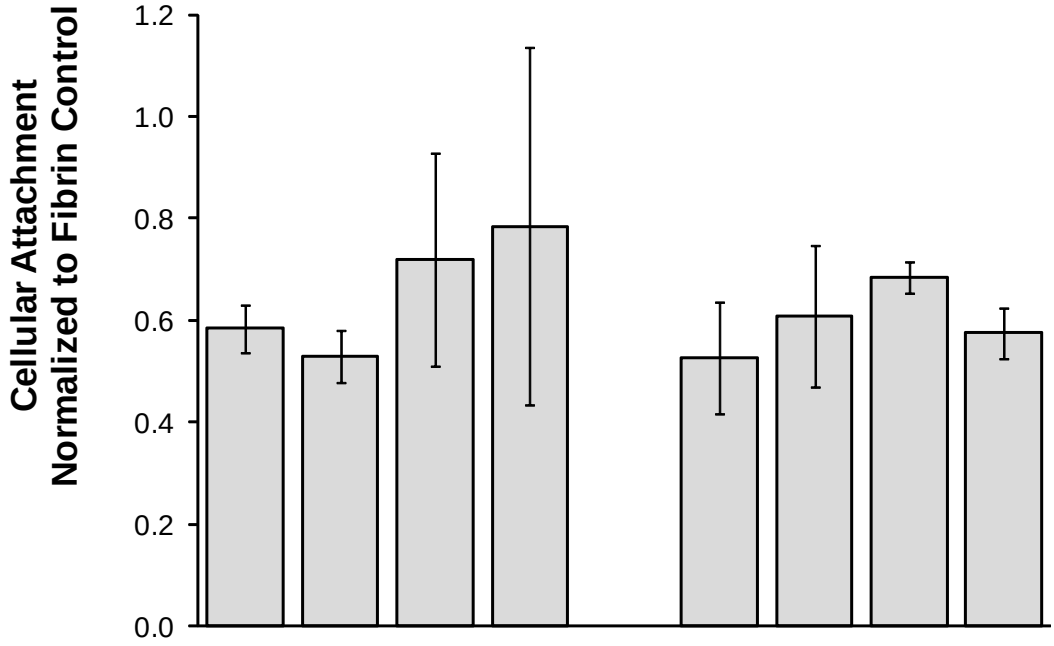

Polymer Chain Length	18.2				22.1			
Peptide Type	N/A	CREKA		CAERK	N/A	CREKA		CAERK
Number of Peptide Units	0	2.4	7.4	2.4	0	2.3	7.1	2.3
Code	P2	P2-L	P2-H	P2-S	P4	P4-L	P4-H	P4-S

Figure 6-20 Normalized cellular attachment data for short PEG chain (M_N = 300) polymers.
Values (M ± SE) represent the degree of cellular attachment, based on DNA assay, normalized to fibrin controls. No statistically significant differences were observed.

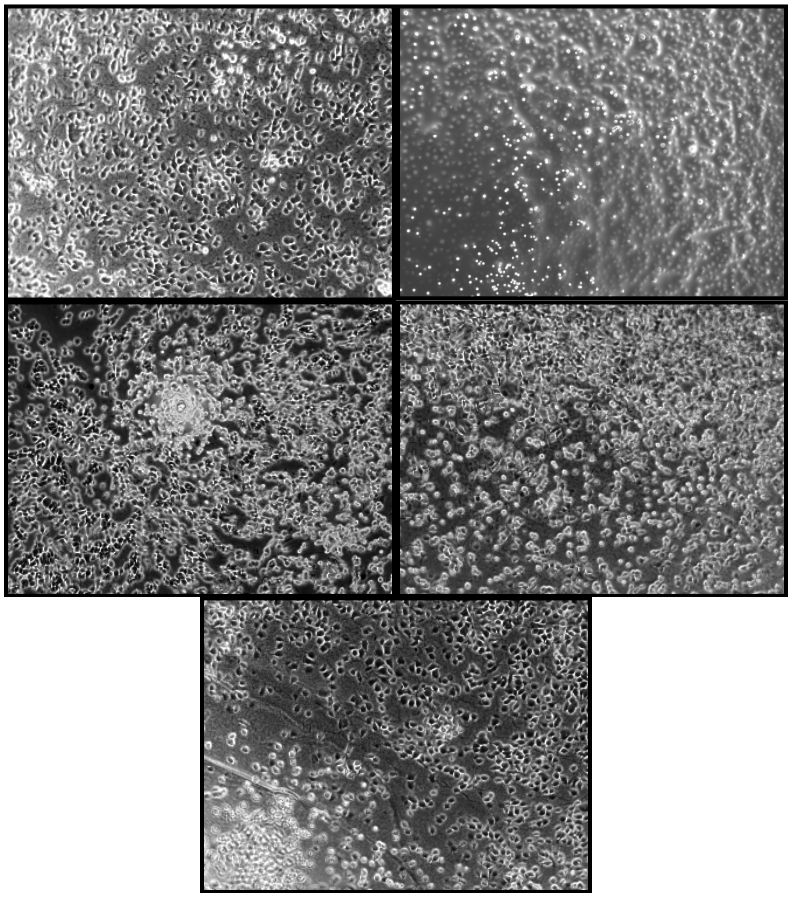

Figure 6-21 Images of cells attached to fibrin gel after treatment with barrier material. These images (Fibrin, TCP, PMAA-S, P1-L, and P1-S, clockwise from top left) are representative of the cells after incubation. The heterogeneous distribution of cells in the wells made accurate visual assessment of the cellular density impossible.

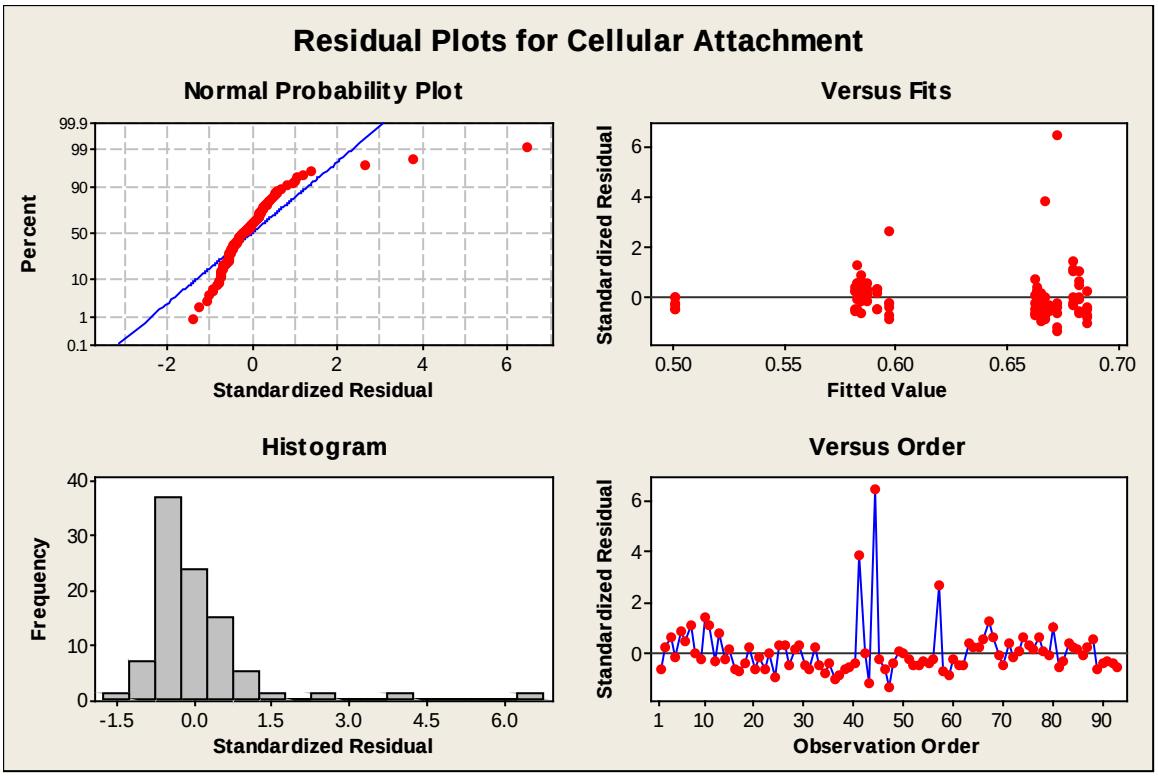

Figure 6-22 Residual plots for attachment of cells to fibrin substrate.
The validity of the general linear model used for the ANOVA for the kinetic analysis of fibrin gel propagation is supported by the residual plots. There are, however, three apparent outliers. These outliers result from P2-H, P2-S, and P3-L. With the exception of these outliers, the linearity of the normal probability plot and random distribution observed in the standardized residual plots indicate a lack of bias in the model fit. The histogram of standardized residuals suggests a normal distribution of residuals. Excepting the outliers, all of the residuals are within the expected range of ± 2 standard deviations. The outliers potentially result from the non-linear nature of the fluorescence assay employed for the quantification of cellular attachment, where small experimental variation can result in large variation in the results.

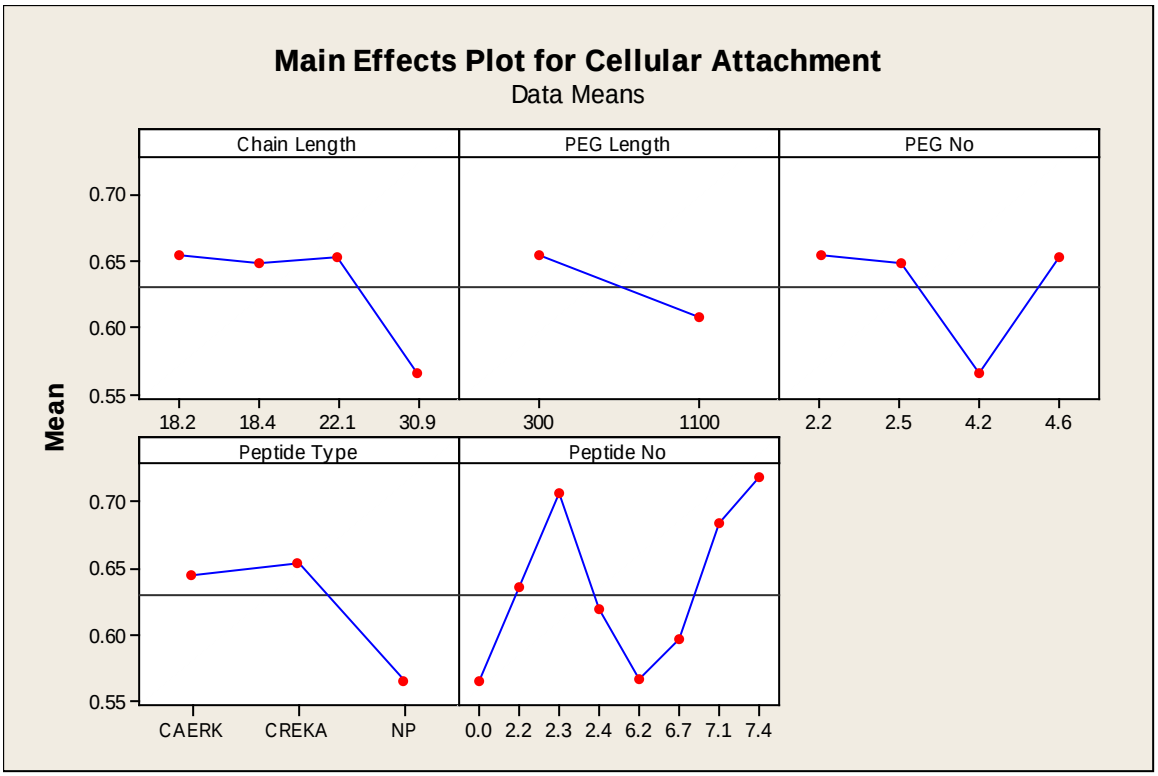

Figure 6-23 Main effects plots for attachment of cells to fibrin substrate.

The main effects plots for the attachment of cells to fibrin substrate provide insight into the importance of the various aspects of polymer architecture that were investigated. As indicated by the strong dependence of the response to the presence of peptide, this factor has the largest influence on the performance in this experiment. No trend is observed for the response with changes in polymer chain length; however, the longest chain length material showed a dramatic decrease in the level of cellular attachment. No statistically significant trend was observed with changes in PEG chain length, number of PEG chains, or number of peptide units.

Table 6-1 Polymers Included in General Linear Model for Targeted Polymer Analysis

Polymer Code	Functional Group	Number of Functional Groups	Chain Length	Number of MA Units	Number of PEG Units	MA/PEG Ratio	PEG Chain Length	Molecular Weight
P1	-	-	18.4	15.9	2.5	6.5	1,100	4,300
P1-L	CREKA	2.3	18.4	15.9	2.5	6.5	1,100	9,300
P1-H	CREKA	6.7	18.4	15.9	2.5	6.5	1,100	14,400
P1-S	CAERK	2.4	18.4	15.9	2.5	6.5	1,100	9,300
P2	-	-	18.2	16.0	2.2	7.3	300	2,200
P2-L	CREKA	2.4	18.2	16.0	2.2	7.3	300	7,300
P2-H	CREKA	7.4	18.2	16.0	2.2	7.3	300	12,800
P2-S	CAERK	2.4	18.2	16.0	2.2	7.3	300	7,300
P3	-	-	30.9	26.7	4.2	6.4	1,100	7,300
P3-L1	CREKA	2.2	30.9	26.7	4.2	6.4	1,100	14,800
P3-H	CREKA	6.2	30.9	26.7	4.2	6.4	1,100	21,000
P3-S	CAERK	2.2	30.9	26.7	4.2	6.4	1,100	14,800
P4	-	-	22.1	17.5	4.6	3.8	300	3,300
P4-L	CREKA	2.3	22.1	17.5	4.6	3.8	300	8,700
P4-H	CREKA	7.1	22.1	17.5	4.6	3.8	300	14,200
P4-S	CAERK	2.3	22.1	17.5	4.6	3.8	300	8,600

Table 6-2 Effects of Variation in Molecular Architecture on Material Performance

		Response			
		Fibrinogen Adsorption Ratio $\left(\frac{Fg_2}{Fg_1}\right)$	**Fibrinogen Deposition Half-Life**	**Initial Rate of Fibrin Gel Propagation**	**Cellular Attachment**
Variable	**Chain Length**				↓*
	PEG Chain Length	↓	↓		
	Number of PEG Units		↓		
	Number of Peptide Units	↓		↓	
	Peptide Type	NS	NS	S	NS

Summary of statistically significant ($p < 0.05$) effects of polymer architecture on performance in *in vitro* and *ex vivo* tests. The "↓" symbol indicates a decrease in the response when the variable value is increased. Designations of "S" and "NS" indicate effects that are specific (S) or not specific (NS) to the type of peptide unit conjugated to the polymer. The "*" symbol indicates that the response only shows negative correlation with the variable for the longest polymer chains.

CHAPTER 7. INVESTIGATION OF INTERACTION BETWEEN CREKA AND FIBRINOGEN

7.1. Introduction

As has been demonstrated in the literature, the pentapeptide CREKA has successfully been used to target nanoparticles to tumor sites based on the high levels of fibrin present due to the well characterized leaky vasculature [168-173]. In addition, the molecular configuration of this material has been characterized under a variety of conditions [175-177]. The work described in **Chapter 6** demonstrates that CREKA can also be incorporated into polymers and used to interrupt the series of events that leads to an extended fibrin gel matrix, promoting post surgical adhesion formation. To date, however, no analysis of the interaction of this peptide with fibrin, or its precursor, fibrinogen, has been reported.

Two complementary approaches were employed to begin the investigation of this important interaction. First, the structure of fibrin gels grown from surfaces treated with a series of polymeric materials was analyzed using a turbidity assay. The powerful optical technique, circular dichroism (CD), was employed to probe the interaction of this peptide with fibrinogen in the solution phase. While a much more detailed investigation of this interaction is warranted, these two studies represent a critical first step in developing an understanding of the nature of these interactions.

7.2. Materials and Methods

For the structural analysis if fibrin, all of the materials listed in **Table 4-2** were employed. Circular dichroism was carried out with the free targeting peptide (CREKA)

and the polymer conjugate deemed to have the best overall performance from previous experiments (P3-H). All materials were prepared as previously described.

7.2.1. Analysis of Fibrin Structure using UV-Visible Turbidity Assay

In order to investigate the structure of fibrin gels grown from the surface of existing fibrin substrates under a variety of conditions, a microplate based turbidity analysis was performed [224-225].

7.2.1.1. Preparation of Fibrin Gel Substrate

A Costar high binding 96-Well EIA/RIA plate was used to maximize the strength of interaction between the fibrin gel and the microplate. In order to create a stable gel on the surface, fibrinogen (50 µL, 2.0 mg/mL), thrombin (20 µL, 2.5 U/mL), and calcium chloride (10 µL, 100 mM) were added to each well. The resulting gel was allowed to cure for 5 hours at room temperature. Each well was then rinsed twice with 200 µL TBS, and care was taken to avoid removing the fibrin gel from the surface. A solution of each material under investigation (50 µL, 0.10 mg/mL in TBS, n = 4) was added to the wells.

7.2.1.2. Assessment of Fibrin Gel Structure

After treating each gel with the material under investigation, 150 µL of fibrinogen (0.5 mg/mL in TBS) was added to each well. A partial UV-visible spectrum (350 – 500 nm) was collected for each well using the CaryWin UV UV-visible spectrophotometer. After 90 minutes, a second UV-visible spectrum was collected. The turbidity of the additional fibrin gel formed during the intervening 90 minutes was determined by subtracting the initial reading from the final reading at each wavelength.

Previously published studies have shown that it is possible to relate the turbidity of the resulting gel to the structure of its composite fibers [223, 230-233]. Turbidity (•) can be calculated from the measured absorbance (Abs) value and the path length (b):

$$\tau = \frac{\ln(10) * \text{Abs}}{\text{b}} \qquad (7\text{-}1).$$

As shown in **Appendix A**, this value can be related to the $\frac{\text{mass}}{\text{length}}$ ratio (μ) of the fibrin fibrils by Equation (7-2):

$$\tau = \frac{6.52 \times 10^{-27}}{\lambda^3} \cdot \mu \qquad (7\text{-}2).$$

As indicated by this expression, a plot of • versus $\left(\frac{6.52 \times 10^{-27}}{\lambda^3}\right)$ should yield a straight line with a slope of μ. Assuming an average well diameter of 0.661 mm, a 150 μL gel results in a path length of 0.437 cm. Equation (7-2) can be employed, and a plot of • versus $\frac{6.52 \times 10^{-27}}{\lambda^3}$ will yield a straight line with a slope equal to the ratio of mass to length ratio of the fibrin fibrils (μ) in $\left(\frac{\text{Da}}{\text{cm}}\right)$ to relate the turbidity of the gel to its structure.

7.2.2. Circular Dichroism of Fibrinogen with Free Peptide and with Targeted Polymeric Adhesion Barrier

Circular dichroism (CD) is a powerful optical technique often employed to investigate the structure of proteins in solution and to probe the interaction of materials with these proteins. Briefly, a sample of the material of interest is dissolved in a solvent

and irradiated alternately with circularly polarized light with opposite polarities. Since proteins fold into chiral structures, they interact differently with these two polarized beams. The absorbed light is measured as a function of wavelength for each beam, and the difference between these absorption values is used to study the structure of the analyte. Numerous articles and books have been written describing the underlying physics of the technique [234-237]. Other manuscripts offer guidance on the experimental and analytical aspects of CD measurement [238]. Because of the nature of the technique, it is necessary that the protein of interest be dissolved in a UV transparent solvent. As a result, direct investigation of the insoluble fibrin molecule is impossible; rather, it is customary to investigate interactions between ligands and fibrinogen and then to apply these results to fibrin [239-241]. In this work, we employ this technique to study the interaction between targeting peptides and solution phase fibrinogen.

7.2.2.1. Preparation of Solutions for CD Measurements

Prior to preparing solutions, PBS was filtered with a 0.22 μm syringe filter. Solutions of fibrinogen (0.1 to 200 μg/mL), CREKA (100 μg/mL), and P3-H (100 μg/mL) were prepared in this PBS buffer solution. These solutions were combined in the appropriate ratios and diluted with PBS to prepare the samples shown in **Table 7-1**. All samples were prepared fresh on the day of the experiment to minimize degradation of the proteins in solution.

7.2.2.2. Circular Dichroism Measurement

All CD measurements were performed at 37 ^{o}C using the Jasco J-810 Spectropolarimeter controlled by the Jasco Spectral Measurement software. Spectra were

collected from 320 to 200 nm. Each measurement is the average of four acquisitions collected in a 1.0 mm quartz cuvette, and each sample was measured three times. In order to avoid contamination between samples, the cuvette was cleaned with 1M nitric acid, rinsed with copious amounts of DI water and ethanol, and dried with acetone between samples. Analysis of blank PBS samples confirmed that this cleaning procedure removed all traced of the sample from the cuvette.

7.2.2.3. CD Data Analysis

In order to estimate the content of • -helical and • -sheet secondary structure in the fibrinogen, each spectrum was analyzed using the K2D2 neural network deconvolution algorithm [242-244]. This algorithm, accessible via an online interface, uses a neural network to assess the structure of proteins in aqueous solution. By comparing the observed CD spectrum with a database of 43 proteins with known structures, the K2D2 network can effectively estimate the • -helical and • -sheet content in the sample.

7.3. Results

7.3.2. Fibrin Structure

As previously described, the structure of the fibrils within a fibrin gel can be probed by analyzing the turbidity of the gel as a function of wavelength. As shown in **Figure 7-1**, a plot of • versus $\left(\frac{6.52\times10^{-27}}{\lambda^3}\right)$, yields a straight line, in good agreement with theory. Using a linear least squares analysis in Excel, data for each well was analyzed. The results of this analysis, shown in **Figure 7-2** – **Figure 7-4**, summarize these results for the materials tested. The control, with no polymer addition, yields a value of

$2.56 \times 10^{12} \pm 1.7 \times 10^{11} \frac{\text{Da}}{\text{cm}}$ and is shown on the figures as a horizontal line for reference. Only EPC exhibited a statistical difference from the TBS control.

The residual plots for μ are shown in **Figure 7-5**. With the possible exception of 1 outlier, the normal probability plot is linear and the residuals are normally distributed. The main effects plots, shown in **Figure 7-6**, indicate mass/length ratio is not affected by the polymer chain length, the number of PEG chains, or the number of peptide units. The value of μ decreases with increasing PEG chain length . No clear difference is observed as a function of peptide type.

7.3.3. CD Analysis

Representative CD spectra for the samples tested are shown in **Figure 7-7**. These spectra indicate a change in secondary protein structure with the addition of either CREKA or polymer. The intensity of the peak at 210 nm decreases with increasing CREKA concentration; the effect of the polymer (100 μg/mL) is approximately equivalent to the effect of 0.2 μg/mL of CREKA.

Circular dichroism measurements of solution phase fibrinogen in the absence of targeting peptides indicate 32.5 ± 7.0 percent •-helical content and 20.4 ± 5.8 percent •-sheet content. These results are in good agreement with previously published structural data (35 – 42 percent •-helix, 20 – 25 percent •-sheet) and validate the accuracy of the subsequent CD measurements [245-246]. As shown in **Table 7-1**, the addition of CREKA or CAERK to the fibrinogen solution does not result in a significant change in the •-helical content. The addition of CREKA at 0.20 and 1.0 μg/mL causes a decrease in the •-sheet content from 20.4 ± 5.8 percent to approximately 12.4 ± 1.2 percent and 12.5 ± 1.5 percent, respectively. A dose dependant decrease in •-sheet content was observed

with the scramble peptide. The addition of 0.20 μg/mL CAERK results in a •-sheet content of 16.0 ± 4.5 percent, while the sample with 1.0 μg/mL CAERK exhibited 10.2 ± 0.2 percent •-sheet content. The addition of 1.0 μg/mL P3-H to the fibrinogen solution caused no decrease in •-helical content but did result in a decrease in •-sheet content to 12.6 percent.

7.4. Discussion

As indicated by the data in this section, the materials tested in these studies had a significant effect on the structure of fibrin gels propagated from an existing fibrin surface. Although the individual comparisons reported in **Figure 7-2** – **Figure 7-4** fail to reveal a strong significant difference among the samples, ANOVA analysis conducted on the entire data set of polymer samples did reveal several important, statistically significant, trends.

The effect of PEG chain length, indicating that longer PEG chains result in a decrease in the mass/length ratio for the fibrin fibrils, suggests that longer PEG chains are effective at inhibiting the deposition of fibrinogen to growing fibrin fibrils. As has been discussed in **Chapter 6**, this result is in good agreement with previously published studies, where the length of PEG chain is an important factor in the ability to suppress protein adsorption. Surprisingly, the number of PEG chains does not appear to impact the structure of the growing fibrin fibrils. This indicates that the steric effect of PEG chains on adjacent monomer units in the polymer fails to result in enhanced protection against protein deposition. It is possible that, in the environment tested, all of the PEG chains form a fully hydrated hydrophilic core. While it was impossible to determine the number of polymer chains adsorbed to the growing fibrin fibril, it is likely that a larger number of

low PEG number polymer chains are able to adhere to the surface. As a result, the total number of PEG chains on the surface may be equivalent despite the difference in molecular architecture.

The somewhat surprising observation that polymer chain length does not affect the resulting fibrin structure may also be explained if it is assumed that the surface of the fibrin fibrils is saturated with polymer. Although the longer polymer chains occupy a larger surface area, the presence of additional polymer chains results in an equivalent effect on the polymerized protein structure.

Although the trend in protein structure that results from changing the peptide is ambiguous, it does appear that the presence of either CREKA or CAERK in the polymer structure results in an increase in the specific mass of the fibrils. This is confirmed by the clear trend observed that increasing the level of peptide conjugation increases the measured value of μ. Two mechanisms may be responsible for this trend. If the presence of the peptide simply increases the affinity for the polymers to the fibrin fibril surface, it is conceivable that the observed increase simply results from the accumulation of polymer around the fibrin core. Another potential explanation for this observation is that the peptides on the polymer chain enhance the deposition of fibrin around these growing fibrils by increasing the interacting with the solution phase protein and the growing fibril. Without additional structural information about the structure of the fibrin generated in these experiments, it is impossible to distinguish between these two potentialities; however, since is appears likely that the surfaces are completely saturated with polymer, the second explanation appears to be more likely.

The observations made with circular dichroism can be used to begin to explain the interaction of CREKA with fibrin and its precursor, fibrinogen. The fibrinogen solution employed was prepared at a concentration of 100 μg/mL, or 0.29 μM. The peptide was employed at concentrations of 0.33 and 1.7 μM. Since CD of the free peptide did not reveal any secondary structure, all structural changes in the protein/peptide mixture were attributed to alterations in the conformation of fibrinogen.

These preliminary circular dichroism measurements revealed what appears to be a strong interaction between the peptide ligands and the fibrinogen molecule. The native protein structure, which is in good agreement with previously published studies, showed a large degree of change when incubated with the targeting peptides [245-249]. At either a low (1.1:1) or high (5.6:1) peptide/protein ratio, the CREKA causes a similar conformational change. The scramble, on the other hand, shows less change at the lower concentration. This result indicates that, while CAERK binds to fibrinogen, it does so with a much lower affinity than CREKA. In addition, since the CD data shows no change in the • -helical content in the protein, it can be concluded that the binding site(s) for the two peptides all reside in the • -sheet domains of the protein. The fact that no additional conformational change is observed with greater than a 1.1:1 ratio of peptide to protein suggests that each fibrinogen molecule contains only one peptide binding site. Although these observations have a high degree of variability and do not provide sufficient detail to discern the precise nature of the interaction between CREKA and fibrinogen, the large conformational change suggests that CREKA interacts strongly with solution phase fibrinogen.

7.5. Conclusion

The materials tested for use as prophylactic treatments for post surgical adhesion prevention demonstrate the ability to bind to growing fibrin fibrils and to affect the structure of the resulting structures. As anticipated, the observed trends indicate that PEG chain length and degree of peptide conjugation are the most important factors in the performance of the materials. The unanticipated results that the number of PEG chains conjugated to the polymer and the overall polymer length are not important factors in modifying the structure of the fibrin fibrils is likely attributable to the existence of a high density of polymer chains bound to the protein surface. Circular dichroism measurements of fibrinogen with free peptide and with peptide-conjugated polymer demonstrate strong interactions with fibrinogen. While the CAERK scramble, used as a control, does bind to the solution phase protein, it exhibits a much lower affinity for the protein than CREKA. This finding confirms the ability of CREKA to serve as a useful moiety for targeting polymers to fibrinogen and fibrin, but suggests that other peptide groups may also be useful in controlling the affinity of the polymeric biomaterials for damaged tissues.

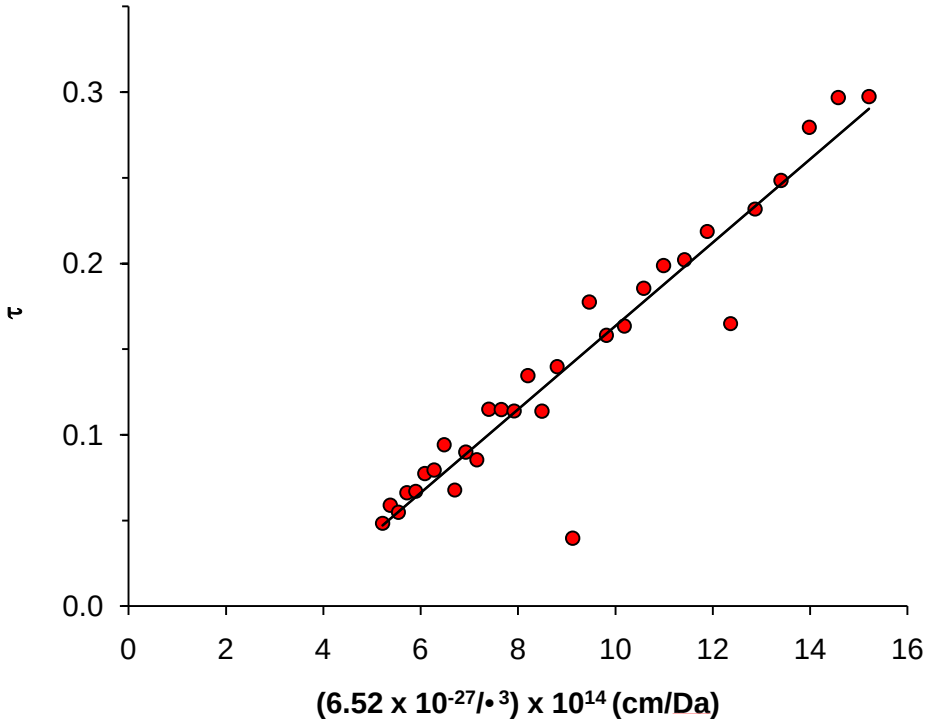

Figure 7-1 Turbidity analysis.

A plot of turbidity (•) versus $\left(\frac{6.52 \times 10^{-27}}{\lambda^{3}}\right)$ for control sample with no polymer. The slope of this graph indicates a fibrin $\frac{\text{mass}}{\text{length}}$ ratio of $2.43 \times 10^{12}\ \frac{\text{Da}}{\text{cm}}$.

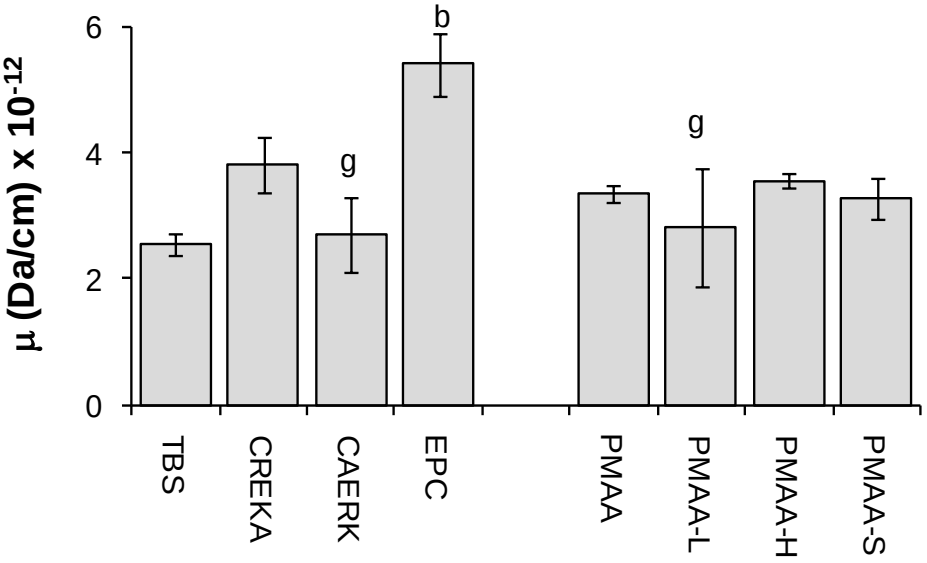

Figure 7-2 Mass/length ratio from turbidity analysis (controls and PMAA polymers). Values (M ± SE) and statistical significance are given: 99% compared to no polymer (b) and 95% compared to EPC (g).

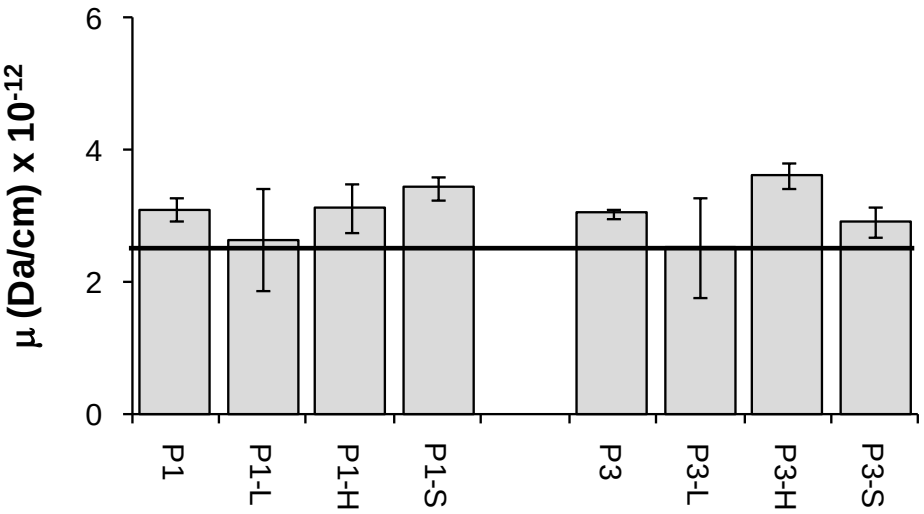

Figure 7-3 Mass/length ratio from turbidity Analysis (long PEG chain polymers). Values (M ± SE) are given. No statistical significance was observed.

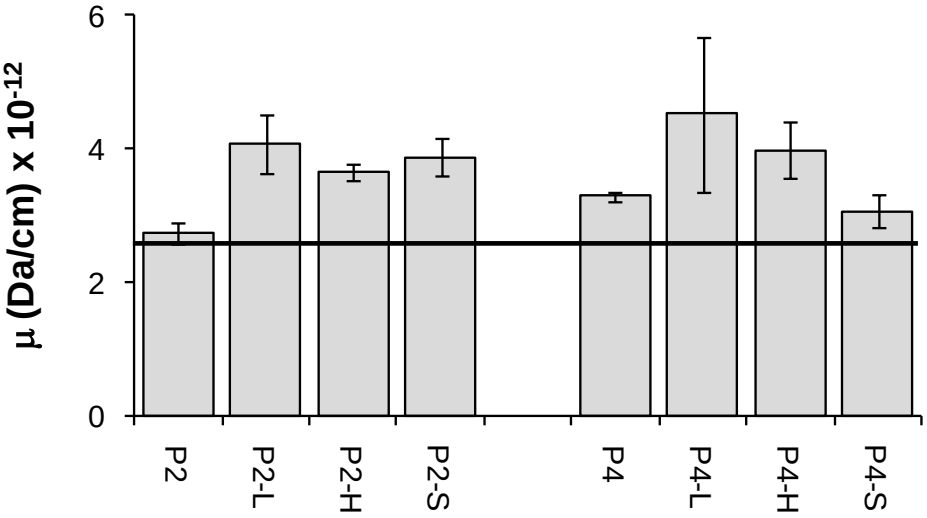

Figure 7-4 Mass/Length Ratio from Turbidity Analysis (short PEG chain polymers). Values (M ± SE) are given. No statistical significance was observed.

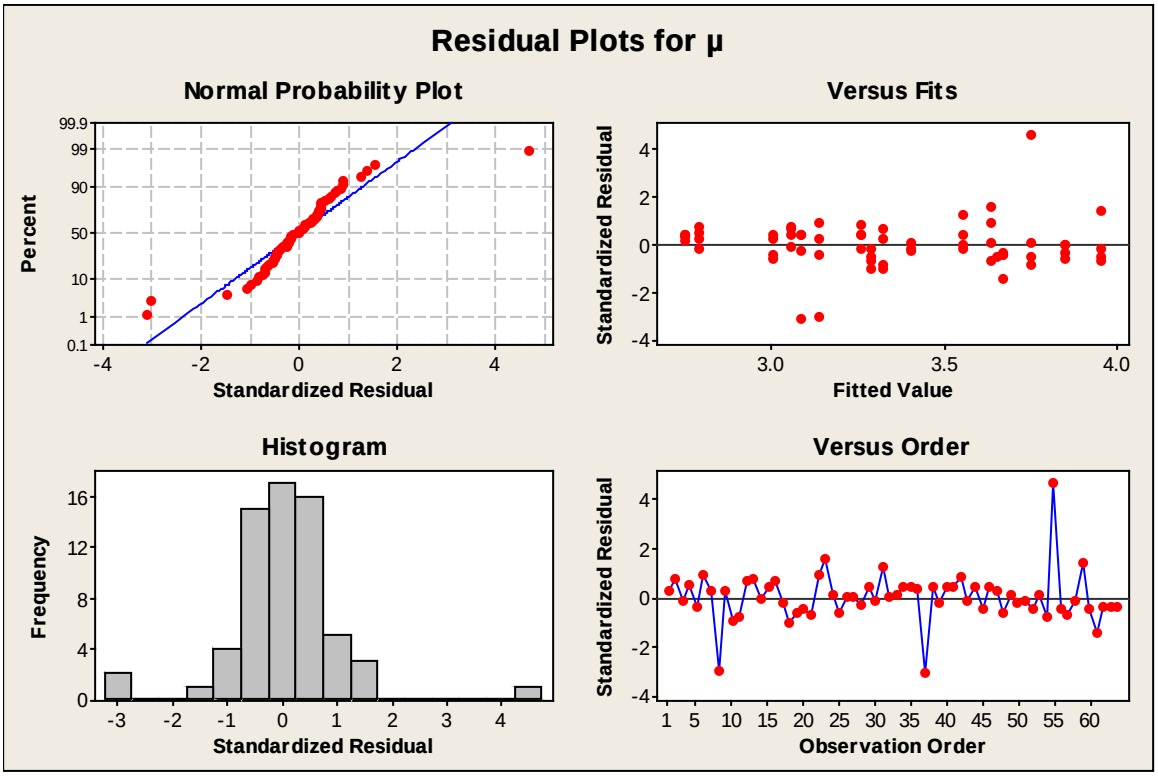

Figure 7-5 Residual plots for fibrin mass/length ratio (μ).
The validity of the general linear model used for the ANOVA for the fibrin $\frac{\text{mass}}{\text{length}}$ ratio is confirmed by the residual plots. Three outliers are observed for P1-L, P3-L, and P4-L. With the exception of these three outliers, the linearity of the normal probability plot and random distribution observed in the standardized residual plots indicate a lack of bias in the model fit. The histogram of standardized residuals indicates a normal distribution of residuals. In addition, the vast majority of the residuals are within the expected range of ± 2 standard deviations. The three outliers with standardized residuals above 3 arise from polymers with the lowest level of CREKA conjugation.

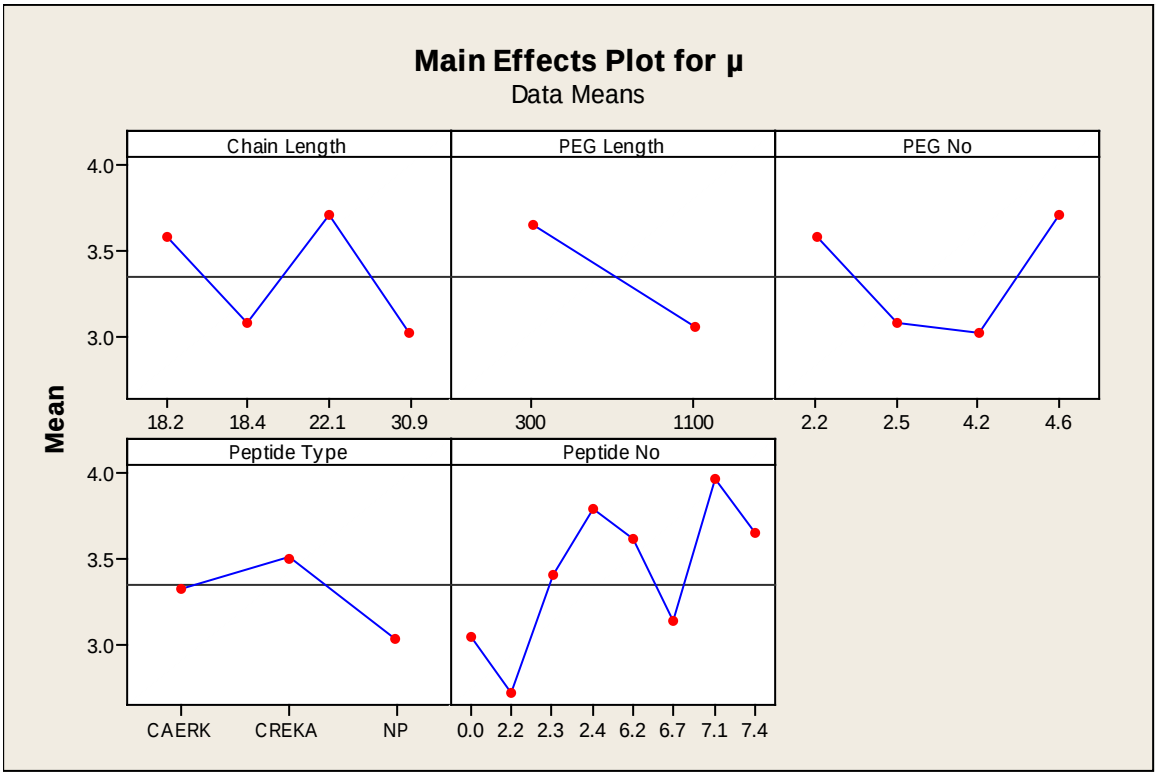

Figure 7-6 Main effects plots for fibrin mass/length ratio (μ).

The main effects plots for the $\frac{\text{mass}}{\text{length}}$ ratio for fibrin provide insight into the importance of the various aspects of polymer architecture that were investigated. No statistically significant dependence was observed for polymer chain length, the number of PEG units, or the number of peptide units. Increases in PEG chain length result in a decrease in the observed value for μ. The impact of peptide type is unclear; however, the presence of peptide units in the polymer appears to result in a larger value for μ.

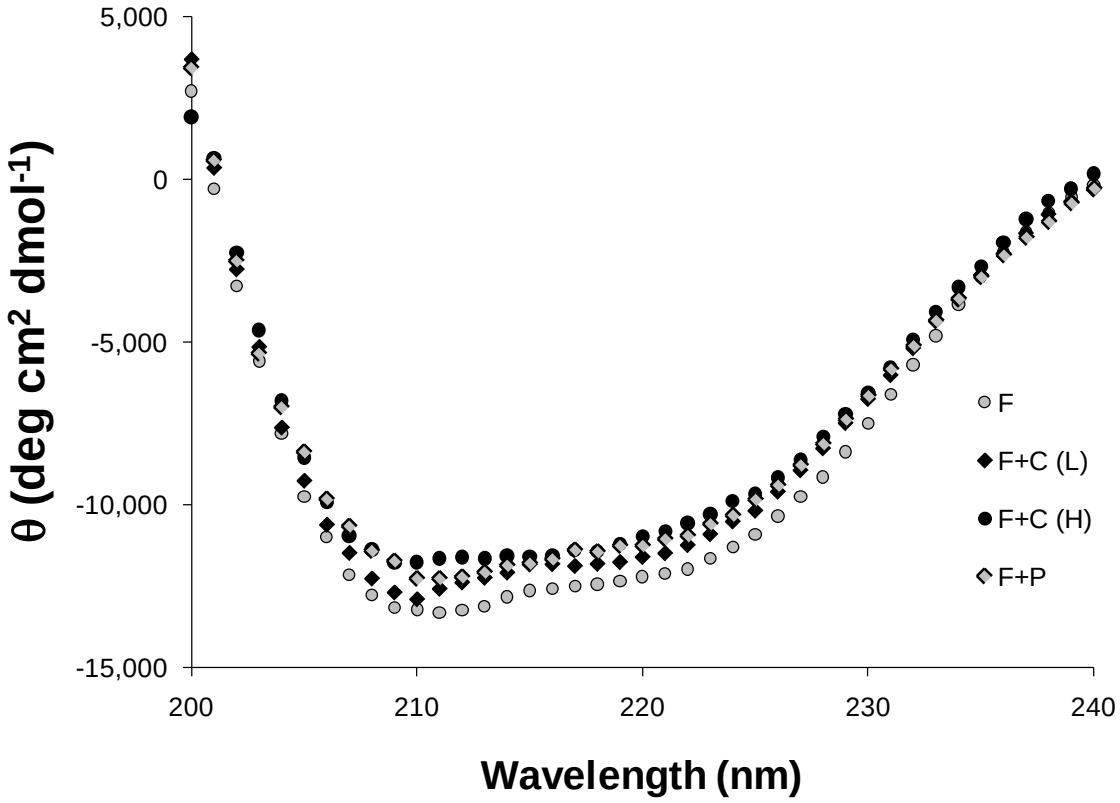

Figure 7-7 Circular dichroism measurements.
A comparison of CD spectra for fibrinogen (F), fibrinogen with 0.20 µg/mL CREKA (F+C (L)), fibrinogen with 1.0 µg/mL CREKA (F+C (H)), and fibrinogen with 100 µg/mL P3-H (F+P). The peak at 210 nm decreases with increasing CREKA; a similar level of decrease is observed with the polymer as with the lower level of CREKA. Both of these peaks correspond to a $\frac{\text{CREKA}}{\text{fibrinogen}}$ ratio of approximately 1:1.

Table 7-1 Results of Circular Dichroism Measurement

Sample	Description	Molar Ratio of Peptide to Fibrinogen	• -Helix Content (Percent) (M ± SE)	• -Sheet Content (Percent) (M ± SE)
F	100 µg/mL Fibrinogen in PBS	0	32.5 ± 7.0	20.4 ± 5.8
F + C (L)	100 µg/mL Fibrinogen + 0.20 µg/mL CREKA in PBS	1.1	34.1 ± 2.5	12.4 ± 1.2
F + S (L)	100 µg/mL Fibrinogen + 0.20 µg/mL CAERK in PBS	1.1	35.3 ± 5.3	16.0 ± 4.5
F + C (H)	100 µg/mL Fibrinogen + 1.0 µg/mL CREKA in PBS	5.6	35.1 ± 3.8	12.5 ± 1.5
F + S (H)	100 µg/mL Fibrinogen + 1.0 µg/mL CAERK in PBS	5.6	39.8 ± 0.4	10.2 ± 0.2
F + P *	100 µg/mL Fibrinogen + 1.0 µg/mL P3-H in PBS	1.0	33.0	12.6

* n = 1

Summary of solutions used for circular dichroism (CD) investigation of fibrinogen interactions. Each peptide was studied at 1.1:1 and 5.6:1 molar ratios to fibrinogen. CREKA conjugated polymer was studied at a concentration that corresponds to 1 peptide unit per protein molecule. With the exception of the polymer (n = 1), each value represents the average of 3 – 4 independently prepared samples.

CHAPTER 8. CONCLUSIONS AND FUTURE STUDIES

In this research, a rational approach for the development of a series of novel biomaterials for the prevention of post surgical adhesions has been employed. Starting with a thorough understanding of the biochemistry and pathology of PSA formation, these materials were developed specifically to meet this significant critical need. Robust methodology to synthesize and characterize functionalized block and statistical copolymers with precisely controlled molecular architecture has been developed. Initial studies, focused on understanding the interaction of non-targeted polymers with positively charged model surfaces, verified the viability of this approach and provided a critical basis for the development of materials. Subsequent investigations of targeted polymers led to an understanding of the relationship between the molecular architecture and performance in a number of *in vitro* tests. The ability of these materials to interact with fibrin as a marker of tissue damage and to reduce the propagation of the fibrin gel matrix can be modulated by controlling the molecular architecture of the polymers. Finally, the results of these experiments were employed to select materials for subsequent *in vivo* experiments to assess their ability to prevent PSA formation in a rabbit model.

The power of this ground up approach to biomaterial development has been validated. The promising preliminary results obtained in these experiments indicate the need for additional studies, including the following:

- The structure-property relationships that have been determined should be employed to design and synthesize additional polymers for testing.
- Investigation of biocompatibility.

  - Efforts to investigate biocompatibility should begin with an assessment of the dose-dependent cytotoxicity of the materials, including the polymers of interest and the targeting peptides. These studies should include multiple cell types, as these materials will be in contact with many types of cells *in vivo*.
  - Additional biocompatibility tests should include histological investigation of the tissues in close proximity to the materials, Ames testing, and LD50 testing.
- The fibrin and fibrinogen binding studies that were conducted indicated a strong interaction between CREKA and fibrinogen. Additional binding studies are warranted in order to develop a better understanding of these interactions.
  - CD can be used to determine the stoichiometry of the interaction between the protein and peptide.
  - Complementary techniques, including ITC and SPR, could be used to investigate the kinetics and thermodynamics of protein-peptide interactions.
  - Additional studies should be conducted to ascertain the precise location of the peptide binding sites in fibrinogen.
- The effect of these materials on fibrin formation has been investigated. In order to develop a better understanding of how these materials affect the fibrin gel matrix formation, their impact on the rate of fibrinolysis should be evaluated *in vitro*.
- Animal studies are needed to assess the *in vivo* performance of these materials compared to existing PSA prevention technologies.

- Stability and biodistribution studies.
  - Degradation of the polymers *in vitro* should be investigated to assess their chemical stability.
  - *In vivo* degradation should be investigated, and the biodistribution of the polymer and degradation products should be studied in order to assess the likelihood of adverse biological reactions.

APPENDIX A. DERIVATION OF RELATIONSHIP BETWEEN FIBRIN STRUCTURE AND TURBIDITY

This derivation, originally reported by Carr and Hermans, has been included for clarity. Additional details, including the physical justification for the assumptions included in the derivation can be found in the literature [230-233].

Turbidity is defined as the total amount of light scattered by a sample. Mathematically, this is expressed as Equation A-1:

$$\tau = \int_0^{\pi} 2\,\pi d \left(\frac{i_\theta}{I_0}\right) \sin\theta\, d\theta \qquad \text{(A-1)},$$

where • is the turbidity, d is the distance from the sample to the detector, i**.** is the intensity of scattered light detected at angle •, and I_0 is the intensity of the intensity of the incident beam. The ratio of the scattered light to the incident light is described by Equation A-2:

$$\left(\frac{i_\theta}{I_0}\right) = \frac{R_\theta\left(1+\cos^2\theta\right)}{d^2} \qquad \text{(A-2)},$$

where R**.** is the Rayleigh scattering ratio and depends on the size and shape of the particles causing the scattering. The value of the Rayleigh ratio can be calculated for rod-shaped particles by Equation A-3:

$$R_\theta = \frac{Ck\lambda\mu}{4\,\eta \sin\left(\frac{\theta}{2}\right)} \qquad \text{(A-3)}.$$

In Equation A-3, C is the concentration of particles in $\left(\frac{g}{cm^3}\right)$, • is the wavelength of the incident light, μ is the $\left(\frac{mass}{length}\right)$ ratio of the particles in $\left(\frac{Dalton}{cm}\right)$, • is the refractive index of the solution, and k is a factor defined by Equation A-4:

$$k = \frac{2\pi^2\eta^2\left(\frac{d\eta}{dc}\right)^2}{N\lambda^4} \qquad \text{(A-4)}.$$

N in Equation A-4 represents Avogadro's number, while $\left(\frac{d\eta}{dc}\right)$ represents the refractive index increment of the solute. Substituting Equations A-2 and A-3 into Equation A-1 yields the following expression for turbidity:

$$\tau = \left(\frac{\pi Ck\lambda\mu}{2\eta}\right)\int_0^{\pi}\frac{(1+\cos^2\theta)(\sin\theta)}{\sin\left(\frac{\theta}{2}\right)}d\theta \qquad \text{(A-5)}.$$

Integration of Equation A-5 yields Equation A-6:

$$\tau = \left(\frac{44\,\pi Ck\lambda\mu}{15\,\eta}\right) \qquad \text{(A-6)}.$$

Substituting Equation A-4 into this expression yields Equation A-7:

$$\tau = \frac{88\,\pi^3\eta\left(\frac{d\eta}{dc}\right)^2 C\mu}{15\,N\lambda^3} \qquad \text{(A-7)}.$$

Values for $\left(\frac{\mathrm{d}\eta}{\mathrm{dc}}\right)$ and • can obtained from literature (0.18 $\frac{cm^3}{g}$ and 1.333, respectively) [230]. Substituting these values, and the fibrinogen concentration of $5.00 \times 10^{-4}\ \frac{\mathrm{g}}{\mathrm{cm}^3}$, Equation A-7 simplifies to Equation A-8:

$$\tau = \frac{6.52 \times 10^{-27}}{\lambda^3}\mu \qquad \text{(A-8).}$$

LIST OF ABBREVIATIONS

ABCR	Bis-(dimethylamino)methylsilane
ACN	Acetonitrile
ANOVA	Analysis of Variance
BSA	Bovine Serum Albumin
CAERK	Cysteine-Alanine-Glutamic Acid-Arginine-Lysine
CD	Circular Dichroism
CMC	Carboxymethylcellulose
CREKA	Cysteine-Arginine-Glutamic Acid-Lysine-Alanine
DCC	N,N'-Dicyclohexylcarbodiimide
DCU	N,N'-Dicyclohexylurea
DI	Deionized
DMEM	Dubecco's Modified Eagle Medium
DNA	Deoxyribonucleic Acid
EDTA	Ethylenediaminetetraacetic acid
EPC	Egg Phosphatidylcholine
FGM	Fibrin Gel Matrix
GPC	Gel Permeation Chromatography
GTP	Group Transfer Polymerization
HA	Hyaluronic Acid
HAc	Acetic Acid
HAx	Crosslinked Hyaluronic Acid
HPLC	High Performance Liquid Chromatography
MA	Methacrylic Acid
M_N	Number Average Molecular Weight
MTS	1-Methoxy-1-(trimethylsiloxy)-2-methyl-1-propene
M_W	Weight Average Molecular Weight
NAEM	N-Aminoethylmaleimide Trifluoroacetic Acid
NHS	N-Hydroxysuccinimide
NMR	Nuclear Magnetic Resonance
ORC	Oxidized Regenerated Cellulose
PAA	Poly(acrylic acid)
PAI-1	Plasminogen Activator Inhibitor-1
PBS	Phosphate Buffered Saline
PD	Polydispersity
PE	Polyethylene
PEG	Poly(ethylene glycol)
PEGMA	Poly(ethylene glycol methacrylate)
PEO	Poly(ethylene oxide)
PLG	Poly(L-glutamate)
PLGA	Poly(lactic-co-glycolic acid)
PLL	Poly(L-lysine)
PMAA	Poly(methacrylic acid)
PMN	Polymorphoneutrophils
PS	Polystyrene

PSA	Post Surgical Adhesion
PTBMA	Poly(t-butyl methacrylate)
PTFE	Poly(tetraflouroethylene)
PTSA	Para-Toluenesulfonic Acid
QCM	Quartz Crystal Microbalance
QCM	Quartz Crystal Microbalance with Dissipation
rt-PA	Recombinant Tissue Plasminogen Activator
r.t.	Retention Time
RID	Refractive Index Detector
SAM	Self-Assembled Monolayer
SD	Standard Deviation
SE	Standard Error
SPIO	Superparamagnetic Iron Oxide
TBABB	tert-Butylammonium bibenzoate
TBMA	tert-Butylmethacrylic acid
TCP	Tissue Culture Polystyrene
TFA	Trifluoroacetic Acid
THF	Tetrahydrofuran
TMS	Trimethylsilyl
tPA	Tissue Plasminogen Activator
UV	Ultraviolet
VASE	Variable Angle Spectroscopic Ellipsometry

REFERENCES

1. Ellis, H., et al., *Adhesion-related hospital readmissions after abdominal and pelvic surgery: a retrospective cohort study.* Lancet, 1999. **353**(9163): p. 1476-80.

2. Risberg, B., *Adhesions: preventive strategies.* Eur J Surg Suppl, 1997(577): p. 32-9.

3. Matthews, B.D., et al., *Assessment of adhesion formation to intra-abdominal polypropylene mesh and polytetrafluoroethylene mesh.* J Surg Res, 2003. **114**(2): p. 126-32.

4. Nagelschmidt, M., T. Minor, and S. Saad, *Polyethylene glycol 4000 attenuates adhesion formation in rats by suppression of peritoneal inflammation and collagen incorporation.* Am J Surg, 1998. **176**(1): p. 76-80.

5. Medley, J.M., et al., *Block copolymers for the rational design of self-forming postsurgical adhesion barriers.* Acta Biomaterialia, 2010. **6**(1): p. 72.

6. Weis, C., et al., *Poly(vinyl alcohol) membranes for adhesion prevention.* J Biomed Mater Res B Appl Biomater, 2004. **70**(2): p. 191-202.

7. diZerega, G.S., *Biochemical events in peritoneal tissue repair.* Eur J Surg Suppl, 1997(577): p. 10-6.

8. Boland, G.M. and R.J. Weigel, *Formation and prevention of postoperative abdominal adhesions.* J Surg Res, 2006. **132**(1): p. 3-12.

9. *Control and prevention of peritoneal adhesions in gynecologic surgery.* Fertil Steril, 2006. **86**(5 Suppl): p. S1-5.

10. Al-Took, S., R. Platt, and T. Tulandi, *Adhesion-related small-bowel obstruction after gynecologic operations.* Am J Obstet Gynecol, 1999. **180**(2 Pt 1): p. 313-5.

11. Miller, G., et al., *Etiology of small bowel obstruction.* Am J Surg, 2000. **180**(1): p. 33-6.

12. Diamond, M.P. and M.L. Freeman, *Clinical implications of postsurgical adhesions.* Hum Reprod Update, 2001. **7**(6): p. 567-76.

13. Tulandi, T. and A. Al-Shahrani, *Adhesion prevention in gynecologic surgery.* Curr Opin Obstet Gynecol, 2005. **17**(4): p. 395-8.

14. Kresch, A.J., et al., *Laparoscopy in 100 women with chronic pelvic pain.* Obstet Gynecol, 1984. **64**(5): p. 672-4.

15. Swank, D.J., et al., *Laparoscopic adhesiolysis in patients with chronic abdominal pain: a blinded randomised controlled multi-centre trial.* Lancet, 2003. **361**(9365): p. 1247-51.

16. Dijkstra, F.R., et al., *Recent clinical developments in pathophysiology, epidemiology, diagnosis and treatment of intra-abdominal adhesions.* Scand J Gastroenterol Suppl, 2000(232): p. 52-9.

17. Brill, A.I., et al., *The incidence of adhesions after prior laparotomy: a laparoscopic appraisal.* Obstet Gynecol, 1995. **85**(2): p. 269-72.

18. Brunelli, G., et al., *Adhesion reduction after knee surgery in a rabbit model by Hyaloglide, a hyaluronan derivative gel.* J Orthop Res, 2005. **23**(6): p. 1377-82.

19. Haq, I., et al., *Postoperative fibrosis after surgical treatment of the porcine spinal cord: a comparison of dural substitutes. Invited submission from the Joint Section Meeting on Disorders of the Spine and Peripheral Nerves, March 2004.* J Neurosurg Spine, 2005. **2**(1): p. 50-4.

20. Lilly, S.I. and T.M. Messer, *Complications after treatment of flexor tendon injuries.* J Am Acad Orthop Surg, 2006. **14**(7): p. 387-96.

21. Nkere, U.U., *Postoperative adhesion formation and the use of adhesion preventing techniques in cardiac and general surgery.* ASAIO J, 2000. **46**(6): p. 654-6.

22. Trescot, A.M., et al., *Systematic review of effectiveness and complications of adhesiolysis in the management of chronic spinal pain: an update.* Pain Physician, 2007. **10**(1): p. 129-46.

23. Zhou, J., et al., *Reduction in postsurgical adhesion formation after cardiac surgery in a rabbit model using N,O-carboxymethyl chitosan to block cell adherence.* J Thorac Cardiovasc Surg, 2008. **135**(4): p. 777-83.

24. Cheong, Y.C., N. Bajekal, and T.C. Li, *Peritoneal closure--to close or not to close.* Hum Reprod, 2001. **16**(8): p. 1548-52.

25. Lyell, D.J., et al., *Peritoneal closure at primary cesarean delivery and adhesions.* Obstet Gynecol, 2005. **106**(2): p. 275-80.

26. Roset, E., M. Boulvain, and O. Irion, *Nonclosure of the peritoneum during caesarean section: long-term follow-up of a randomised controlled trial.* Eur J Obstet Gynecol Reprod Biol, 2003. **108**(1): p. 40-4.

27. Setzen, G. and E.F. Williams, 3rd, *Tissue response to suture materials implanted subcutaneously in a rabbit model.* Plast Reconstr Surg, 1997. **100**(7): p. 1788-95.

28. Merad, F., et al., *Prophylactic abdominal drainage after elective colonic resection and suprapromontory anastomosis: a multicenter study controlled by randomization. French Associations for Surgical Research.* Arch Surg, 1998. **133**(3): p. 309-14.

29. Memon, M.A., et al., *The uses and abuses of drains in abdominal surgery.* Hosp Med, 2002. **63**(5): p. 282-8.

30. Memon, M.A., M.I. Memon, and J.H. Donohue, *Abdominal drains: a brief historical review.* Ir Med J, 2001. **94**(6): p. 164-6.

31. Bertram, P., et al., *Effects of intra-abdominal drainages on adhesion formation and prevention by phospholipids in a rat model. Drainages and adhesion formation.* Eur Surg Res, 2003. **35**(2): p. 92-7.

32. Schein, M., *To drain or not to drain? The role of drainage in the contaminated and infected abdomen: an international and personal perspective.* World J Surg, 2008. **32**(2): p. 312-21.

33. Matsuzaki, S., et al., *Effects of supplemental perioperative oxygen on post-operative abdominal wound adhesions in a mouse laparotomy model with controlled respiratory support.* Hum Reprod, 2007. **22**(10): p. 2702-6.

34. Gutt, C.N., et al., *Fewer adhesions induced by laparoscopic surgery?* Surg Endosc, 2004. **18**(6): p. 898-906.

35. Milingos, S., et al., *Adhesions: laparoscopic surgery versus laparotomy.* Ann N Y Acad Sci, 2000. **900**: p. 272-85.

36. Pattaras, J.G., et al., *Incidence of postoperative adhesion formation after transperitoneal genitourinary laparoscopic surgery.* Urology, 2002. **59**(1): p. 37-41.

37. Muller, S.A., et al., *Adhesion prevention comparing liquid and solid barriers in the rabbit uterine horn model.* Eur J Obstet Gynecol Reprod Biol, 2005. **120**(2): p. 222-6.

38. Cooper, K., et al., *Reduction of post-surgical adhesion formation with tranilast.* J Surg Res, 2007. **141**(2): p. 153-61.

39. Stramer, B.M., R. Mori, and P. Martin, *The inflammation-fibrosis link? A Jekyll and Hyde role for blood cells during wound repair.* J Invest Dermatol, 2007. **127**(5): p. 1009-17.

40. Knight, J.A., *Review: Free radicals, antioxidants, and the immune system.* Ann Clin Lab Sci, 2000. **30**(2): p. 145-58.

41. Peterhans, E., *Oxidants and antioxidants in viral diseases: disease mechanisms and metabolic regulation.* J Nutr, 1997. **127**(5 Suppl): p. 962S-965S.

42. Prakash Kumar, B. and K. Shivakumar, *Alterations in collagen metabolism and increased fibroproliferation in the heart in cerium-treated rats: implications for the pathogenesis of endomyocardial fibrosis.* Biol Trace Elem Res, 1998. **63**(1): p. 73-9.

43. Wilgus, T.A., et al., *Hydrogen peroxide disrupts scarless fetal wound repair.* Wound Repair Regen, 2005. **13**(5): p. 513-9.

44. ten Raa, S., et al., *The role of neutrophils and oxygen free radicals in post-operative adhesions.* J Surg Res, 2006. **136**(1): p. 45-52.

45. de la Portilla, F., et al., *Prevention of peritoneal adhesions by intraperitoneal administration of vitamin E: an experimental study in rats.* Dis Colon Rectum, 2004. **47**(12): p. 2157-61.

46. Demirbag, S., et al., *Comparison of hyaluronate/carboxymethylcellulose membrane and melatonin for prevention of adhesion formation in a rat model.* Hum Reprod, 2005. **20**(7): p. 2021-4.

47. Yuzbasioglu, M.F., et al., *The effect of intraperitoneal catalase on prevention of peritoneal adhesion formation in rats.* J Invest Surg, 2008. **21**(2): p. 65-9.

48. Johns, A., *Evidence-based prevention of post-operative adhesions.* Hum Reprod Update, 2001. **7**(6): p. 577-9.

49. Hellebrekers, B.W.J., et al., *A role for the fibrinolytic system in postsurgical adhesion formation.* Fertility and sterility, 2005. **83**(1): p. 122-129.

50. Hellebrekers, B.W., et al., *Short-term effect of surgical trauma on rat peritoneal fibrinolytic activity and its role in adhesion formation.* Thromb Haemost, 2000. **84**(5): p. 876-81.

51. Hellebrekers, B.W., et al., *Use of fibrinolytic agents in the prevention of postoperative adhesion formation.* Fertil Steril, 2000. **74**(2): p. 203-12.

52. Whitting, H.W. and B.A. Young, *The effect of varidase in carboxymethylcellulose jelly on peritoneal adhesion formation.* Virchows Arch Pathol Anat Physiol Klin Med, 1966. **341**(2): p. 155-63.

53. D'Amico, G., *[Experimental research on the effect of varidase on peritoneal adhesions.]*. Riv Patol Clin, 1954. **9**(1): p. 23-36.

54. Schutze, U., et al., *[Prophylaxis of peritoneal adhesions with streptokinase and streptodornase (Varidase). An experimental study in animals (author's transl)]*. MMW Munch Med Wochenschr, 1977. **119**(4): p. 123-6.

55. Hill-West, J.L., R.C. Dunn, and J.A. Hubbell, *Local release of fibrinolytic agents for adhesion prevention.* J Surg Res, 1995. **59**(6): p. 759-63.

56. Jewett, T.C., Jr., et al., *Effects of Fibrinolytic Enzymes on Experimentally Induced Peritoneal Adhesions.* Surgery, 1965. **57**: p. 280-4.

57. Armstrong, P.W. and M.J. Mant, *Bleeding risks, risk factors and management of bleeding complications after treatment with anticoagulants, specific antithrombins, thrombolytics IIb-IIIa receptor blockers.* Eur Heart J, 1995. **16 Suppl L**: p. 75-80.

58. Derex, L. and N. Nighoghossian, *Intracerebral haemorrhage after thrombolysis for acute ischaemic stroke: an update.* J Neurol Neurosurg Psychiatry, 2008. **79**(10): p. 1093-9.

59. Okamoto, Y., S. Takai, and M. Miyazaki, *Oral administration of a novel chymase inhibitor, NK3201, prevents peritoneal adhesion formation in hamsters.* Jpn J Pharmacol, 2002. **90**(1): p. 94-6.

60. David-Raoudi, M., et al., *Differential effects of hyaluronan and its fragments on fibroblasts: relation to wound healing.* Wound Repair Regen, 2008. **16**(2): p. 274-87.

61. Turley, E.A., *Hyaluronan and cell locomotion.* Cancer Metastasis Rev, 1992. **11**(1): p. 21-30.

62. Moore, A.R., et al., *The chemotactic properties of cartilage glycosaminoglycans for polymorphonuclear neutrophils.* Int J Tissue React, 1989. **11**(6): p. 301-7.

63. Gao, F., et al., *Hyaluronan oligosaccharides are potential stimulators to angiogenesis via RHAMM mediated signal pathway in wound healing.* Clin Invest Med, 2008. **31**(3): p. E106-16.

64. Sawada, T., et al., *Adhesion preventive effect of hyaluronic acid after intraperitoneal surgery in mice.* Hum Reprod, 1999. **14**(6): p. 1470-2.

65. Shushan, A., et al., *Hyaluronic acid for preventing experimental postoperative intraperitoneal adhesions.* J Reprod Med, 1994. **39**(5): p. 398-402.

66. Detchev, R., et al., *Prevention of de novo adhesion by ferric hyaluronate gel after laparoscopic surgery in an animal model.* JSLS, 2004. **8**(3): p. 263-8.

67. Johns, D.B., et al., *Reduction of postsurgical adhesions with Intergel adhesion prevention solution: a multicenter study of safety and efficacy after conservative gynecologic surgery.* Fertil Steril, 2001. **76**(3): p. 595-604.

68. Wiseman, D.M., *Possible Intergel Reaction Syndrome (pIRS).* Ann Surg, 2006. **244**(4): p. 630-2.

69. Yeo, Y., et al., *In situ cross-linkable hyaluronic acid hydrogels prevent post-operative abdominal adhesions in a rabbit model.* Biomaterials, 2006. **27**(27): p. 4698-705.

70. Guida, M., et al., *Effectiveness of auto-crosslinked hyaluronic acid gel in the prevention of intrauterine adhesions after hysteroscopic surgery: a prospective, randomized, controlled study.* Hum Reprod, 2004. **19**(6): p. 1461-4.

71. Pellicano, M., et al., *Effectiveness of autocrosslinked hyaluronic acid gel after laparoscopic myomectomy in infertile patients: a prospective, randomized, controlled study.* Fertil Steril, 2003. **80**(2): p. 441-4.

72. Mazzone, A., et al., *Pharmacological effect of hyaluronic acid (HA) on phagocytes: hypothesis for an HA-induced monocyte chemotactic factor for neutrophils.* Clin Ther, 1986. **8**(5): p. 527-36.

73. Bulpitt, P. and D. Aeschlimann, *New strategy for chemical modification of hyaluronic acid: preparation of functionalized derivatives and their use in the formation of novel biocompatible hydrogels.* J Biomed Mater Res, 1999. **47**(2): p. 152-69.

74. Jia, X., et al., *Prolongation of sciatic nerve blockade by in situ cross-linked hyaluronic acid.* Biomaterials, 2004. **25**(19): p. 4797-804.

75. Ito, T., et al., *The prevention of peritoneal adhesions by in situ cross-linking hydrogels of hyaluronic acid and cellulose derivatives.* Biomaterials, 2007. **28**(6): p. 975-83.

76. Diamond, M.P., *Reduction of adhesions after uterine myomectomy by Seprafilm membrane (HAL-F): a blinded, prospective, randomized, multicenter clinical study. Seprafilm Adhesion Study Group.* Fertil Steril, 1996. **66**(6): p. 904-10.

77. Kelekci, S., et al., *The efficacy of a hyaluronate/carboxymethylcellulose membrane in prevention of postoperative adhesion in a rat uterine horn model.* Tohoku J Exp Med, 2004. **204**(3): p. 189-94.

78. *FDA Panel Recommends Against Approval of Genzyme General's Sepracoat* 1997 [cited 2008 September 16, 2008]; Available from: www.prnewswire.com.

79. Hills, B.A., B.D. Butler, and R.E. Barrow, *Boundary lubrication imparted by pleural surfactants and their identification.* J Appl Physiol, 1982. **53**(2): p. 463-9.

80. Muller, S.A., et al., *Efficacy of adhesion prevention and impact on wound healing of intraperitoneal phospholipids.* J Surg Res, 2001. **96**(1): p. 68-74.

81. Muller, S.A., et al., *Influence of intraperitoneal phospholipid dosage on adhesion formation and wound healing at different intervals after surgery.* Langenbecks Arch Surg, 2001. **386**(4): p. 278-84.

82. Treutner, K.H., et al., *Prevention of postoperative adhesions by single intraperitoneal medication.* J Surg Res, 1995. **59**(6): p. 764-71.

83. Baxter, *ADEPT Instructions for Use*: Deerfield, IL.

84. Verco, S.J., et al., *Development of a novel glucose polymer solution (icodextrin) for adhesion prevention: pre-clinical studies.* Hum Reprod, 2000. **15**(8): p. 1764-72.

85. Hosie, K., et al., *Fluid Dynamics in Man of an Intraperitoneal Drug Delivery Solution: 4% Icodextrin.* Drug Delivery, 2001. **8**(1): p. 9-12.

86. Menzies, D., et al., *Use of icodextrin 4% solution in the prevention of adhesion formation following general surgery: from the multicentre ARIEL Registry.* Ann R Coll Surg Engl, 2006. **88**(4): p. 375-82.

87. van den Tol, P., et al., *Icodextrin reduces postoperative adhesion formation in rats without affecting peritoneal metastasis.* Surgery, 2005. **137**(3): p. 348-54.

88. Brown, C.B., et al., *Adept (icodextrin 4% solution) reduces adhesions after laparoscopic surgery for adhesiolysis: a double-blind, randomized, controlled study.* Fertil Steril, 2007. **88**(5): p. 1413-26.

89. Wallwiener, M., et al., *Innovative barriers for peritoneal adhesion prevention: liquid or solid? A rat uterine horn model.* Fertil Steril, 2006. **86 Suppl 4**: p. 1266-76.

90. Krsko, P. and M. Libera, *Biointeractive hydrogels.* Materials Today, 2005. **8**(12): p. 36-44.

91. Hildebrand, H.F., et al., *Surface coatings for biological activation and functionalization of medical devices.* Surface and Coatings Technology, 2006. **200**: p. 6318-6324.

92. Lundorff, P., et al., *Clinical evaluation of a viscoelastic gel for reduction of adhesions following gynaecological surgery by laparoscopy in Europe.* Hum Reprod, 2005. **20**(2): p. 514-20.

93. Nehez, L., et al., *Prevention of postoperative peritoneal adhesions: effects of lysozyme, polylysine and polyglutamate versus hyaluronic acid.* Scand J Gastroenterol, 2005. **40**(9): p. 1118-23.

94. Nehez, L., et al., *Differently charged polypeptides in the prevention of post-surgical peritoneal adhesions.* Scand J Gastroenterol, 2007. **42**(4): p. 519-23.

95. Kapadia, M.R., D.A. Popowich, and M.R. Kibbe, *Modified prosthetic vascular conduits.* Circulation, 2008. **117**(14): p. 1873-82.

96. Adam, D.J., et al., *Antiplatelet and anticoagulant therapy to prevent bypass graft thrombosis in patients with lower extremity arterial occlusive disease.* Int Angiol, 2001. **20**(1): p. 90-8.

97. Kenny, D.A., et al., *Experimental comparison of the thrombogenicity of fibrin and PTFE flow surfaces.* Ann Surg, 1980. **191**(3): p. 355-61.

98. Patel, M., et al., *Experimental evaluation of ten clinically used arterial prostheses.* Ann Vasc Surg, 1992. **6**(3): p. 244-51.

99. Harris, E.S., R.F. Morgan, and G.T. Rodeheaver, *Analysis of the kinetics of peritoneal adhesion formation in the rat and evaluation of potential antiadhesive agents.* Surgery, 1995. **117**(6): p. 663-9.

100. Hellebrekers, B.W., et al., *Effects of five different barrier materials on postsurgical adhesion formation in the rat.* Hum Reprod, 2000. **15**(6): p. 1358-63.

101. Montz, F.J., B.J. Monk, and S.M. Lacy, *The Gore-Tex Surgical Membrane: effectiveness as a barrier to inhibit postradical pelvic surgery adhesions in a porcine model.* Gynecol Oncol, 1992. **45**(3): p. 290-3.

102. Haney, A.F. and E. Doty, *A barrier composed of chemically cross-linked hyaluronic acid (Incert) reduces postoperative adhesion formation.* Fertil Steril, 1998. **70**(1): p. 145-51.

103. Himeda, Y., et al., *Application of Biocompatible Gel of Hyaluronic Acid in Adhesion Prevention.* Journal of Gynecologic Surgery, 2004. **20**(2): p. 39-46.

104. Stuart, M., *Breaking the Surgical Adhesion Barrier.* Start-Up, 2005. **April**: p. 16-22.

105. Ferland, R., D. Mulani, and P.K. Campbell, *Evaluation of a sprayable polyethylene glycol adhesion barrier in a porcine efficacy model.* Hum Reprod, 2001. **16**(12): p. 2718-23.

106. Dunn, R., et al., *Evaluation of the SprayGel adhesion barrier in the rat cecum abrasion and rabbit uterine horn adhesion models.* Fertil Steril, 2001. **75**(2): p. 411-6.

107. Rodgers, K., et al., *Evaluation of polyethylene glycol/polylactic acid films in the prevention of adhesions in the rabbit adhesion formation and reformation sidewall models.* Fertil Steril, 1998. **69**(3): p. 403-8.

108. Zeng, Q., et al., *Efficacy and safety of Seprafilm for preventing postoperative abdominal adhesion: systematic review and meta-analysis.* World J Surg, 2007. **31**(11): p. 2125-31; discussion 2132.

109. Shinohara, T., et al., *A simple and novel technique for the placement of antiadhesive membrane in laparoscopic surgery.* Surg Laparosc Endosc Percutan Tech, 2008. **18**(2): p. 188-91.

110. Mettler, L., et al., *A randomized, prospective, controlled, multicenter clinical trial of a sprayable, site-specific adhesion barrier system in patients undergoing myomectomy.* Fertil Steril, 2004. **82**(2): p. 398-404.

111. Jackson, J.K., et al., *Paclitaxel-loaded crosslinked hyaluronic acid films for the prevention of postsurgical adhesions.* Pharm Res, 2002. **19**(4): p. 411-7.

112. Yagmurlu, A., et al., *Reduction of surgery-induced peritoneal adhesions by continuous release of streptokinase from a drug delivery system.* Eur Surg Res, 2003. **35**(1): p. 46-9.

113. Yeo, Y., et al., *Prevention of peritoneal adhesions with an in situ cross-linkable hyaluronan hydrogel delivering budesonide.* J Control Release, 2007. **120**(3): p. 178-85.

114. Leach, R.E., et al., *Reduction of postsurgical adhesion formation in the rabbit uterine horn model with use of hyaluronate/carboxymethylcellulose gel.* Fertil Steril, 1998. **69**(3): p. 415-8.

115. Cheung, M., *Development of a Swine Model for the Evaluation of Novel Compounds in the Prevention of Pelvic Adhesions*, in *2008 North Central Regional AICHE Student Conference*. 2008: University of Akron.

116. Black, J., *The education of the biomaterialist: report of a survey, 1980-81.* J Biomed Mater Res, 1982. **16**(2): p. 159-67.

117. Park, J.B., *Biomaterials Science and Engineering*. 1984, New York: Plenum

118. Ratner, B.D. and S.J. Bryant, *Biomaterials: where we have been and where we are going.* Annu Rev Biomed Eng, 2004. **6**: p. 41-75.

119. Williams, D.F. *Definitions in Biomaterials. Proceedings of a Concensus Conference of the Eurpoean Society for Biomaterials*. 1987. Chester, Englans: Elsevier.

120. Ratner, B.D., *A History of Biomaterials*, in *Biomaterial Science: An Introduction to Materials in Medicine*, B.D. Ratner, et al., Editors. 2004, Elsevier: New York. p. 10-19.

121. Ratner, B.D., et al., *Biomaterials Science: A Multidisciplinary Endeavor*, in *Biomaterials Science: An Introduction to Materials in Medicine*, B.D. Ratner, et al., Editors. 2004, Elsevier: New York. p. 1-9.

122. Anderson, J.M., *Inflammation, Wound Healing, and the Foreign Body Response*, in *Biomaterials Science: An Introduction to Materials in Medicine*, B.D. Ratner, et al., Editors. 2004, Elsevier: New York. p. 296-304.

123. Anderson, J.M., *In Vitro and In Vivo Monocyte, Macrophage, Foreign Body Giant Cell, and Lymphocyte Interactions with Biomaterials*, in *Biological Interactions on Materials Surfaces: Understanding and Controlling Protein, Cell, and Tissue Responses*, D.A. Puleo and R. Bizios, Editors. 2009, Springer: New York. p. 225-244.

124. Schoen, F.J. and R.N. Mitchell, *Tissues, the Extracellular Matrix, and Cell-Biomaterial Interactions*, in *Biomaterials Science: An Introduction to Materials in Medicine*, B.D. Ratner, et al., Editors. 2004, Elsevier: New Youk. p. 260-281.

125. Dee, K.C., D.A. Puleo, and R. Bizios, *An introduction to tissue-biomaterial interactions*. 2002, Hoboken, N.J.: Wiley-Liss. xx, 228 p.

126. diZerega, G.S. and J.D. Campeau, *Peritoneal repair and post-surgical adhesion formation.* Hum Reprod Update, 2001. **7**(6): p. 547-55.

127. Bakker, D., et al., *Effect of implantation site on phagocyte/polymer interaction and fibrous capsule formation.* Biomaterials, 1988. **9**(1): p. 14-23.

128. Barbosa, J.N., et al., *The influence of functional groups of self-assembled monolayers on fibrous capsule formation and cell recruitment.* J Biomed Mater Res A, 2006. **76**(4): p. 737-43.

129. Imber, G., et al., *Fibrous capsule formation after subcutaneous implanation of synthetic materials in experimental animals.* Plast Reconstr Surg, 1974. **54**(2): p. 183-6.

130. Jansson, E., et al., *On the formation of fibrous capsule and fluid space around machined and porous blood plasma clot coated titanium.* J Mater Sci Mater Med, 2001. **12**(10-12): p. 1019-24.

131. Suska, F., et al., *Fibrous capsule formation around titanium and copper.* J Biomed Mater Res A, 2008. **85**(4): p. 888-96.

132. Sittinger, M., et al., *Tissue engineering and autologous transplant formation: practical approaches with resorbable biomaterials and new cell culture techniques.* Biomaterials, 1996. **17**(3): p. 237-42.

133. Tsourapasa, G., et al., *Surface spectroscopic imaging of PEG-PLA tissue engineering constructs with ToF-SIMS.* Applied Surface Science, 2006. **252**(19): p. 6693.

134. Saltzman, W.M., *Drug delivery : engineering principles for drug therapy*. 2001, Oxford England ; New York: Oxford University Press. xi, 372.

135. Albertorio, F., et al., *Fluid and air-stable lipopolymer membranes for biosensor applications.* Langmuir, 2005. **21**(16): p. 7476-82.

136. Hartmann, J.T., et al., *Tyrosine Kinase Inhibitors - A Review on Pharmacology, Metabolism and Side Effects.* Curr Drug Metab, 2009.

137. Henke, M., et al., *Erythropoietin to treat head and neck cancer patients with anaemia undergoing radiotherapy: randomised, double-blind, placebo-controlled trial.* Lancet, 2003. **362**(9392): p. 1255-60.

138. Julie, L., M. Elizabeth, and P. Louise, *Chemotherapy-induced alopecia and effects on quality of life among women with breast cancer: a literature review.* Psycho-Oncology, 2008. **17**(4): p. 317-328.

139. Knight, K., S. Wade, and L. Balducci, *Prevalence and outcomes of anemia in cancer: a systematic review of the literature.* Am J Med, 2004. **116 Suppl 7A**: p. 11S-26S.

140. Spivak, J.L., *The anaemia of cancer: death by a thousand cuts.* Nat Rev Cancer, 2005. **5**(7): p. 543-55.

141. Bussemer, T., I. Otto, and R. Bodmeier, *Pulsatile drug-delivery systems.* Crit Rev Ther Drug Carrier Syst, 2001. **18**(5): p. 433-58.

142. El-Maradny, H.A., *Modulation of a pulsatile release drug delivery system using different swellable/rupturable materials.* Drug Deliv, 2007. **14**(8): p. 539-46.

143. Gotfried, M.H., *Clarithromycin (Biaxin) extended-release tablet: a therapeutic review.* Expert Rev Anti Infect Ther, 2003. **1**(1): p. 9-20.

144. Maroni, A., et al., *Oral pulsatile drug delivery systems.* Expert Opin Drug Deliv, 2005. **2**(5): p. 855-71.

145. Sloan, P.A. and R.L. Barkin, *Oxymorphone and oxymorphone extended release: a pharmacotherapeutic review.* J Opioid Manag, 2008. **4**(3): p. 131-44.

146. Hoffman, A.S., *The origins and evolution of "controlled" drug delivery systems.* J Control Release, 2008. **132**(3): p. 153-63.

147. Maeda, H., *The enhanced permeability and retention (EPR) effect in tumor vasculature: the key role of tumor-selective macromolecular drug targeting.* Adv Enzyme Regul, 2001. **41**: p. 189-207.

148. Maeda, H., G.Y. Bharate, and J. Daruwalla, *Polymeric drugs for efficient tumor-targeted drug delivery based on EPR-effect.* Eur J Pharm Biopharm, 2009. **71**(3): p. 409-19.

149. Tanaka, T., et al., *Tumor targeting based on the effect of enhanced permeability and retention (EPR) and the mechanism of receptor-mediated endocytosis (RME).* Int J Pharm, 2004. **277**(1-2): p. 39-61.

150. Brannon-Peppas, L. and J.O. Blanchette, *Nanoparticle and targeted systems for cancer therapy.* Adv Drug Deliv Rev, 2004. **56**(11): p. 1649-59.

151. Farokhzad, O.C. and R. Langer, *Impact of Nanotechnology on Drug Delivery.* ACS Nano, 2009. **3**(1): p. 16-20.

152. Langer, R., *Drugs on Target.* Science, 2001. **293**(5527): p. 58.

153. Ding, B.S., et al., *Advanced drug delivery systems that target the vascular endothelium.* Mol Interv, 2006. **6**(2): p. 98-112.

154. Alemany, R., *Designing adenoviral vectors for tumor-specific targeting.* Methods Mol Biol, 2009. **542**: p. 57-74.

155. Engelman, J.A., *Targeting PI3K signalling in cancer: opportunities, challenges and limitations.* Nat Rev Cancer, 2009. **9**(8): p. 550-62.

156. Gordon, I.O., et al., *Update in neoplastic lung diseases and mesothelioma.* Arch Pathol Lab Med, 2009. **133**(7): p. 1106-15.

157. Jia, L.J. and Z.C. Hua, *Development of bacterial vectors for tumor-targeted gene therapy.* Methods Mol Biol, 2009. **542**: p. 131-54.

158. Sandoval, D.A., S. Obici, and R.J. Seeley, *Targeting the CNS to treat type 2 diabetes.* Nat Rev Drug Discov, 2009. **8**(5): p. 386-98.

159. Telvekar, V.N. and H.S. Kundaikar, *GPR40 carboxylic acid receptor family and diabetes: a new drug target.* Curr Drug Targets, 2008. **9**(10): p. 899-910.

160. Yu, X., E. Patterson, and D.C. Kem, *Targeting proteasomes for cardioprotection.* Curr Opin Pharmacol, 2009. **9**(2): p. 167-72.

161. Blakey, D.C., *Drug Targeting with Monoclonal Antibodies: A review.* Acta Oncologica, 1992. **31**(1): p. 91-97.

162. Bunka, D.H. and P.G. Stockley, *Aptamers come of age - at last.* Nat Rev Microbiol, 2006. **4**(8): p. 588-96.

163. Yan, A.C. and M. Levy, *Aptamers and aptamer targeted delivery.* RNA Biology, 2009. **6**(3): p. 316.

164. Smith, G.P. and V.A. Petrenko, *Phage Display.* Chem Rev, 1997. **97**(2): p. 391-410.

165. Cao, Y. and L. Lam, *Bispecific antibody conjugates in therapeutics.* Adv Drug Deliv Rev, 2003. **55**(2): p. 171-97.

166. Nobs, L., et al., *Current methods for attaching targeting ligands to liposomes and nanoparticles.* J Pharm Sci, 2004. **93**(8): p. 1980-92.

167. Pangburn, T.O., et al., *Peptide- and aptamer-functionalized nanovectors for targeted delivery of therapeutics.* J Biomech Eng, 2009. **131**(7): p. 074005.

168. Anderson, J.C., B.C. McFarland, and C.L. Gladson, *New molecular targets in angiogenic vessels of glioblastoma tumours.* Expert Rev Mol Med, 2008. **10**: p. e23.

169. Brown, J.M. and A.J. Giaccia, *The unique physiology of solid tumors: opportunities (and problems) for cancer therapy.* Cancer Res, 1998. **58**(7): p. 1408-16.

170. Dvorak, H.F., *Leaky tumor vessels: consequences for tumor stroma generation and for solid tumor therapy.* Prog Clin Biol Res, 1990. **354A**: p. 317-30.

171. Simberg, D., et al., *Biomimetic amplification of nanoparticle homing to tumors.* Proc Natl Acad Sci U S A, 2007. **104**(3): p. 932-6.

172. Karmali, P.P., et al., *Targeting of albumin-embedded paclitaxel nanoparticles to tumors.* Nanomedicine, 2009. **5**(1): p. 73-82.

173. Park, J.H., et al., *Systematic surface engineering of magnetic nanoworms for in vivo tumor targeting.* Small, 2009. **5**(6): p. 694-700.

174. Peters, D.T., *Targeting Atherosclerosis: Nanoparticle Delivery for Diagnosis and Treatment*, in *Biomedical Sciences*. 2009, University of California: San Diego. p. 79.

175. Zanuy, D., et al., *The energy landscape of a selective tumor-homing pentapeptide.* J Phys Chem B, 2008. **112**(29): p. 8692-700.

176. Zanuy, D., et al., *Influence of the dye presence on the conformational preferences of CREKA, a tumor homing linear pentapeptide.* Biopolymers, 2009. **92**(2): p. 83-93.

177. Zanuy, D., et al., *In Silico Molecular Engineering for a Targeted Replacement in a Tumor-Homing Peptide.* J Phys Chem B, 2009.

178. Kutlay, J., et al., *Comparative effectiveness of several agents for preventing postoperative adhesions.* World J Surg, 2004. **28**(7): p. 662-5.

179. Moreira, H., Jr., et al., *Use of bioresorbable membrane (sodium hyaluronate + carboxymethylcellulose) after controlled bowel injuries in a rabbit model.* Dis Colon Rectum, 2000. **43**(2): p. 182-7.

180. Doan, K.T., R.J. Olson, and N. Mamalis, *Survey of intraocular lens material and design.* Curr Opin Ophthalmol, 2002. **13**(1): p. 24-9.

181. Eppley, B.L. and B. Dadvand, *Injectable soft-tissue fillers: clinical overview.* Plast Reconstr Surg, 2006. **118**(4): p. 98e-106e.

182. Revell, P.A., M. Braden, and M.A. Freeman, *Review of the biological response to a novel bone cement containing poly(ethyl methacrylate) and n-butyl methacrylate.* Biomaterials, 1998. **19**(17): p. 1579-86.

183. Sclafani, A.P. and T. Romo, 3rd, *Injectable fillers for facial soft tissue enhancement.* Facial Plast Surg, 2000. **16**(1): p. 29-34.

184. Hilgers, L.A., et al., *Alkyl-esters of polyacrylic acid as vaccine adjuvants.* Vaccine, 1998. **16**(16): p. 1575-81.

185. Oka, T., et al., *Influenza vaccine: enhancement of immune response by application of carboxy-vinylpolymer.* Vaccine, 1990. **8**(6): p. 573-6.

186. Ho, D.H., et al., *Clinical pharmacology of polyethylene glycol-L-asparaginase.* Drug Metab Dispos, 1986. **14**(3): p. 349-52.

187. Saiki, I., et al., *Antimetastatic activity of polymeric RGDT peptides conjugated with poly(ethylene glycol).* Jpn J Cancer Res, 1993. **84**(5): p. 558-65.

188. Teppler, H., et al., *Prolonged immunostimulatory effect of low-dose polyethylene glycol interleukin 2 in patients with human immunodeficiency virus type 1 infection.* J Exp Med, 1993. **177**(2): p. 483-92.

189. Gref, R., et al., *'Stealth' corona-core nanoparticles surface modified by polyethylene glycol (PEG): influences of the corona (PEG chain length and surface density) and of the core composition on phagocytic uptake and plasma protein adsorption.* Colloids Surf B Biointerfaces, 2000. **18**(3-4): p. 301-313.

190. Butun, V., et al., *Synthesis and aqueous solution properties of novel neutral/acidic block copolymers.* Polymer, 2000. **41**(9): p. 3173-3182.

191. Hadjiyannakou, S.C., M. Vamvakaki, and C.S. Patrickios, *Synthesis, characterization and evaluation of amphiphilic diblock copolymer emulsifiers based on methoxy hexa(ethylene glycol) methacrylate and benzyl methacrylate.* Polymer, 2004. **45**(8): p. 2433-2442.

192. Triftaridou, A.I., M. Vamvakaki, and C.S. Patrickios, *Amphiphilic diblock and ABC triblock methacrylate copolymers: synthesis and aqueous solution characterization.* Polymer, 2002. **43**(10): p. 2921-2926.

193. Vamvakaki, M., N.C. Billingham, and S.P. Armes, *Synthesis of water-soluble statistical copolymers and terpolymers containing pendent oligo(ethylene glycol derivatives).* Polymer, 1999. **40**(18): p. 5161-5171.

194. Rannard, S.P., et al., *Synthesis of monodisperse block copolymers containing methacrylic acid segments by group transfer polymerization: choice of protecting group and catalyst.* European Polymer Journal, 1993. **29**(2/3): p. 407-414.

195. Dicker, I.B., et al., *Oxyanions Catalyze Group-Transfer Polymerization To Give Living Polymers.* Macromolecules, 1990. **23**: p. 4034-4041.

196. Arano, Y., et al., *Reassessment of diethylenetriaminepentaacetic acid (DTPA) as a chelating agent for indium-111 labeling of polypeptides using a newly synthesized monoreactive DTPA derivative.* J Med Chem, 1996. **39**(18): p. 3451-60.

197. Boeckler, C., B. Frisch, and F. Schuber, *Design and synthesis of thiol-reactive lipopeptides.* Bioorg Med Chem Lett, 1998. **8**(15): p. 2055-8.

198. Neises, B. and W. Steglich, *Simple Method for the Esterification of Carboxylic Acids.* Angew. Chem. Int. Ed. Engl., 1978. **17**(7): p. 522-524.

199. Sheehan, J.C. and G.P. Hess, *A New Method of Forming Peptide Bonds.* Journal of the American Chemical Society, 1955. **77**(4): p. 1067-1068.

200. Odian, G.G., *Principles of polymerization*. 4th ed. 2004, Hoboken, N.J.: Wiley-Interscience. xxiv, 812.

201. *How to Prepare Self-Assembled Monolayers*, in *Self-Assembling Molecules*. 2005, Asemblon, Inc. p. 2-6.

202. *Variations in the Assembly Protocol for Carboxy- and Amine-Terminated Alkanethiols*, in *Self-Assembly Procedure for Carboxy- and Amine-Terminated Alkanethiols*. 2005, Asemblon, Inc. p. 2-3.

203. Wang, H., et al., *Improved Method for the Preparation of Carboxylic Acid and Amine Terminated Self-Assembled Monolayers of Alkanethiolates.* Langmuir, 2005. **21**(7): p. 2633-2636.

204. *Cleaning-UVO Treatment*, in *Methods and Protocols*. 2007, Q-Sense Methods and Protocols. p. 1-16.

205. Sauerbrey, G., Zeitschrift für Physik, 1959. **155**: p. 206.

206. Reimhult, K., K. Petersson, and A. Krozer, *QCM-D analysis of the performance of blocking agents on gold and polystyrene surfaces.* Langmuir, 2008. **24**(16): p. 8695-700.

207. Höök, F., et al., *A comparative study of protein adsorption on titanium oxide surfaces using in situ ellipsometry, optical waveguide lightmode spectroscopy, and quartz crystal microbalance/dissipation.* Colloids and Surfaces B: Biointerfaces, 2002. **24**(2): p. 155-170.

208. Tompkins, H.G. and W.A. McGahan, *Spectroscopic ellipsometry and reflectometry : a user's guide*. 1999, New York: Wiley. xiv, 228 p.

209. Hanson, A.D., et al., *Effects of oxygen plasma treatment on adipose-derived human mesenchymal stem cell adherence to poly(L-lactic acid) scaffolds.* J Biomater Sci Polym Ed, 2007. **18**(11): p. 1387-400.

210. Morra, M., et al., *Collagen I-coated titanium surfaces: mesenchymal cell adhesion and in vivo evaluation in trabecular bone implants.* J Biomed Mater Res A, 2006. **78**(3): p. 449-58.

211. Ahmed, T.A., E.V. Dare, and M. Hincke, *Fibrin: A Versatile Scaffold for Tissue Engineering Applications.* Tissue Eng Part B Rev, 2008.

212. Ahn, H.H., et al., *Polyethyleneimine-mediated gene delivery into human adipose derived stem cells.* Biomaterials, 2008. **29**(15): p. 2415-22.

213. Jeon, J.H., M.V. Thomas, and D.A. Puleo, *Bioerodible devices for intermittent release of simvastatin acid.* Int J Pharm, 2007. **340**(1-2): p. 6-12.

214. Labarca, C. and K. Paigen, *A simple, rapid, and sensitive DNA assay procedure.* Anal Biochem, 1980. **102**(2): p. 344-52.

215. Höök, F., et al., *Energy dissipation kinetics for protein and antibody-antigen adsorption under shear oscillation on a quartz crystal microbalance.* Langmuir, 1998. **14**(4): p. 729-734.

216. Fan, X., L. Lin, and P.B. Messersmith, *Cell fouling resistance of polymer brushes grafted from ti substrates by surface-initiated polymerization: effect of ethylene glycol side chain length.* Biomacromolecules, 2006. **7**(8): p. 2443-8.

217. Nappi, C., et al., *Prevention of adhesions in gynaecological endoscopy.* Hum Reprod Update, 2007. **13**(4): p. 379-94.

218. Höök, F. and B. Kasemo, *The QCM-D Technique for Probing Biomacromolecular Recognition Reactions*, in *Piezoelectric Sensors*. 2007. p. 425-447.

219. Höök, F., et al., *Dissipative QCM-D technique: Interfacial phenomena and sensor applications for proteins, biomembranes, living cells and polymers.* Proceedings of the Annual IEEE International Frequency Control Symposium, 1999. **2**: p. 966-972.

220. Reimhult, E., et al., *Simultaneous surface plasmon resonance and quartz crystal microbalance with dissipation monitoring measurements of biomolecular adsorption events involving structural transformations and variations in coupled water.* Analytical Chemistry, 2004. **76**(24): p. 7211-7220.

221. Medley, J.M. and T.D. Dziubla, *Prevention of Post-Surgical Adhesions: A Biomaterials Perspective*, in *Biological Interactions on Materials Surfaces: Understanding and Controlling Protein, Cell, and Tissue Responses*, R. Bizios and D.A. Puleo, Editors. 2009, Elsevier: New York.

222. Jung, H., et al., *Change of viscoelastic property and morphology of fibrin affected by antithrombin III and heparin: QCM-Z and AFM study.* Colloids Surf B Biointerfaces, 2009. **68**(1): p. 111-9.

223. Riedel, T., et al., *Controlled preparation of thin fibrin films immobilized at solid surfaces.* J Biomed Mater Res A, 2009. **88**(2): p. 437-47.

224. Kroh, H.K., P. Panizzi, and P.E. Bock, *Von Willebrand factor-binding protein is a hysteretic conformational activator of prothrombin.* Proc Natl Acad Sci U S A, 2009. **106**(19): p. 7786-91.

225. Wolberg, A.S., D.A. Gabriel, and M. Hoffman, *Analyzing fibrin clot structure using a microplate reader.* Blood Coagul Fibrinolysis, 2002. **13**(6): p. 533-9.

226. Williams, J.D., *Statistical Methods*. 1996, Lanham, MD: University Press of America.

227. Walpole, R.E. and R.H. Myers, *Probability and Statistics for Engineers and Scientists*. 3rd ed. 1985, New York: Macmillan.

228. National Institute of Standards and Technology (U.S.) and International SEMATECH. *Engineering Statistics Handbook*. 2009 October 15, 2009]; Available from: http://www.itl.nist.gov/div898/handbook/index2.htm.

229. Vardeman, S.B., *Statistics for Engineering Problem Solving*. 1994, Boston, MA: PWS Publishing.

230. Carr, M.E. and D.A. Gabriel, *Dextran-Induced Changes in Fibrin Fiber Size and Density Based on Wavelength Dependence of Gel Turbidity.* Macromolecules, 1980. **13**: p. 1473-1477.

231. Carr, M.E., Jr. and J. Hermans, *Size and density of fibrin fibers from turbidity.* Macromolecules, 1978. **11**(1): p. 46-50.

232. Sato, H. and A. Nakajima, *Kinetic study on the initial stage of the fibrinogen-fibrin conversion by thrombin. (1) Application of mathematical treatment to turbidimetrical method.* Thromb Res, 1984. **33**(6): p. 645-51.

233. Sato, H., E. Nakanishi, and A. Nakajima, *Kinetic Study on the Initial Stage of Fibrinogen-Fibrin Conversion by Turbidimetry.* Colloid and Polymer Science, 1981. **259**: p. 1246-1248.

234. Berova, N., K. Nakanishi, and R.W. Woody, *Circular Dichroism: Principles and Applications*. 2nd ed. 2000, New York: Wiley.

235. Fasman, G.D., *Circular Dichroism and the Conformational Analysis of Biomolecules*. 1st ed. 2007, New York: Springer-Verlag.

236. Kelly, S.M. and N.C. Price, *The use of circular dichroism in the investigation of protein structure and function.* Curr Protein Pept Sci, 2000. **1**(4): p. 349-84.

237. Rodger, A. and B. Norden, *Circular Dichroism and Linear Dichroism*. 1997, New York: Oxford University Press.

238. Kelly, S.M., T.J. Jess, and N.C. Price, *How to study proteins by circular dichroism.* Biochim Biophys Acta, 2005. **1751**(2): p. 119-39.

239. da Silva, J.O., et al., *Triterpenoid saponins, new metalloprotease snake venom inhibitors isolated from Pentaclethra macroloba.* Toxicon, 2007. **50**(2): p. 283-91.

240. Fenton, J.W., 2nd, et al., *Thrombin inhibition by hirudin: how hirudin inhibits thrombin.* Haemostasis, 1991. **21 Suppl 1**: p. 27-31.

241. Sillanpaa, J., et al., *A family of fibrinogen-binding MSCRAMMs from Enterococcus faecalis.* Microbiology, 2009. **155**(Pt 7): p. 2390-400.

242. Andrade, M.A., et al., *Evaluation of secondary structure of proteins from UV circular dichroism spectra using an unsupervised learning neural network.* Protein Eng, 1993. **6**(4): p. 383-90.

243. Perez-Iratxeta, C. and M. Andrade. *K2D2: Estimating Protein Secondary Structure from CD Spectra*. [cited 2009 August 23]; Available from: http://www.ogic.ca/projects/k2d2/orainaldia.html.

244. Perez-Iratxeta, C. and M.A. Andrade-Navarro, *K2D2: Estimation of protein secondary structure from circular dichroism spectra.* BMC Struct Biol, 2008. **8**: p. 25.

245. Chen, Y., et al., *Thermal conformational changes of bovine fibrinogen by differential scanning calorimetry and circular dichroism.* Int J Biol Macromol, 1999. **26**(2-3): p. 129-34.

246. Ohta, N. and T. Yotsuyanagi, *Alteration of fibrinogen secondary structure by cis-diamminedichloroplatinum(II) and calcium protection.* Biol Pharm Bull, 1993. **16**(7): p. 631-4.

247. Doolittle, R.F. and J.M. Kollman, *Natively unfolded regions of the vertebrate fibrinogen molecule.* Proteins, 2006. **63**(2): p. 391-7.

248. Martin, S.C. and I. Bjork, *Conformational changes in human fibrinogen after in vitro phosphorylation and their relation to fibrinogen behaviour.* FEBS Lett, 1990. **272**(1-2): p. 103-5.

249. Tsurupa, G., L. Tsonev, and L. Medved, *Structural organization of the fibrin(ogen) alpha C-domain.* Biochemistry, 2002. **41**(20): p. 6449-59.

VITA

John Medley was born in Owensboro, Kentucky, on April 28th, 1974. He graduated from Owensboro Catholic High School and went on to earn his Bachelor of Arts Degree in Chemistry from Transylvania University. After completing a Master of Science degree in Chemistry from the University of Michigan and a Master of Science degree in Chemical Engineering, he pursued an industrial career. As a development engineer at Lexmark, International, in Lexington, Kentucky, he was an inventor on four United States patent applications. Following his tenure as an engineer in the Materials and Processes Engineering department at United Space Alliance in Cape Canaveral, Florida, John returned to the University of Kentucky to pursue a Doctorate of Philosophy in Chemical Engineering. After completion of his dissertation research, John joined the faculty of Centre College in Danville, Kentucky, as a visiting instructor of chemistry.

Awards and Honors

2007-2009	University of Kentucky Graduate Student Academic Year Fellowship
2007	Q-Sense Users Meeting, Runner-up, Best Student Presentation
2006-2009	University of Kentucky Whalen Graduate Fellowship
2006-2007	University of Kentucky Research Challenge Trust Fund Fellowship
1996-1997	University of Michigan President's Fellowship
1995	National Science Foundation Research Experience for Undergraduates, University of Chicago

Publications and Presentations

Book Chapters

Medley, John M. and Thomas D. Dziubla. "Prevention of Post-Surgical Adhesions: A Biomaterials Perspective." Biological Interactions on Materials Surfaces: Understanding and Controlling Protein, Cell, and Tissue Responses. Ed. Rena Bizios, David A. Puleo. Elsevier, New York, 2009.

Journal Articles

Medley, John M., Eric J. Beane, S.K.C. Sundararaj, Eugene Kaplan, David A. Puleo, and Thomas D. Dziubla. “Targeted Block Copolymers for the Prevention of Post-Surgical Adhesions.” Manuscript in preparation.

Medley, John M., Eric J. Beane, and Thomas D. Dziubla. “Synthesis and Characterization of CREKA-Targeted Polymers for the Disruption of Fibrin Gel Matrix Propagation.” Manuscript in preparation.

Medley, John M., Mandeep Saini, Fran Lockwood, Kazunori Kuwana, and Eric Grulke. “A Mechanism for Formation of Low Friction MoS2 Films.” Manuscript in preparation.

Medley, John M., Eric J. Beane, S.K.C. Sundararaj, Eugene Kaplan, David A. Puleo, and Thomas D. Dziubla. “Block Copolymers for the Rational Design of Self-Forming Postsurgical Adhesion Barriers.” Acta Biomaterialia, 2009, 6 (1): p. 72.

Medley, John M. “Semiempirical Predictive Kinetic Model of Light Induced Magenta Dye-Based Ink Jet Ink Fading on Polymer-Coated Photomedia.” Journal of Imaging Science and Technology, July/August 2009, 53 (4), p. 040501-(6).

Presentations

Medley, John M. (Presenter), Thomas D. Dziubla, Eugene Kaplan, and Eric J. Beane. “Targeted Block Copolymers for the Prevention of Post-Surgical Adhesions.” American Institute of Chemical Engineering, Annual Meeting, November 19, 2008.

Medley, John M. “No Boundaries: Chemistry in Research.” Centre College Departmental Seminar, April 16, 2008.

Medley, John M. (Presenter), Eugene Kaplan, Eric Beane, and Thomas D. Dziubla. “Structure-Property Relationships in Self-Assembled Barriers for the Prevention of Post-Surgical Adhesions.” University of Kentucky Graduate Student Interdisciplinary Conference, March 28, 2008.

Medley, John M. (Presenter), Eugene Kaplan, Eric Beane, and Thomas D. Dziubla. “Hydrophilic Anionic-Neutral Block Copolymers for the Prevention of Post-Surgical Adhesions.” Q-Sense Users Meeting, Runner-up, Best Student Presentation, November 27, 2007.

Medley, John M. (Presenter), Eugene Kaplan, Eric Beane, and Thomas D. Dziubla. “Synthesis and Characterization of Hydrophilic Anionic-Neutral Block

Copolymers for the Prevention of Post-Surgical Adhesions." American Institute of Chemical Engineering, Annual Meeting, November 8, 2007.

Patents and Patent Applications

Dziubla, T., E. Kaplan, and J.M. Medley, Jr. "Compounds and Methods for Reducing the Occurrence of Post-Surgical Adhesions." US Patent Application, November 16, 2009.

McCain, S.H. and J.M. Medley. "Pigment Black and Dilute Dye Inks in Ink Set." US Patent Application 20070171268, July 26, 2007.

McCain, S.H., J.M. Medley, and AK Zimmer. "Inkjet Ink Having Yellow Dye Mixture." US Patent 7,040,746, May 9, 2006.

McCain, S.H. and J.M. Medley. "Pigment Black and Dilute Dye Inks in Ink Set." US Patent Application 20050183629, August 25, 2005.

Zimmer, A.K., et al. "Inkjet Ink, Dye Set, Ink Set, and Method of Use Thereof." US Patent 6,843,838, January 18, 2005.